Australian Government
Department of the Environment
Supervising Scientist

internal report **628**

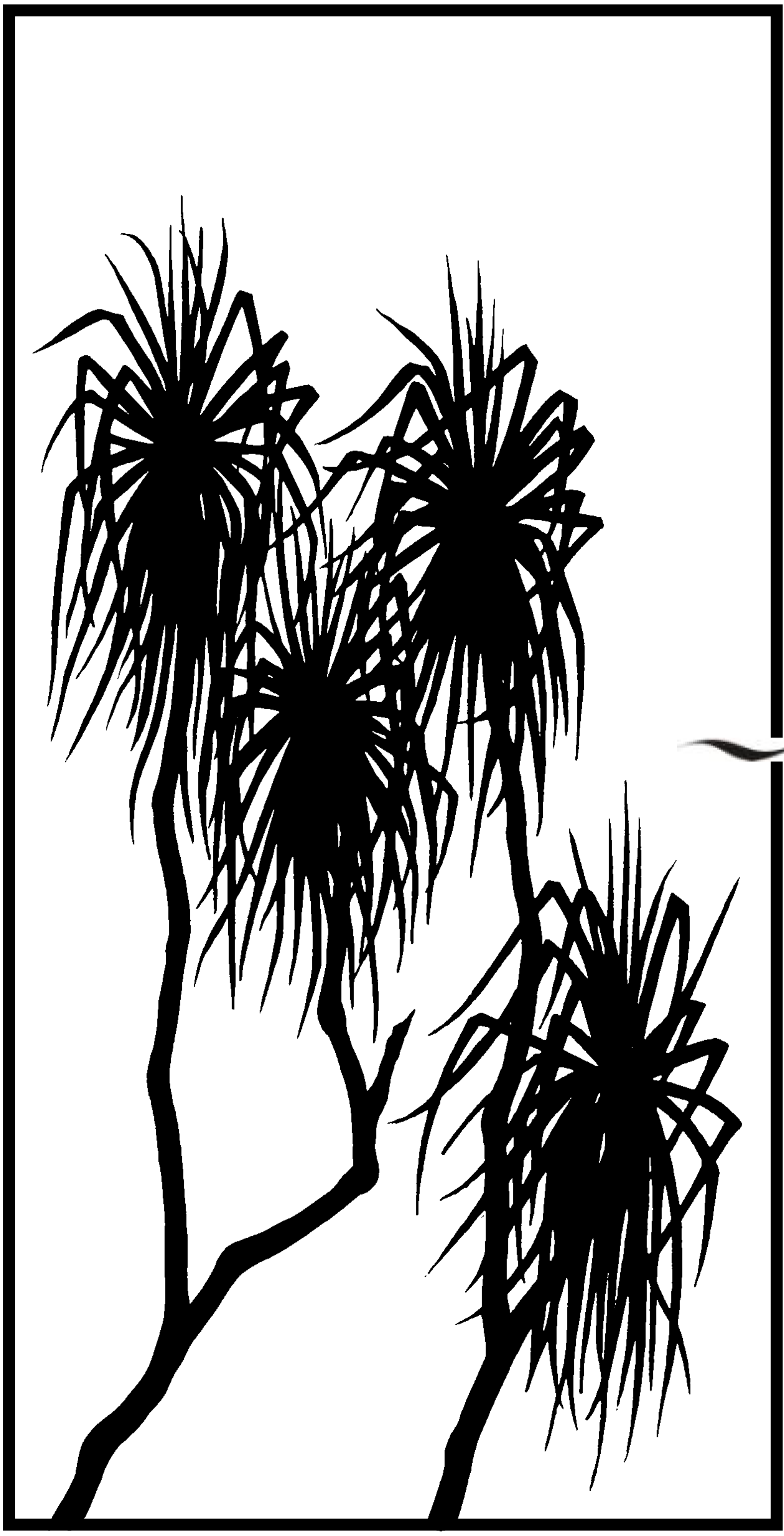

Vegetation map for Magela Creek floodplain using WorldView - 2 multispectral image data

T Whiteside & R Bartolo

April 2014

Release status – unrestricted

Project number – RES-2012-011

This page has been left blank intentionally.

Vegetation map for Magela Creek floodplain using WorldView - 2 multispectral image data

T Whiteside & R Bartolo

Supervising Scientist Division

GPO Box 461, Darwin NT 0801

April 2014

Project number RES-2012-011

(Release status – unrestricted)

Australian Government

Department of the Environment

Supervising Scientist

T Whiteside & R Bartolo 2014. Vegetation map for Magela Creek floodplain using WorldView -2 multispectral image data. Internal Report 628, April, Supervising Scientist, Darwin.

Project number – RES-2012-011

Authors of this report:

Tim Whiteside – Environmental Research Institute of the Supervising Scientist, GPO Box 461, Darwin NT 0801, Australia

Renee Bartolo – Environmental Research Institute of the Supervising Scientist, GPO Box 461, Darwin NT 0801, Australia

The Supervising Scientist is a division of the Australian Government Department of the Environment.

Supervising Scientist
Department of the Environment
GPO Box 461, Darwin NT 0801 Australia

Internet: environment.gov.au/ssd/publications

Printed and bound in Darwin NT by Supervising Scientist Division

Contents

List of Figures

List of Tables

Executive summary

The significance of the wetlands of the Magela Creek floodplain in northern Australia and their biodiversity has been recognised through their listing by the Ramsar Convention on Wetlands. The wetlands have been identified as being at risk from a number of sources, chiefly the landscape-scale risks of weeds, fire and climate change. In addition, the Magela Creek floodplain is a downstream receiving environment for the Ranger uranium mine. Offsite monitoring of this area will become increasingly important in the years following closure and rehabilitation of the minesite (post 2026), as a key component of an integrated environmental monitoring framework (particularly relevant to Key Knowledge Need 2.6.2 pertaining to off-site monitoring).

Vegetation within the wetland is spatially and temporally variable and, therefore, a robust methodology for mapping wetland vegetation at scales that can detect the variability is required. In addition, time series mapping of floodplain vegetation will provide a contemporary baseline of annual vegetation dynamics on the floodplain to assist with analysing change during and after minesite rehabilitation.

The aim of this project is to:

To establish a baseline dataset of natural variability in vegetation that could be used to monitor potential mine impacts through the production of a series of high resolution vegetation maps 2010–2014.

Specifically, the objectives of this report are to:

a. Document the procedures for producing a map of the floodplain vegetation for 2010 in a large wetland downstream from Ranger Uranium Mine.
b. Determine the applicability of high spatial resolution (HSR) satellite imagery to map and monitor vegetation on the floodplain.
c. Develop and record a GEOBIA-based methodology suitable for mapping and monitoring the offsite environment.

HSR satellite imagery consists of pixels with a ground sample distance (GSD) less than 5 m. HSR imagery, such as WorldView-2 provides data for spatially detailed analysis of landscapes. The increased spatial heterogeneity associated with the finer resolution of the data requires data aggregation to assist with classification. The research described here uses geographic object-based image analysis (GEOBIA) to classify the floodplain vegetation from 2010 WorldView-2 imagery. The GEOBIA used consisted of a step-wise rule-set driven approach using a series of segmentations and classifications. The rule-set implemented a number of well-known spectral indices and sensor band specific ratios to: (1) create and classify objects representing the major landscape units (floodplain and non-floodplain) and mask non-target land covers, and (2) extract objects representative of the vegetation communities within the floodplain. The input of a digital elevation model enabled the delineation of the floodplain boundary.

The main output of this project is a map of the major 12 vegetation communities that exist on the Magela Creek floodplain and their distribution for May 2010. Based on the reference data the overall accuracy of the map is 78%. The rule set was able to distinguish the majority of the floodplain classes. Most of the error appears to be associated with confusion between classes that are spectrally similar such as the classes dominated by grasses. The other main output from this project is the development of a robust methodology for mapping the vegetation on the Magela Creek floodplain for 2010 and subsequent years using WorldView-2 imagery.

The major findings of this project are that WorldView-2 multispectral imagery is an appropriate data set for a vegetation classification of the Magela Creek floodplain. The application of a GEOBIA methodology is a suitable method for the increase within field spectral variation associated with HSR data.

The use of WV-2 high spatial resolution imagery enables boundary delineation between classes and also aids in the identification of individual or small clusters of plants. The red edge band within the imagery was useful for discrimination of a number of the classes. Limitations of the WV-2 data include the narrow spectral range (350–940 nm) and different view angle for the different images. The advantages of using a GEOBIA method included the ability to compile a rule set that is repeatable and potentially transferrable to other data, although it is limiting in lengthy processing time. The inclusion of a Canopy Height Model (CHM) was beneficial in enabling the accurate identification and mapping of treed areas within the floodplain although the coverage was not entire and is a different date to the WV-2 data.

The methodology described in this report will be applied to the WV-2 imagery acquired annually by ***eriss*** for 2011–2014. Vegetation maps from each year will be used in analysis of the spatial and temporal variability of the communities. This analysis will inform the temporal frequency of image acquisitions over the region as part of an ongoing monitoring program during and post mine site rehabilitation.

Related publications

Whiteside, T, Bartolo, R & Staben, G 2012. A rule-based approach to segment and classify floodplain vegetation from WorldView-2 imagery. In *Proceedings of 16th Australasian Remote Sensing and Photogrammetry Conference*, 25 August–1 September 2012, Melbourne, Victoria.

Whiteside, T, Bartolo, R, Pfitzner, K & Staben, G 2013. Geometric & radiometric correction of multispectral WorldView-2 satellite imagery, Internal report 617, May, Supervising Scientist, Darwin.

Acknowledgments

The authors would like to thank James Boyden, Krissy Kai-Nielsen, Annamarie Beraldo and Grant Staben for their contributions towards the collection of the field data for this report. Also thank you to Michael Saynor for providing Magela Creek 009 gauging station discharge data.

Abbreviations

AGL	Above ground level
AHD	Australian Height Datum
ARR	Alligator Rivers Region
CHM	Canopy height model
DEM	Digital elevation model
DSM	Digital surface model
EM	Electromagnetic
EVI	Enhanced vegetation index
FDI	Forest discrimination index
FNEA	Fractal Net Evolution Approach
GCP	Ground control point
GEOBIA	Geographical object-based image analysis
GIS	Geographic information system
GPS	Global positioning system
GSD	Ground sample distance
HSR	High spatial resolution
KNP	Kakadu National Park
LI	Lily index
LiDAR	Light detection and ranging
MSR	Moderate spatial resolution
NDVI	Normalised vegetation index
NIR	Near infrared
RE	Red edge
RGB	Red, green, blue
RMSE	Root means square error
RPC	Rational polynomial coefficient
SRTM	Shuttle Radar Topography Mission
SP	Scale parameter
SPOT	Satellite Pour l'Observation de la Terre
SSD	Supervising Scientist Division
TM	Thematic mapper
VNIR	Visible and near infrared
WV-2	WorldView-2

1 Introduction

1.1 Project definition

This report presents work undertaken by ***eriss*** staff during 2010–2012 to map the floodplain vegetation in a large ecologically significant wetland downstream from Ranger Uranium Mine using data for May 2010 captured by the satellite-based WorldView-2 (WV-2) sensor. Within the project the goals were to determine the applicability of high spatial resolution multispectral satellite data for mapping and monitoring floodplain vegetation and develop a methodology that would be transferable to WV-2 imagery for future years. The time series mapping of floodplain vegetation will provide a contemporary baseline of annual vegetation dynamics on the floodplain to assist with monitoring and analysing off-site change during and after rehabilitation.

The aims of this project are to:

1. To produce high resolution maps of the vegetation communities of the Magela Creek floodplain for the years 2010–2013 to as a baseline.

2. To map and analyse annual change within vegetation communities on the floodplain.

More specifically, the objectives of this report are to:

a. Determine the applicability of very high resolution satellite imagery to map and monitor vegetation on the floodplain and thus establish a baseline dataset of variability that can be used monitor the potential impacts downstream from the rehabilitation of Ranger Uranium Mine.
b. Develop a GEOBIA-based methodology suitable for mapping and monitoring the offsite environment.

The outcomes of this project are:

- A vegetation map of the Magela Creek floodplain for May 2010
- The development of a methodology capable of producing vegetation maps of the Magela Creek floodplain for WorldView-2 imagery captured in May 2011, June 2012 and June 2013.

1.2 Project focus

The geographical focus of this project is the Magela Creek floodplain (Figure 1.1) within the East Alligator River catchment of the Alligators Rivers Region of the Northern Territory of Australia. The floodplain is a downstream receiving environment for the Ranger Uranium Mine.

Figure 1.1 Location of Magela Creek floodplain, the study area for this project.

The research focus of this project is twofold. Firstly, the project is assessing the utility of high spatial resolution satellite imagery (in this instance WorldView-2 multispectral imagery) for mapping Magela Creek floodplain vegetation. WorldView-2 data have increased spectral range compared to other high spatial resolution satellite imagery acquired by ***eriss***, namely QuickBird and IKONOS imagery. Secondly the project is focussed on developing a methodology for mapping the floodplain vegetation for 2010 and subsequent years to establish a baseline for the natural variability of vegetation within the Magela Creek floodplain. This baseline will assist with monitoring the potential downstream impacts associated with minesite rehabilitation.Vegetation community mapping will also inform ecological risk assessment for management of the floodplain. Current landscape level ecological risks within the region are identified as weeds, feral animals and unmanaged wildfire. The research undertaken for this project will also provide valuable information that will inform research such as the National Environmental Research Program's North Australia Hub remote sensing of coastal habitats program.

1.3 Background

According to the criteria of the Ramsar Wetlands Convention, the wetlands within Kakadu National Park (KNP) have been designated as internationally important (Finlayson et al. 2006). The wetlands, including the floodplain within the Magela Creek catchment are significant not only in their biogeographical context, but also for the diversity of plant communities (Finlayson et al. 2006) and as habitat refuges for abundant and diverse waterbird populations (Bayliss & Yeomans 1990, Bellio et al. 2004). Previous research has identified 10 major vegetation communities within the Magela Creek floodplain (Finlayson et al. 1989) and the species composition of these communities is seasonally dynamic (Finlayson et al. 2006). The spatial distribution of a number of the communities is annually dynamic, although reasons for the dynamics are not fully understood. It is uncertain whether the annual change is a naturally occurring phenomenon, the result of anthropogenic influence or a combination of both and, despite the importance of these wetlands, there has been little research on the dynamics (Finlayson et al. 2006). Accurate mapping of the communities within the floodplain at the appropriate spatial and temporal scale will provide data that will enable analysis that may determine the drivers of the dynamics. Vegetation community mapping of the floodplain also informs the ecological risk assessment underlying park management strategies (Bayliss et al. 2012). Current landscape level ecological risks within the region are identified as weeds, feral animals (Figure 1.2) and unmanaged wildfire (Bayliss et al. 2012). In addition, the Magela Creek floodplain is a down-stream receiving environment for the Ranger uranium minesite and as such off-site monitoring of this area will become increasingly important in the years following mine closure and rehabilitation (post 2026).

Figure 1.2 Two of the ecological risks identified for Magela Creek floodplain; feral animals (pigs) and weeds (Para grass). Photo: Krissy Kai-Nielsen.

1.4 Previous mapping of the Magela Floodplain

The most recent community level vegetation map for the Magela Creek floodplain was created using a nearest neighbour supervised classification of a time series of four Landsat 5 TM images (May–September) captured in 2006 (Boyden et al. 2013). This classification provided 16 classes which were then aggregated into 10 vegetation community types and described to an extent the seasonalvariation for that year. Prior to the 2006 map, the last published vegetation map for the floodplain was produced in 1989 based on aerial photo interpretation and extensive field campaigns (Finlayson et al. 1989). The 1989 map consisted of ten classes accounting for the seasonal variations in vegetation cover. Each class was derived from several years data collected at times of peak growth (typically during the wet season) with the names used for each class either reflecting the observed indicator species at the period of peak biomass (wet to early dry season), or else the class was assigned a general descriptive name. At the time, Finlayson et al. (1989) postulated that the major determinant in the composition of flora was the duration and period of inundation, with lesser contributions from other factors such as water flow velocity and depth (Finlayson et al. 1989).

There have been three studies examining temporal change of the distribution of *Melaleuca* spp. on the floodplain. An analysis of aerial photography (Williams 1984) determined that, although the area covered by *Melaleuca* trees did not change between 1950 and 1975, tree density in a number of areas decreased by up to 37%. Another study of aerial photography for 1975 and 1994 (Riley & Lowry 2002), found the tree densities to be greater in 1975 than Williams (1984) had measured. The study also found, although the distribution had increased, *Melaleuca* densities had declined by 21% between 1975 and 1994. In addition, a study of the spatial and temporal distribution of *Melaleuca* spp. on a portion of the floodplain was undertaken using four dates of aerial photographs over a 54 year period and an object-based image analysis (Staben 2008). This work showed that while overall canopy cover has remained relatively constant, the spatial distribution has been dynamic.

1.5 Use of satellite data for wetland mapping

Multispectral remote sensing has been used as a source of data to successfully map and monitor vegetation at a range of scales from local (Boyden et al. 2013), regional (Hayder 2001), continental (Lymburner et al. 2011) to global (Herold et al. 2008). Remote sensing is a relatively low cost means of acquiring continuous data over remote, inaccessible and potentially hazardous areas such as tropical wetlands. Higher spatial resolution (HSR) data (with a ground sample distance (GSD) < 5 m) has shown potential for vegetation mapping (Moffett & Gorelick 2012, Mutanga et al. 2012, Jawak & Luis 2013). This is despite HSR imagery typically not having the range across the electromagnetic spectrum (EM) that is covered by moderate resolution sensors such as the Landsat satellite series. For example, WV-2 imagery while having 8 bands only captures data from the visible and near infrared (VNIR) portion of the EM spectrum, whereas Landsat data (with a GSD 30 m), also capturing 8 bands, covers the VNIR, the short-wave infrared and long-wave infrared regions.

Medium spatial resolution (MSR) imagery (10–30 m GSD), such as Landsat TM and SPOT data have proven insufficient for discriminating vegetation species in detailed wetland environments (Harvey and Hill 2001; McCarthy et al. 2005; May et al. 1997). According to Adam et al. (2010), this is due to three factors. Firstly, it is difficult to distinguish the fine ecological divisions between certain vegetation species in MSR data. Secondly, the broad nature of the spectral wavebands in the data results in difficulty detecting sharp ecological gradients within narrow vegetation units in wetland ecosystems. Thirdly, MSR data lacks the finer spectral and spatial resolution needed for the detection and mapping of vegetation types beneath a canopy of vegetation in densely vegetated wetlands. Harvey and Hill (2001) found that the spatial resolution of aerial photography was superior to medium resolution satellite imagery (SPOT and Landsat TM) for detailed mapping of tropical wetlands. They also found the increased spectral information available in Landsat TM data provided a more accurate classification than the higher spatial resolution SPOT data. Boyden et al. (2013) identified a number of challenges for remote sensing of monsoonal wetland environments, mostly associated with the highly variable annual rainfall and subsequent variation in water extent and levels within the floodplain. These issues are of concern when applying image analysis methods based purely on per-pixel information. QuickBird multispectral data captured mid-Dry season has been used to successfully map primarily para grass (*Urochloa mutica*) on the central portion of the Magela Creek floodplain (Boyden et al. 2007).The study found that para grass typically displayed higher normalised difference vegetation index (NDVI) values than other vegetation types at that time of year, although NDVI variation within Para grass infestations was associated with variation in floodplain moisture.

1.6 GEOBIA

An issue associated with the use of HSR data, particularly for vegetation mapping, is that the pixels are typically much smaller than the objects that are to be mapped. To ensure the likelihood of greater mapping accuracy there needs to be some form of aggregation of pixels to reduce the within class spectral variability (Blaschke 2010). One potential means to address this issue is to apply a geographic object-based image analysis (GEOBIA) methodology to the imagery. GEOBIA combines image segmentation and spatial, spectral and geographic information along with analyst experience with image-objects in order to model geographic entities (Blaschke & Hay 2001). In other words, GEOBIA involves the partitioning of remotely sensed imagery into meaningful image-objects, and analysing their characteristics through spatial, spectral and temporal scales. The requisites for GEOBIA are image segmentation, the attribution and classification of objects, and the ability to query and link individual objects based upon their spectral, spatial and temporal features (Hay & Castilla 2008).

Image pixels are cells within an arbitrary grid (Hay et al. 2005) whose ground resolution is determined in earth observation by the resolution of the particular sensor. Subsequently, pixels bear little resemblance to real world features (Fisher 1997, Cracknell 1998). Pixels within medium to low resolution imagery (e.g. Landsat with a 30 m GSD) may contain combined or integrated signals from a number of land cover features, whereas pixels within a high resolution image will more closely approximate these features or their components (Hay et al. 2003). In addition, as the spatial resolution of imagery increases (or the GSD decreases) so does heterogeneity (or spectral within-field variability). This is particularly evident within recently commercially available high spatial resolution (HSR) imagery (such as WorldView-2) with a GSD of less than 5 metres (Wulder et al. 2004).

Pixel-based classifiers (such as the Maximum Likelihood and Nearest Neighbour classification algorithms) rely purely on the spectral values of the pixels and do not consider the spatial characteristics inherent in an image (Blaschke & Strobl 2001). By not considering the spatial context of the features represented in remotely sensed data within the classification process, the misclassification of pixels within a particular land cover can occur providing ‘noise’ or a ‘salt and pepper’ effect (Willhauck et al. 2000). Methods used to minimise this effect usually involve the reduction of the spatial complexity or heterogeneity of an image either by using some form of low pass filtering before or after the classification, the manual editing of the classification within a GIS, or by grouping pixels into regions or objects displaying homogeneous characteristics (image segmentation) prior to the classification. The latter method is the basis for GEOBIA which is increasingly the preferred image analysis method for classifying HSR data and the associated increase of spectral variability within land covers (Blaschke 2010).

GEOBIA methodologies have been used successfully for a number of vegetation classification studies including deriving land cover classes for tropical savanna from MSR data (Whiteside et al 2011), forest delineation and tree crown extraction from very high spatial resolution hyperspectral data (Bunting & Lucas 2006) and mapping the biophysical parameters of riparian vegetation from HSR imagery (Johansen et al. 2008) and LiDAR (Johansen et al. 2010). Given the in-field spectral variability of HSR imagery (such as WorldView-2 data) and the fine detail vegetation variation shown in northern Australian floodplains, GEOBIA as a method is well suited for classifying the vegetation of the Magela Creek floodplain.

1.7 Outline of the report

This section (section 1) of the report has provided the definition, focus, aims and objectives of the report as well as background information regarding the application of remote sensing for mapping of wetland vegetation. Section 2 of this report describes the study site and its biophysical characteristics. Section 3 of this report describes the methods including the data sets used and their acquisition, the pre-processing of the data, and the analysis of the data to create the classified map. Section 3 also includes the data and method used to assess the accuracy of the classification. Section 4 describes the results of the analysis including the vegetation map for the Magela Creek floodplain and the description of the classes as well as the results of the accuracy assessment of the classification. Section 5 is a discussion of the results, implications of the uncertainty based on the accuracy assessment and the advantages and limitations of the data used and the application of the GEOBIA methodology.

2 Study site

The Magela Creek sub-catchment is located on the boundary between Kakadu National Park and western Arnhem Land, in the Alligator Rivers Region (ARR) of Australia's Northern Territory about 250 km east of Darwin (Figure 1.1). The 118.8 km long creek is a seasonally-flowing tributary of the East Alligator River, originating in the sandstone Arnhem Land plateau (Williams 1979). The creek has been classified into ten reaches (Saynor & Erskine 2013) which can be grouped into five distinct sections: the channels intersecting the escarpment (Reaches 1–7); the braided sandbed channels of the lowlands (adjacent to Ranger Uranium Mine) (Reach 8); the narrow Mudginberri Corridor (a series of billabongs and connecting channels) and the Magela Creek floodplain (consisting mostly of seasonally-inundated black-clay with a number of permanent billabongs) (Reach 9); and a single channel that flows into the East Alligator River (Reach 10). The corridor and floodplain sections are the focus of this report. The floodplain extent is approximately 220 km^2.

2.1 Landscape

The Magela Creek floodplain is typical of the low-relief sub-coastal Holocene floodplains that have formed along lower reaches of the region's rivers and are typically 3–4 m above AHD (Australian Height Datum) and 0.2 to 1.2 m above the maximum high tide level. Thus the floodplains of the region are potentially at risk of salt water intrusion resulting from future potential sea level rise that has been associated with climate change (Bartolo et al. 2008, Schaeffer et al. 2012). Soils of the floodplain typically consist of alluvial 'cracking clay' sediments belonging to the class Vertosols, as described by Isbell (1996).

2.2 Climate

The regional climate is tropical monsoonal with two distinct seasons, a shorter hot and humid Wet season (typically December - March) and a longer slightly cooler Dry season. From 36 years of recorded weather observations (www.bom.gov.au), the mean annual rainfall for Jabiru Airport is 1584 mm with nearly all rain occurring in the Wet season (Figure 2.1). The period January–March has the highest mean monthly rainfall with 354, 370 and 321 mm respectively for each month, whilst the mean monthly rainfall for November and December are 143 and 235 mm respectively. The mean maximum temperatures for Jabiru Airport range between 31.6–37.6ºC, with the hottest month being October and the coolest months, June–July (Figure 2.2). July has the lowest mean minimum temperature (18.5ºC) while the highest mean minimum (24.9ºC) occurs in November and December. While the floodplains in the region reliably receive an annual inundation, 95% of these areas are typically dry by the end of the dry season (Russell-Smith et al. 1995).

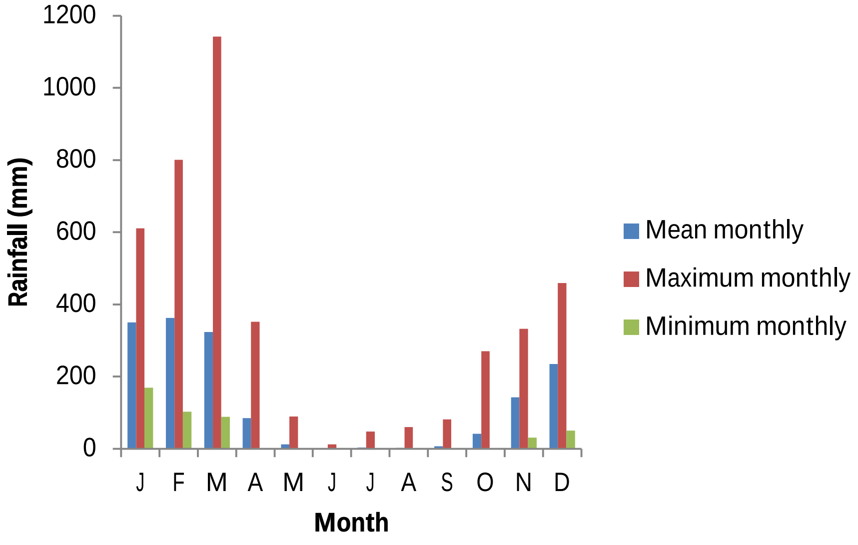

Figure 2.1 Mean, maximum and minimum monthly rainfall statistics for Jabiru Airport (1971–2013). Source: www.bom.gov.au

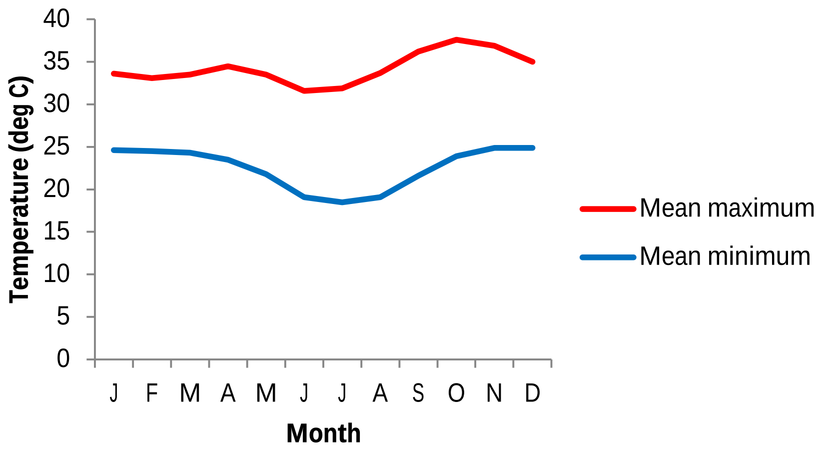

Figure 2.2 Mean maximum and mean minimum monthly temperatures for Jabiru Airport, 1971–2013. Source: www.bom.gov.au

2.3 Drivers of variability

The major drivers of variability of vegetation community distribution in the Magela Creek floodplain are identified as primarily the hydrological cycle (mostly the duration and period of inundation) (Finlayson et al. 1989) and to a lesser extent fire (Roberts 1997). The duration and period of inundation is linked to rainfall and discharge from the Magela Creek upstream.

2.3.1 Rainfall and discharge

The climate descriptors above in section 2.2, while giving an indication of the general patterns, tend to mask the variation in the timing and variation of the monsoonal activity (Finlayson 2005). Primarily, inundation of the large floodplains of northern Australia is determined by the onset of the monsoon, its duration and intensity, including the impact of individual low pressure systems within the monsoon (Wasson & Bayliss 2010). Figure

2.3 displays a generalised hydrological cycle for the Magela Creek floodplain. The dashed line on the diagram represents the variability that is present in the cycle predominant due to the annual variation in monsoonal activity.

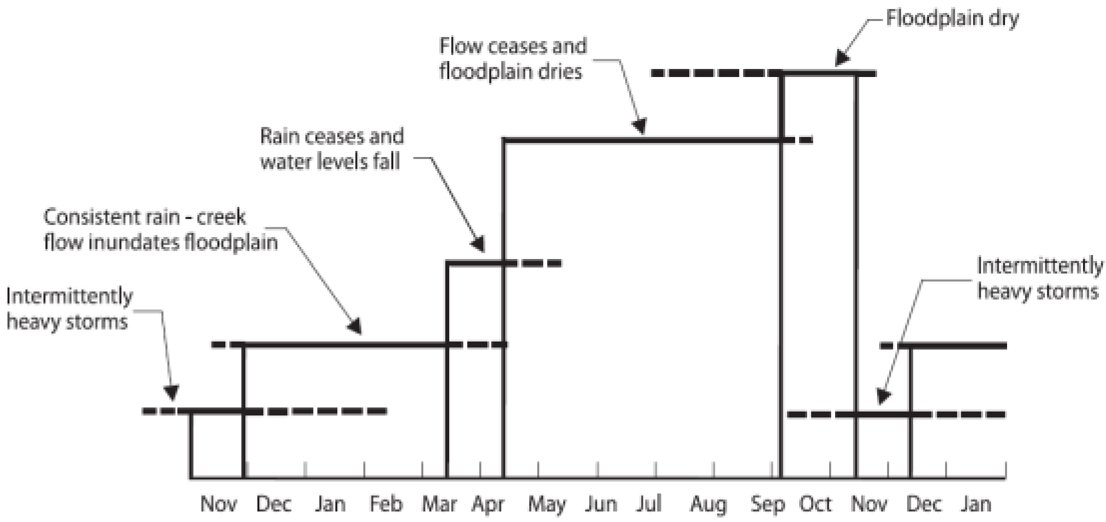

Figure 2.3 Generalised hydrological change on the Magela Creek floodplain. The dashed line represents variability. The diagram was adapted from Sanderson et al. (1983) by Finlayson et al. (1990).

Discharge in the Magela Creek is strongly influenced by El Nino Southern Oscillation (Wasson & Bayliss 2010) although other events such as cyclones also have an impact. Although the period of records is limited, rainfall and annual river flow for the Magela Creek have shown a decadal cycle of approximately 20 years (Wasson & Bayliss 2010). The maximum and minimum monthly rainfall bars in Figure 2.1 do indicate the potential for variability within rainfall in the region. The annual rainfall totals for Jabiru Airport for the period 1971–2012, while an incomplete record, show the interannual variation in rainfall (Figure 2.4). The discharge data recorded over 40 years (1971–2013) for the Magela Creek 009 gauging station (located upstream from the floodplain) also display the seasonal and interannual variability (Figure 2.5). Peak discharge is closely related to high rainfall events.

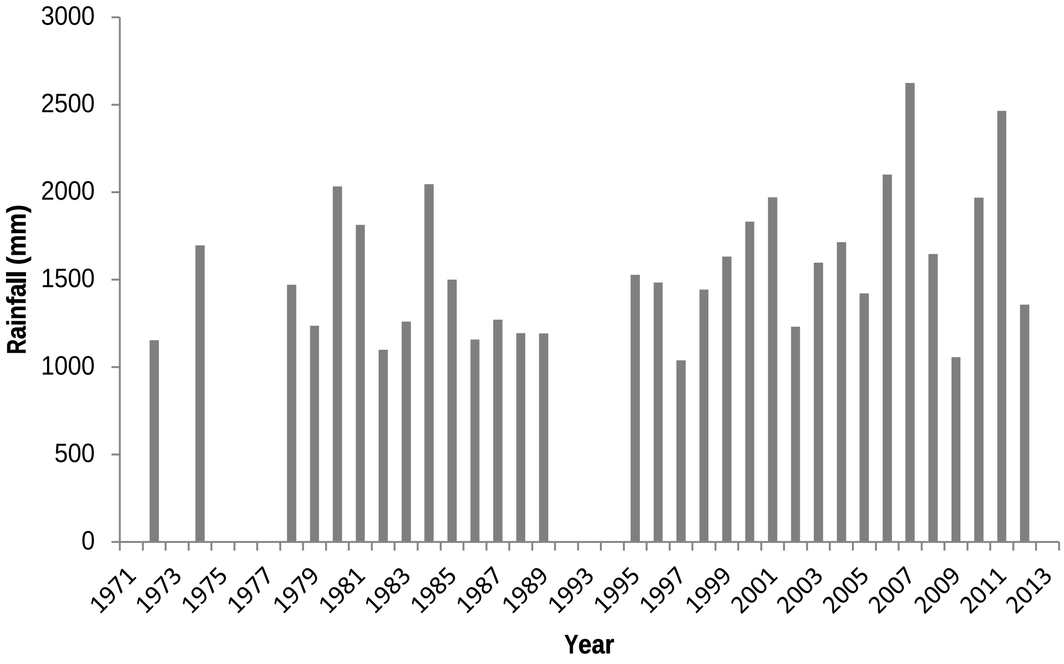

Figure 2.4 Annual total rainfall for Jabiru Airport, 1971–2012. Absent bar indicates that there are incomplete records for that year. Source: www.bom.gov.au

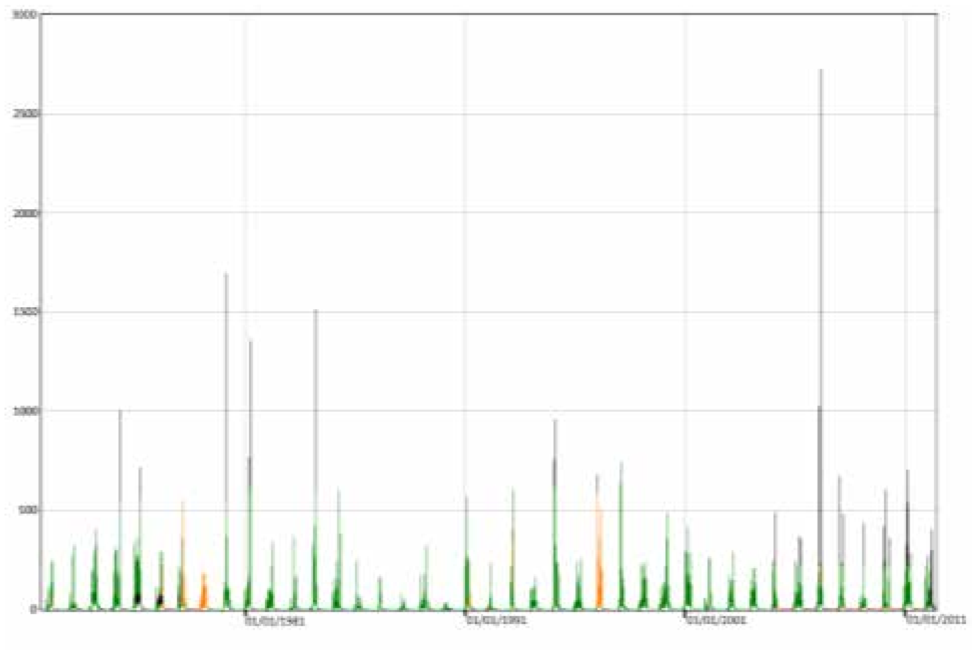

Figure 2.5 Hydrograph showing discharge rates (cubic metres per second) for the Magela Creek 009 gauging station for the period September 1971 to June 2013. Black records indicated good quality continuous data, dark green represents good quality edited data, and orange represents satisfactory quality data. Discharge Source: ***eriss***

2.3.2 Fire

Fire is seen as a major influence in the prevalent savanna vegetation communities of northern Australia (Andersen et al. 2003, Rossiter et al. 2003, Beringer et al. 2007) and modification of fire regimes affects the tree/grass balance within these ecosystems. Reductions in fire frequency and intensity tend to result in an increase in tree recruitment whereas increased fire frequencies and intensities favour the grass component of savanna by suppressing tree growth and establishment (Beringer et al. 2007). Within the floodplains, humic fires have been observed to have a detrimental impact (Williams 1984, Russell-Smith et al. 1995). Fire has also been shown to have an impact on woody species (*Melaleuca* spp.) within the floodplains of Kakadu National Park (Roberts 1997). Tree mortality is significantly higher in areas exposed to fire, with high fire intensity (as experienced in the late dry season) causing high levels of mortality (Roberts 1997). There has been little to no research of the impact of fire on the distribution of non-woody vegetation on the Magela floodplain.

The North Australia Fire Information website (www.firenorth.org.au) provides spatial data sets of fire frequency for northern Australia using fire scar mapping derived from multi-temporal satellite data. Figure 2.6a shows the fire frequency over the Magela Creek floodplain for the period 2000 to 2012. The map shows that most of the floodplain has been burnt in 6 years or less within the 13 years period which contrasts noticeably with the surrounding savanna landscape. Figure 2.6b shows the frequency of late fires (after 31st July) on the Magela Creek floodplain. Late fires can assumed as a surrogate for fire intensity. As can be seen from the map, most fires that do occur on the floodplain are not late fires.

Figure 2.6 Fire frequencies over the Magela Creek floodplain for the period 2000–2012 (a) and the frequency of late fires (fires after 31st July) for the same period (b). Source: www.firenorth.org.au

2.4 Vegetation

The vegetation on the Magela Creek floodplain consists of paperbark forests and woodlands, open perennial and annual swamps, billabongs and grass/sedge/herb fields. Williams (1979) identified 6 major vegetation communities related to water depth based on data collected from non-peak vegetative growth periods and consequently, according to Finlayson et al. (1989), failed to identify classes containing seasonal vegetation such as grass species, e.g. *Oryza* spp. In another study, peak Wet season herbaceous aquatic vegetation was mapped by Morley (1981) providing a classification consisting of 36 communities, which were further clustered together into 8 major classes (Sanderson et al. 1983). Eight key floodplain communities (Figure 2.7) have been identified by previous research and described based upon their dominant species (Story 1976, Finlayson et al. 1989). Descriptions of the major communites are in Appendix B.

Figure 2.7 Vegetation communities of the Magela Creek floodplain mapped by Finlayson et al. 1989.

3 Methods

3.1 Data sets and data acquisition

3.1.1 Multispectral data

The primary data set for this project consisted of three overlapping scenes of WorldView-2 (WV-2) multispectral data captured at approximately 1130 CST, 11 May 2010. The sensors onboard the WV-2 satellite capture data in 11-bit format. After geometric correction image pixels represent 2 m ground sample distance (GSD) at nadir. The multispectral data consist of 8 spectral bands (coastal, blue, green, yellow, red, red edge, NIR1, and NIR2). Also acquired was the WV-2 panchromatic imagery for the region. Data in the panchromatic band has a GSD of 0.5 m after geometric correction. Wavelength characteristics for each band are displayed in Table 3.1. A detailed description of the sensor and data characteristics may be found in (Updike & Comp 2010).

Table 3.1 Spectral bands of the WorldView-2 sensor.

Spectral band	Wavelength centre (nm)	Wavelength min - max (nm)
Coastal	427	400 - 450
Blue	478	450 - 510
Green	546	510 - 580
Yellow	608	585 - 625
Red	659	630 - 690
Red edge	724	705 - 745
Near infrared 1 (NIR1)	831	770 - 895
Near infrared 2 (NIR2)	908	860 - 1040
Panchromatic	630	450 - 800

A feature that distinguishes WV-2 data from other HSR multispectral satellite data is the inclusion of coastal (400–450 nm), yellow (585–625) and red edge (705–745 nm) bands. Of these bands, the one with most potential for this project is the red edge band, which is optimised for the spectral characterisation of chlorophyll and water content in vegetation biomass, thus the band is useful for detecting vegetation under stress (Clevers et al. 2002). Filella and Penuelas (1994) found a high correlation between the wavelength of the red edge peak and chlorophyll content.

The imagery acquired covered approximately 730 km^2 of the Magela Creek -catchment including the 225 km^2 of the Magela floodplain (Figure 3.1). As the requested area for data capture exceeded the maximum swath width of the WorldView-2 satellite, three images were acquired during the satellite overpass. Table 2.3 lists the scene parameters for each image. There is approximately a 1 km^2 and 40 km^2 overlap between the imagery covering Regions 1and 2, and Regions 2 and 3, respectively. All imagery was supplied in a format suitable for scientific analysis (with no radiometric or geometric enhancements) and according to the specifications detailed in Appendix B of Whiteside et al. (2013).

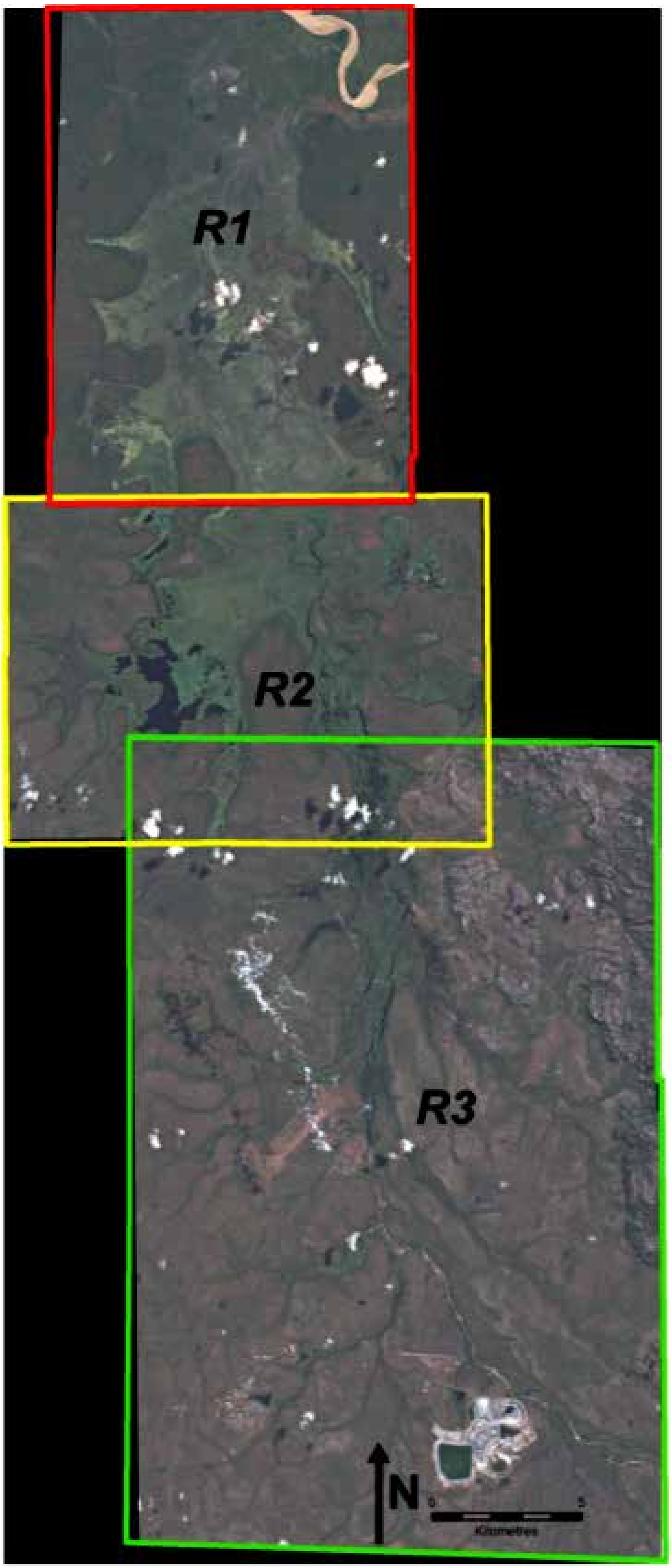

Figure 3.1 WorldView-2 images captured on 11 May 2010. Red polygon is the extent of Region 1 (R1), yellow polygon is boundary of region 2 (R2) and green polygon is extent of Region 3 (R3).

Table 3.2 Summary of the specifications for the three WorldView-2 images acquired for this study.

11 May 2010	Region 1	Region 2	Region 3
Time of capture	11:15:19 CST	11:14:28 CST	11:14:41 CST
Scene centre	12° 19' 26.28" S 132° 50' 7.23" E	12° 26' 56.68" S 132° 50' 19.5" E	12° 32' 21.55" S 132° 53' 6.92" E
Mean off-nadir view angle	19.2°	18.3°	16.5°
Mean satellite azimuth	237.2°	323.2°	311.2°
Mean satellite elevation	68.4°	69.3°	71.3°
Area covered	196 km^2	183 km^2	479 km^2
Proportional cloud cover	0.012	0.009	0.014

The Region 1 image had a noticeable difference in mean satellite azimuth to Regions 2 and 3 (Figure 3.2). As a result there was visible sun glint from patches of water in Region 1, where this is not evident in Regions 2 and 3 (Figure 3.3). Sun glint is the specular reflection of directly transmitted sunlight from the water surface and occurs in imagery when the water surface orientation is such that the sun is directly reflected towards the sensor (Kay et al. 2009). The result of sun glint is an increase in reflected radiance by a factor of 2 or more (Kay et al. 2009), and in extreme cases the saturation of the sensor, making retrieval of information very difficult. Methods for correcting for sun glint in HSR data are based on algorithms that do not account for surface vegetation (Kay et al. 2009) and as such would not function in a wetland scenario.

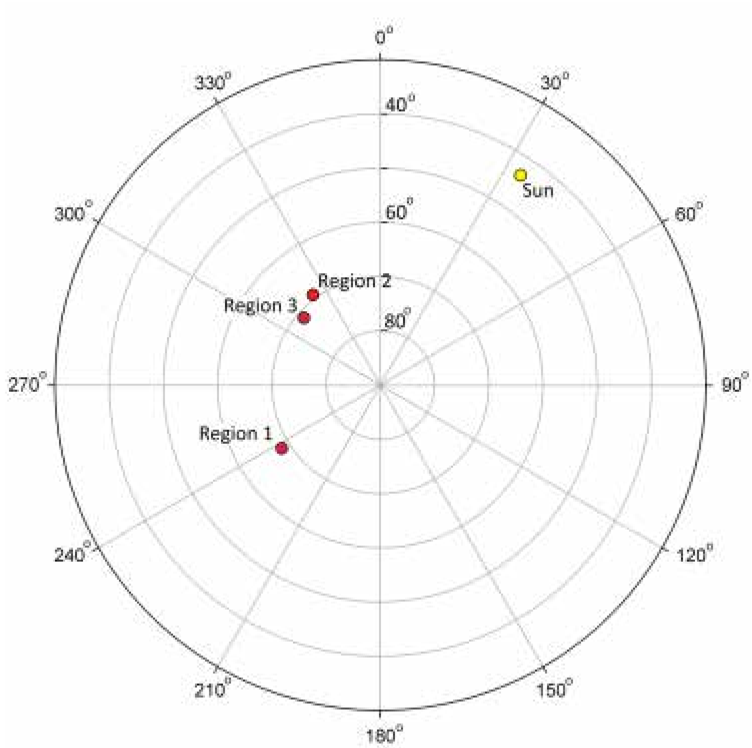

Figure 3.2 The position of the WV-2 satellite relative to the sun during image capture over the Magela Creek floodplain, 11 May 2010. The position of the red circles represents the mean azimuth (angle) and elevation (radial) of the satellite for each of the images. The yellow circle represents the solar azimuth and elevation at the time of image capture.

Figure 3.3 A subsample of the radiometrically calibrated imagery showing the effect of sun glint on Region 1 (upper) compared to Region 2 (lower).

3.2 Ancillary data

3.2.1 Digital elevation models

The following ancillary data were incorporated into the project to aid in delineating the floodplain/uplands boundary and in masking out non-target land covers such as savanna and escarpment outliers. Terrain information in the form of two digital elevation models (DEMs) was included. The first DEM was Geoscience Australia's 1 Second Digital Elevation Model Version 1.0 derived from the Shuttle Radar Topography Mission (SRTM) (Figure 3.4a). The DEM, based on the SRTM data captured in 2000, has a horizontal spatial resolution of 30 m and was incorporated to enable the delineation the floodplain boundary. A finer 10 m horizontal resolution DEM derived from a 2004 aerial photograph survey of KNP was included for the purpose of delineating the upper reaches of the floodplain that were not well defined in the SRTM DEM (Figure 3.4b). Both DEMs fully covered the spatial extent of the study area. The incorporation of terrain information has been shown to improve vegetation classification involving HSR imagery (Devhari & Heck 2009, Whiteside et al. 2011).

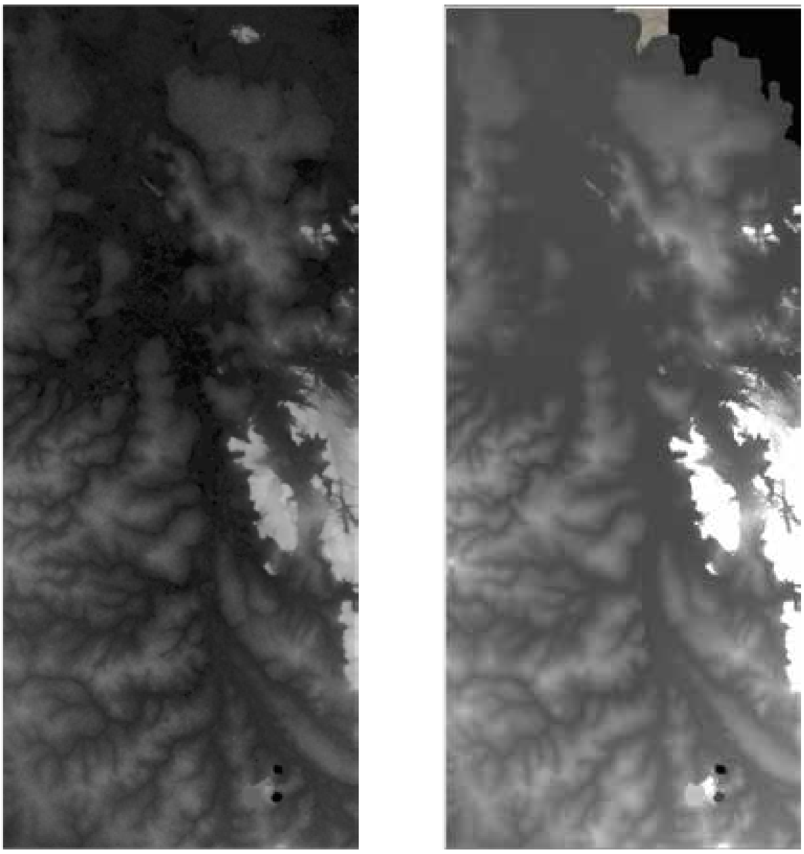

(a) (b)

Figure 3.4 DEMs of the Magela Creek floodplain region. (a) the 30 m SRTM based DEM and (b) is the 10 m DEM derived from 2004 aerial photography.

3.2.2 Canopy height model

A canopy height model (CHM) was incorporated with the intent to differentiate between treed land cover and spectrally similar but non-treed land cover (Figure 3.5a). The CHM was derived from a LiDAR capture conducted within KNP between 22 October and 16 November 2011. A Leica ALS60 laser scanner was used to collect the discrete multiple return data. The horizontal and vertical accuracy of the data were 0.8 m and 0.3 m, respectively. The average point spacing was 2 m^{-2}; the laser beam footprint was 0.32 m, and the flying height was 1409 AGL. A CHM is calculated by subtracting the bare earth model or DEM from the LiDAR data from the digital surface model (DSM) (Figure 3.5b). The DEM is derived from last returns which are assumed to have hit the ground (Figure 3.6). The DSM is derived from first returns which are assumed to hit the top of vegetation. The derived CHM has a resolution of 2 m GSD.

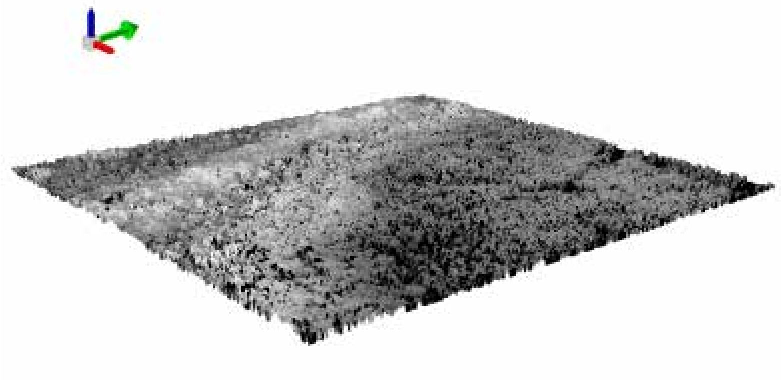

(a)

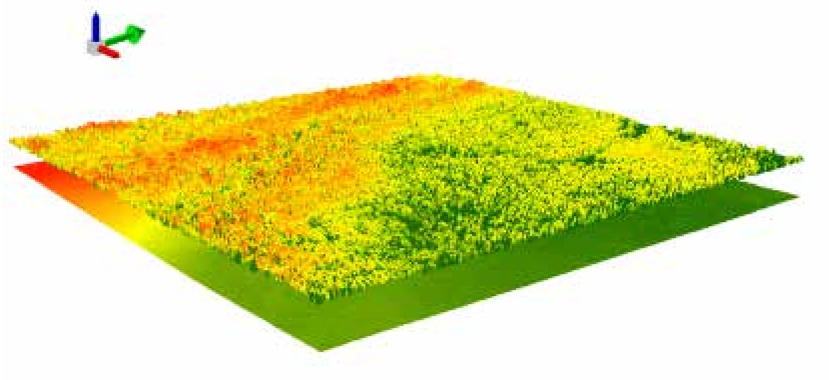

(b)

Figure 3.5 A heavily treed tile from the (a) CHM and (b) the DSM draped over the DEM.

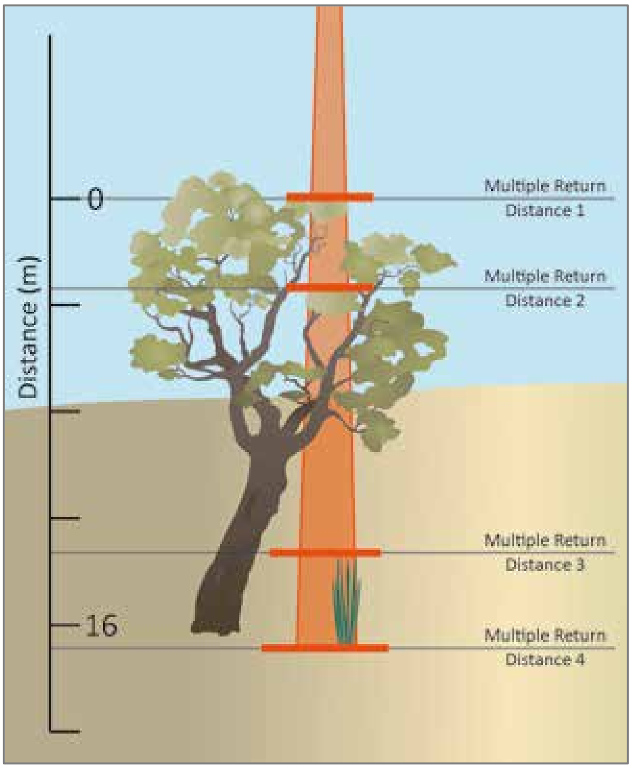

Figure 3.6 Returns for discrete LiDAR. Distance 1 is the first return and distance 4 is the last return.

3.3 Image pre-processing and analysis

The steps within the image analysis approach used to produce the Magela Creek floodplain vegetation map are shown in Figure 3.7. Section 3.3.1 summarises the pre-processing steps, section 0 describes the image analysis steps, section 3.5.1 describes the reference data used for accuracy assessment, while section 3.5.2 describes the accuracy assessment methods.

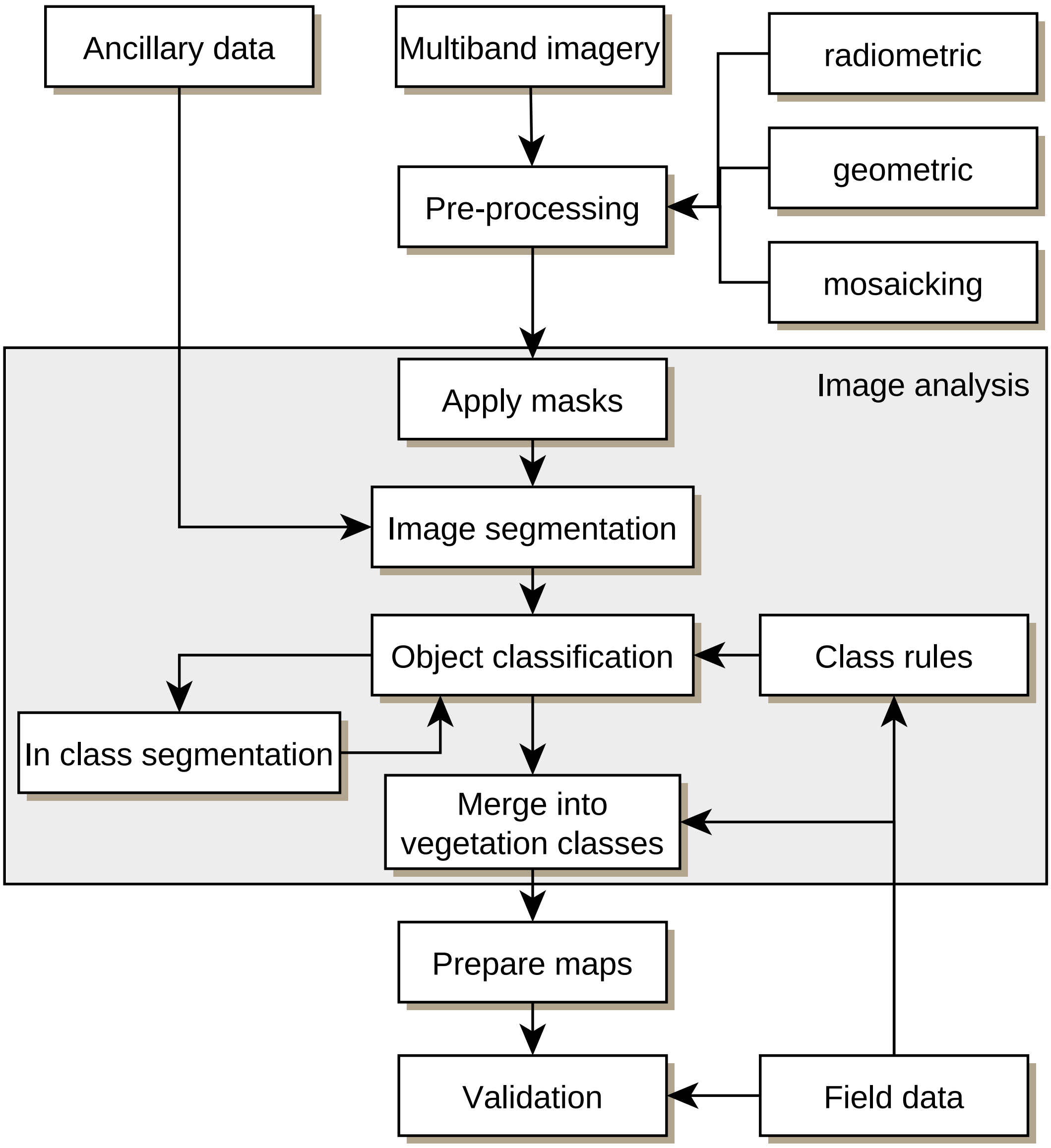

Figure 3.7 The image analysis approach used for wetland vegetation mapping.

3.3.1 Pre-processing

Pre-processing of the data was undertaken to geometrically and radiometrically correct the imagery to characterise the floodplain and involved three steps: geometric rectification, radiometric calibration and mosaicking of the three images. Details of the procedures for both the geometric and radiometric correction of this imagery are described in detail in Whiteside et al. (2013) and summarised in sections 3.3.2 and 3.3.3.

3.3.2 Geometric rectification

All imagery were geometrically orthorectified using the sensor's rational polynomial coefficients (RPCs) and ground control points (GCPs) based on easily identifiable tarpaulins place throughout the scene with locations recorded using a differential GPS. The surface model for the orthorectification was the SRTM DEM data set. Accuracy assessment of the rectification was based on 6 independent GCPs with the mean RMSE 1.82 m (Staben et al. 2012, Whiteside et al. 2013).

3.3.3 Radiometric correction

Radiometric correction of the imagery involved converting the 11-bit digital numbers (DNs) recorded directly by the sensor to floating point surface reflectance. First, the at-sensor DNs were converted to top-of-atmosphere spectral radiance (L_{TOA}) using the following equation (1):

$$L_{TOA} = \frac{K_{Band} Q_{Pixel,Band}}{\Delta_{\lambda,Band}}, \quad (1)$$

where L_{TOA} represents the top-of-atmosphere spectral radiance image pixels in a given band, K_{Band} is the absolute radiometric calibration factor for a given band, $Q_{Pixel,Band}$ is the radiometrically corrected image pixel (DN), and $\Delta_{\lambda,Band}$ is the effective bandwidth for a given band at wavelength, λ (Updike & Comp 2010). Both K_{Band} and $\Delta_{\lambda,Band}$ are obtained from the metadata supplied with imagery. The L_{TOA} images were then converted to surface reflectance (P_s) using the physics-based Fast Line-of-sight Atmospheric Adjustment using Spectral Hypercubes (FLAASH) atmospheric correction algorithm (Adler-Golden et al. 1999). The FLAASH algorithm, which is available as a module within ENVI image analysis software, utilises sensor orientation data and the MODTRAN5 radiative transfer model (Berk et al. 2006). Reflectance was scaled by a factor of 10000 to reduce processing time.

3.3.4 Image mosaic

Prior to creating a mosaic of the three reflectance images, null pixels (edge pixels that are not part of the imagery) were converted from the value 0 to -1500. If the default value of 0 for null pixels was kept pixels within the reflectance images with an actual value of 0 in some bands (some pixels within water and shadows) would result in null sections within the image during the mosaic process. A mosaic was firstly created from the region 2 and 3 images. The region 2 image was colour adjusted to the fixed Region 3 values using statistics from the overlapping areas in the regions and resampled using the Nearest Neighbour algorithm. Region 1 was then added to the Region 2 and 3 mosaic by colour adjusting Region 1 to the fixed mosaic of Region 2 and 3. Any null pixels in the final mosaic of all three images were given the value -1500 making it easy to eliminate these pixels from the analysis.

3.4 Image analysis and classification

A GEOBIA approach was used to analyse and classify the WV-2 imagery. GEOBIA is typically a stepwise process involving a series of rules that implement segmentation, reshaping and classification algorithms. These rules establish and operate within a series of object and classification hierarchies (Figure 3.8).

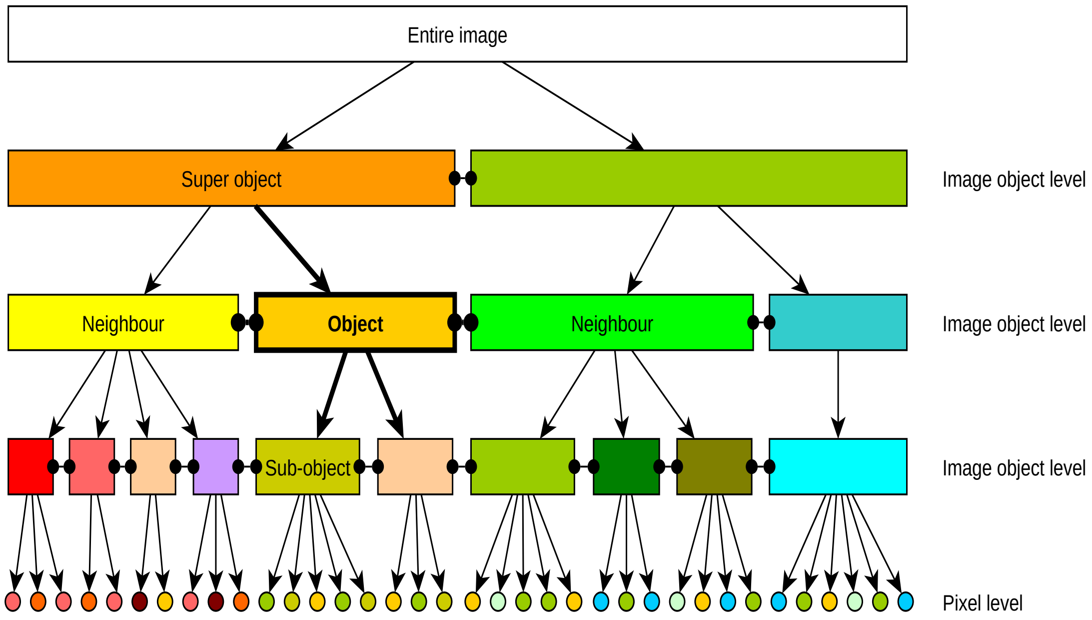

Figure 3.8 Image object hierarchy. Each object is topologically linked to its neighbours, its super object and its sub objects.

For this project, the GEOBIA rule set was created using the eCognition software package. Figure 3.9 shows the project set up dialogue where the image data, thematic layers and extent are selected.

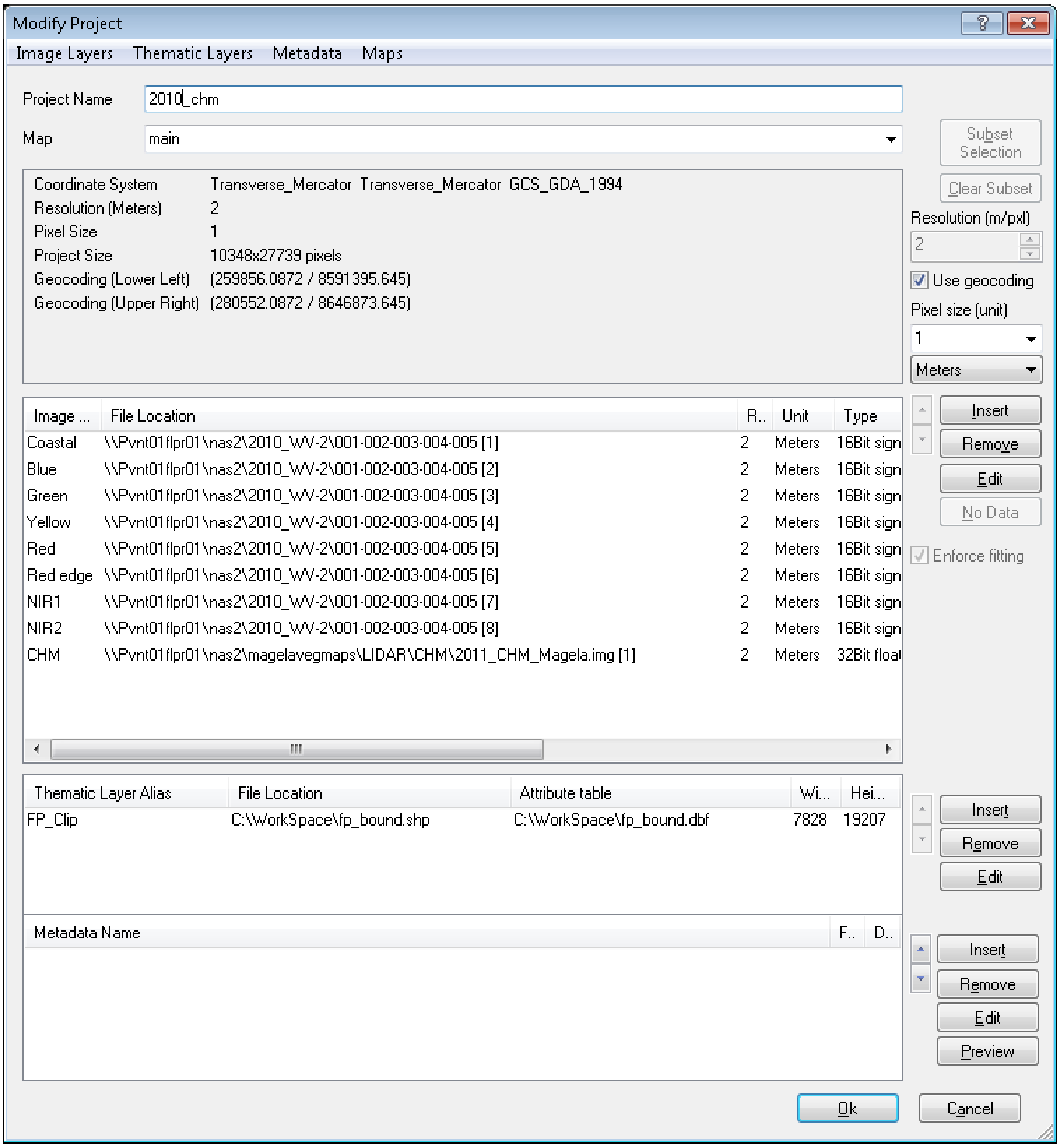

Figure 3.9 The Open/Modify project dialogue within the eCognition software.

3.4.1 Masks

Prior to any discrimination of the vegetation within the floodplain, a series of masks were applied to the mosaic to exclude regions of non-interest from the analysis (Figure 3.10). This was done to reduce unnecessary analysis involving non-relevant regions and redundant processing steps.

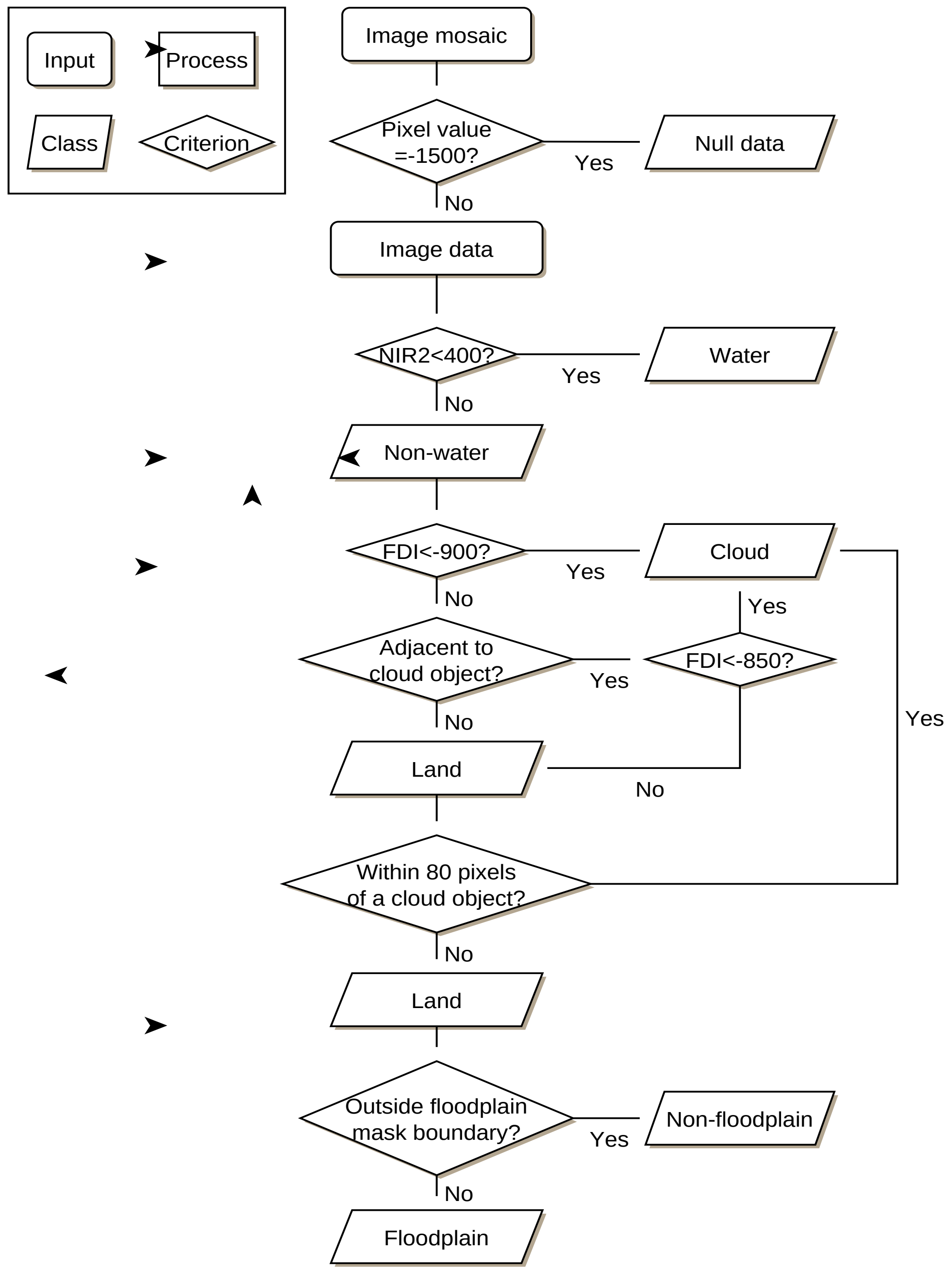

Figure 3.10 Flow diagram for the application of masks upon the WV-2 and ancillary data. FDI is Forest Discrimination Index (Bunting & Lucas 2006).

3.4.2 Masking out of non-image pixels

When setting up the project in eCognition, a null data value can be assigned by clicking the No Data button seen in the Open Project dialogue (Figure 3.9) to eliminate null data pixels from the analysis. In this case, -1500 was used as the value for null data pixels as assigned during the creation of the mosaic (Figure 3.11).

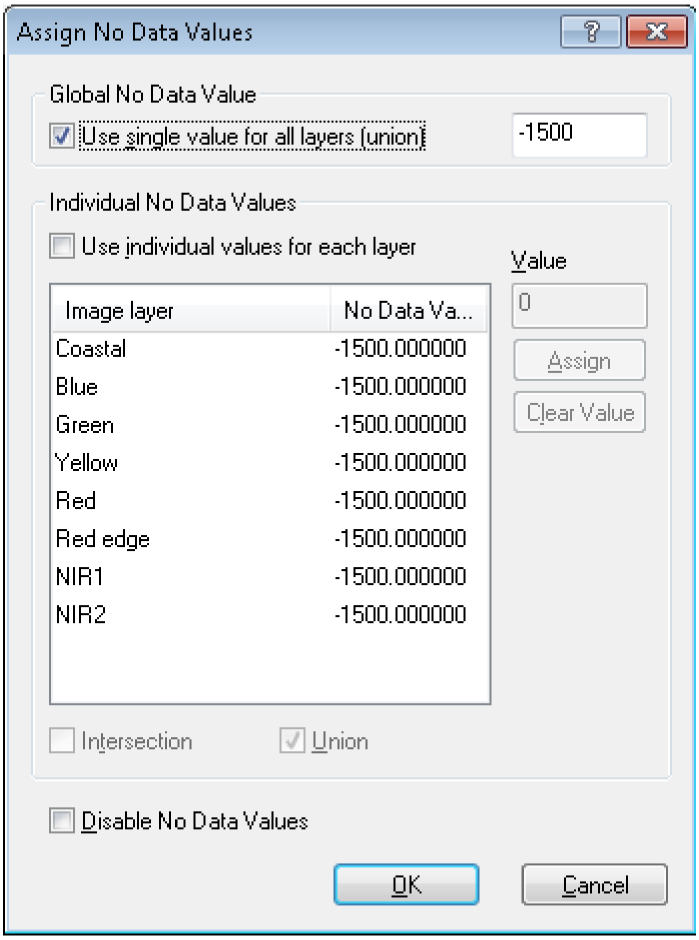

Figure 3.11 The Assign No Data Values dialogue enabled the elimination of null data from the analysis.

3.4.3 Water mask

The NIR1 band (770–895 nm) displays low reflectance values over water bodies. Therefore, it was possible to delineate open water from the image mosaic by utilising a threshold based on the NIR1 band as well as a reshaping routine (Figure 3.12). The process involved creating seed objects for the water class using the multi-threshold segmentation algorithm that splits the image into objects belonging to two or more classes based on pixel values above or below the user-defined thresholds (Trimble 2012). In this instance, water seed objects were created for Regions 2 and 3 from pixels below the threshold value of 400 for the NIR1 band. The threshold for Region 1 was 200. The reshaping routine involved the growing of the seed objects into neighbouring pixels to ensure surface water was sufficiently covered by the objects and shrinking to smooth the boundaries of the objects (Figure 3.13).

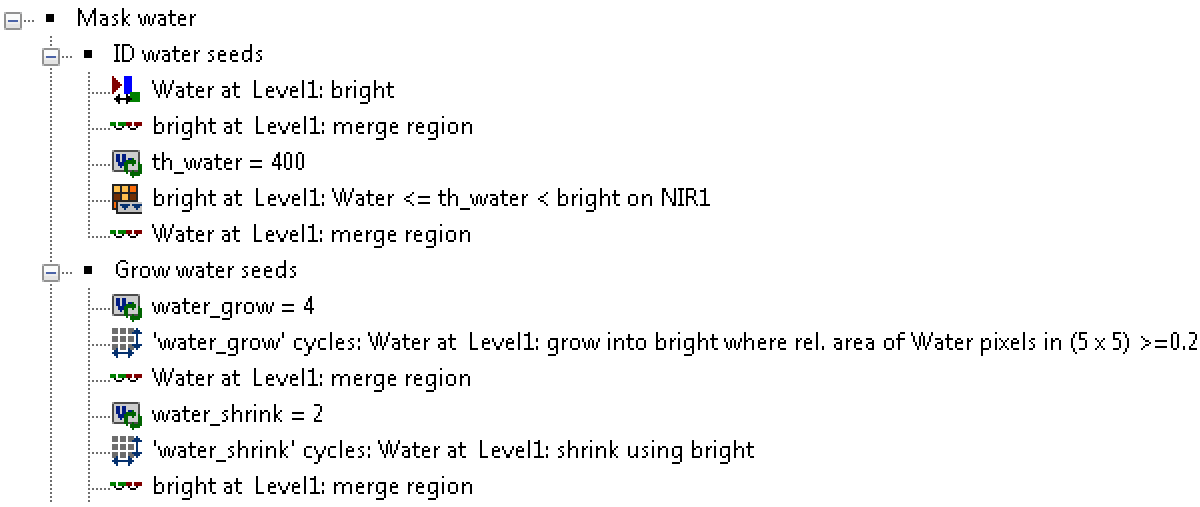

Figure 3.12 Water mask ruleset for Regions 2 and 3.

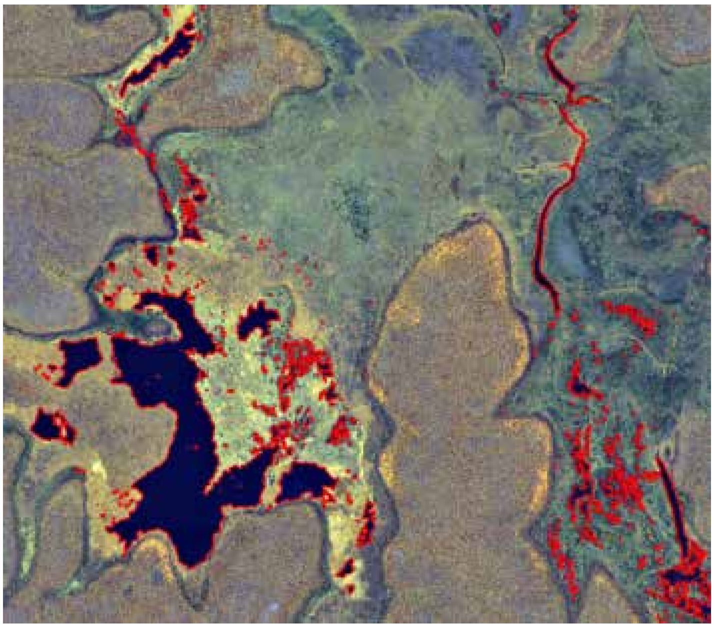

Figure 3.13 Water objects (outlined in red) created as a result of the water mask.

3.4.4 Cloud masks

The Forest Discrimination Index (FDI), a spectral index developed by Bunting and Lucas (2006), was used as a basis to delineate clouds (Equation 5):

$$FDI = NIR2 - (RE + Blue) \qquad (2)$$

where *NIR2*, *RE* and *Blue* are the near infrared 2 (860–1040 nm), red edge (705–745 nm) and blue (450–510 nm) bands of the WV-2 imagery respectively. The index was useful for extracting clouds because although clouds have high values in the NIR2 and Red edge bands so does actively photosynthesising vegetation, and clouds also have high values for the Blue band as do highly reflective rocky outcrops. Thus by using FDI it is possible to readily differentiate clouds from other bright features in the landscape.

A mask to extract clouds based on this index was created using a chessboard segmentation creating a grid of square objects, containing 10 x 10 pixels, and assigning objects to the ‘Cloud’ class if their mean object FDI value was less than -900 (Figure 3.14). Adjacent 100 m^2 objects assigned to the ‘Cloud’ class were then merged to create ‘Cloud’ object seeds, and the boundaries of the ‘Cloud’ object seeds were then grown iteratively to subsume neighbouring pixels with FDI value less than -850 (Figure 3.15). The boundary of the ‘Cloud’ mask was then buffered (extended) by a distance of 80 pixels to ensure capturing as much cloud within the imagery as possible.

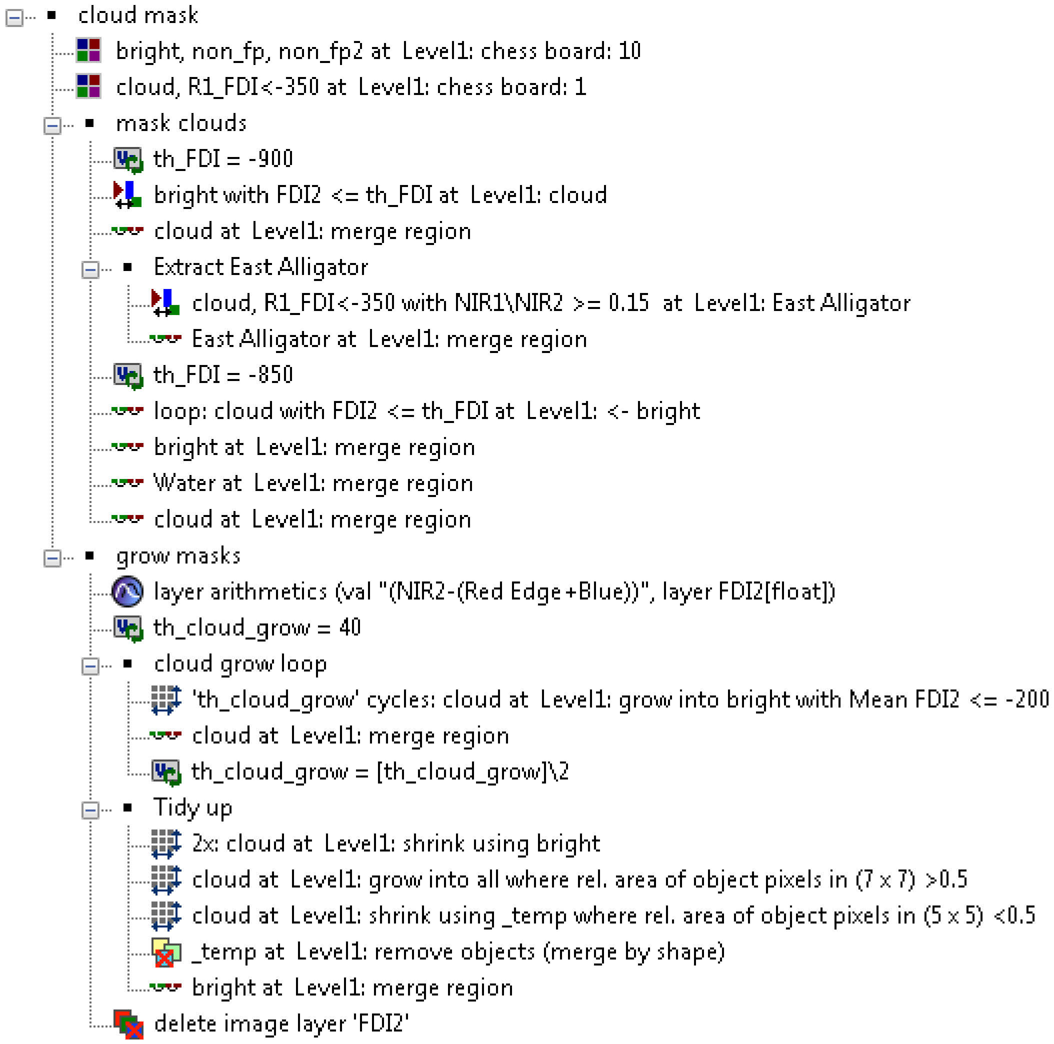

Figure 3.14 The cloud mask rule set.

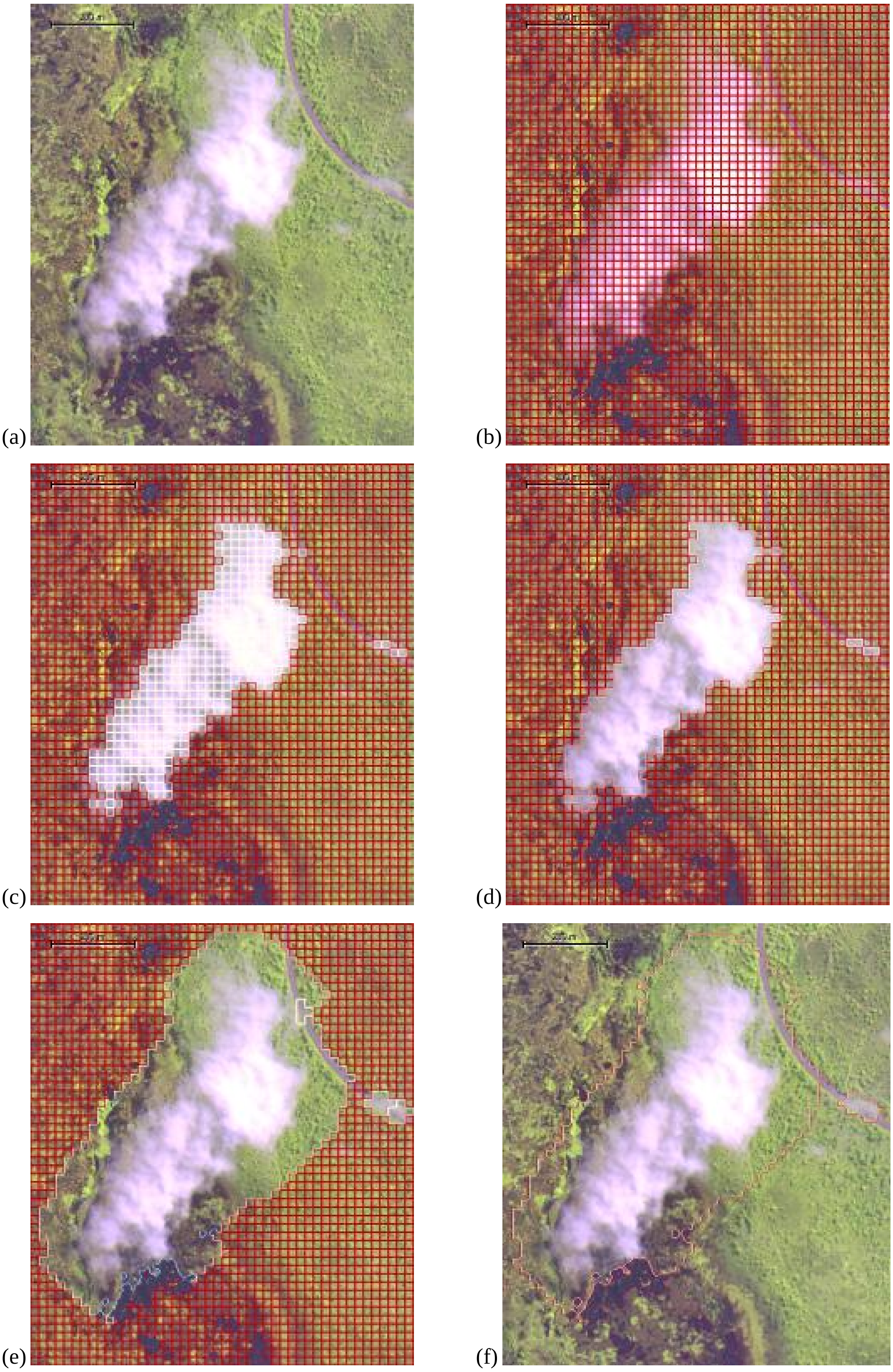

Figure 3.15 The cloud mask at work: (a) a cloud in the image, (b) the chessboard segmentation, (c) the initial cloud objects, (d) merged cloud objects, (e) buffered cloud objects, and (f) the final cloud objects.

The East Alligator River in the northern section of Region 1 was not detected by the water mask (Section 3.4.3) due to pixels representing the river showing high reflectance values in the bands that typically absorb clear water. This was most likely due to a combination of the sun and sensor angles associated with the image as well as high levels of suspended material and surface roughness in the (tidal) portion of the river. Consequently, with the FDI threshold used delineate cloud objects, the river was included in the ‘Cloud’ class. The river was able to be extracted from ‘Cloud’ objects using a NIR1 / NIR2 ratio threshold with the value for the East Alligator object being greater than 0.15.

3.4.5 Floodplain differentiation

After the various masks were applied, the next step involved partitioning the remaining imagery into floodplain and non-floodplain regions. Initially, the floodplain boundary was delineated using a height-based threshold based on digital elevation model (DEM) values. Two DEMs were trialled to evaluate their efficacy: version 1 of the Geoscience Australia DEM derived from the Shuttle Radar Topography Mission (SRTM) with 30 m pixels and a 10 m photogrammetry-derived DEM produced from a 2004 aerial photography capture of KNP.

A threshold height (z) value of 6 m based on the SRTM DEM was used to split the imagery into floodplain ($z < 6$ m) and non-floodplain ($z \geq 6$ m) super-objects. The lack of spatial detail in the coarser resolution DEM (30 m pixel) and potential mis-registration between the DEM and the WorldView-2 data appeared to affect the accuracy of delineating the floodplain boundary. This was particularly evident in the upper reaches of the floodplain (towards the southern extent of the imagery) where the boundary was poorly defined (Figure 3.16a). To attempt to compensate for this, the finer scale aerial photography based DEM (10 m pixel) was used for boundary delineation with the same threshold value. The boundary created by the aerial photography based DEM was better defined in the upper reaches but there were still issues with delineation further downstream (Figure 3.16b), where there was less accurate boundary delineation and a large area discarded in the northern section of the floodplain. Both DEMs displayed artefacts resulting from the influence of the flat terrain of the region (Figure 3.16c and d) and / or vegetation.

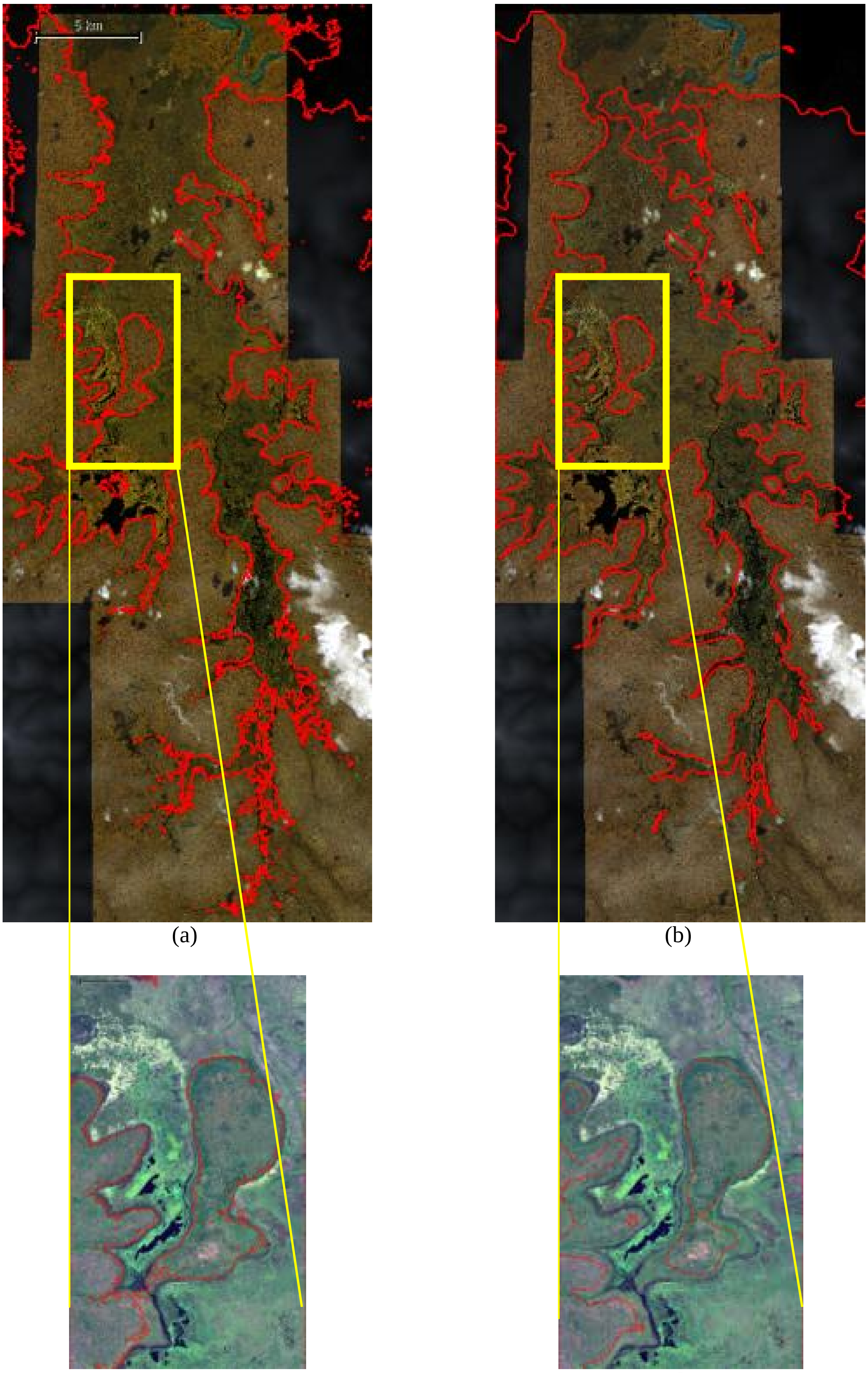

Figure 3.16 The issues associated with using a DEM-based height threshold to delineate the floodplain boundary. The boundary as delineated by a 6 m threshold based on the 30m SRTM DEM (a), the boundary as delineated by the same threshold based on the 10 m aerial photography DEM (a). Insets showing detail (c) and (d).

Using height thresholds, neither DEM was totally successful in providing a boundary that aligned with the observed floodplain boundary. However, by combining the objects derived from the 6 m threshold applied to both DEMs and using this as a boundary proxy. The outline was then manually adjusted within a GIS using visual interpretation of the WV-2 imagery to provide a more comprehensive and accurate floodplain boundary.

3.4.6 Floodplain analysis and classification

The floodplain portion of the imagery then underwent multiresolution segmentation (Benz et al. 2004) whereby the image was partitioned into homogeneous clusters of pixels or image-objects. The multiresolution segmentation algorithm is based on the fractal net evolution approach (FNEA) (Baatz & Schäpe 2000, Benz et al. 2004), whereby the segmentation of an image into image-objects is influenced by three parameters: scale, colour and form (Willhauck et al. 2000). The algorithm is primarily an iterative bottom-up segmentation method starting with individual pixels and merging these pixels based upon pixel heterogeneity and object shape and colour. These features are determined within the algorithm by two parameters; (a) colour versus form (homogeneity) and (b) scale (heterogeneity). The first parameter (a) within FNEA is the composition of homogeneity of the image objects (Figure 3.17). There are four criteria which define the relative homogeneity of image objects. These four criteria are grouped into two pairings: (i) colour versus shape and (ii) smoothness versus compactness. In the first pairing (i), the shape criterion is a measure of spatial homogeneity while the colour criterion refers to the spectral homogeneity. By assigning less emphasis to the shape criterion the contribution of the spectral values of image layers is increased. The shape criterion is influenced by the second pairing (ii). The smoothness criterion optimises image objects in relation to the smoothness of the borders whereas the compactness criterion optimises objects that are compact (Figure 3.18). The sum of the weightings for colour and shape combined equal one and the same applies for the sum of the weightings for smoothness and compactness. The second parameter (b) is the scale parameter (SP) which, although unit-less, determines the maximum allowable heterogeneity of pixels within objects, and hence the size of the objects resulting from segmentation. In addition each band within the image can be weighted to either increase or decrease that band's importance in the segmentation.

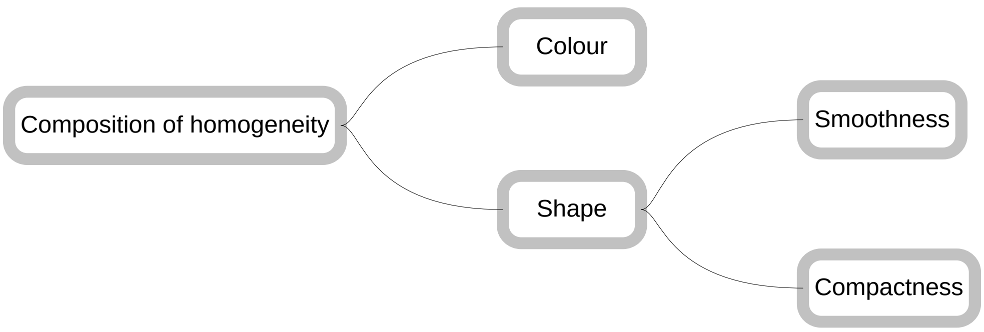

Figure 3.17 The four criteria that determine the composition of homogeneity parameter during an image segmentation (after Trimble 2012).

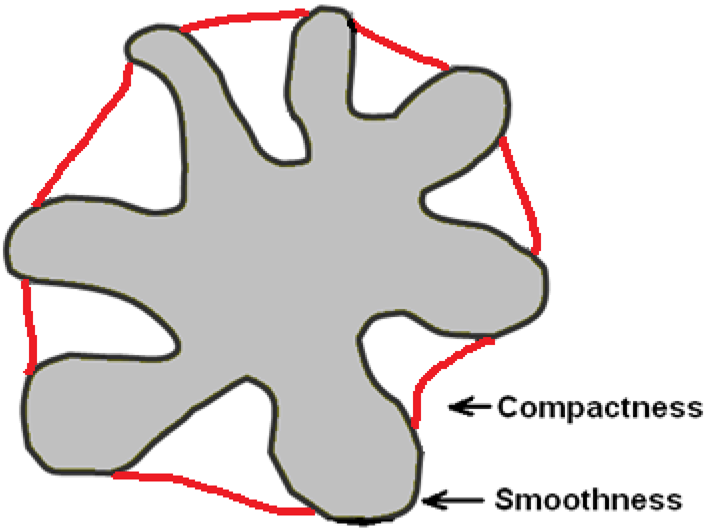

Figure 3.18 Diagram showing the effect on an object boundary of the weighting for smoothness versus compactness criterion. Increased weighting for smoothness provides optimised smooth borders (following the black border), whereas increased weighting for compactness optimises compact objects (i.e. following the red boundary).

3.4.7 Trees versus no trees

The LiDAR derived CHM was used to distinguish objects that contained trees from objects with no trees (Figure 3.19). The first step identified objects that were potential candidates containing trees (Figure 3.19 a and b). This was done by using a mean height threshold of 0.8 m. This threshold value assumed that objects with a mean height above the threshold potentially contained trees. Within these potentially treed objects, sub-objects representing trees or clusters were created using the threshold segmentation algorithm with trees assumed as being the areas within the CHM above 4 m (Figure 3.19c). Sub-objects with spurious high values were removed from the tree sub-objects class using 25 m as a ceiling value. Objects were eliminated from the potentially treed class if they contained no tree sub-objects. The remaining treed objects were then assigned to a tree class depending on the proportion of tree sub-objects per treed object: Open forest was greater than 50% proportional cover, Woodland 10–50% proportional cover, Open Woodland less than 10% proportional cover. These proportions are consistent with those described in the Australian Soil and Land Survey Field Handbook (Hnatiuk et al. 2009).

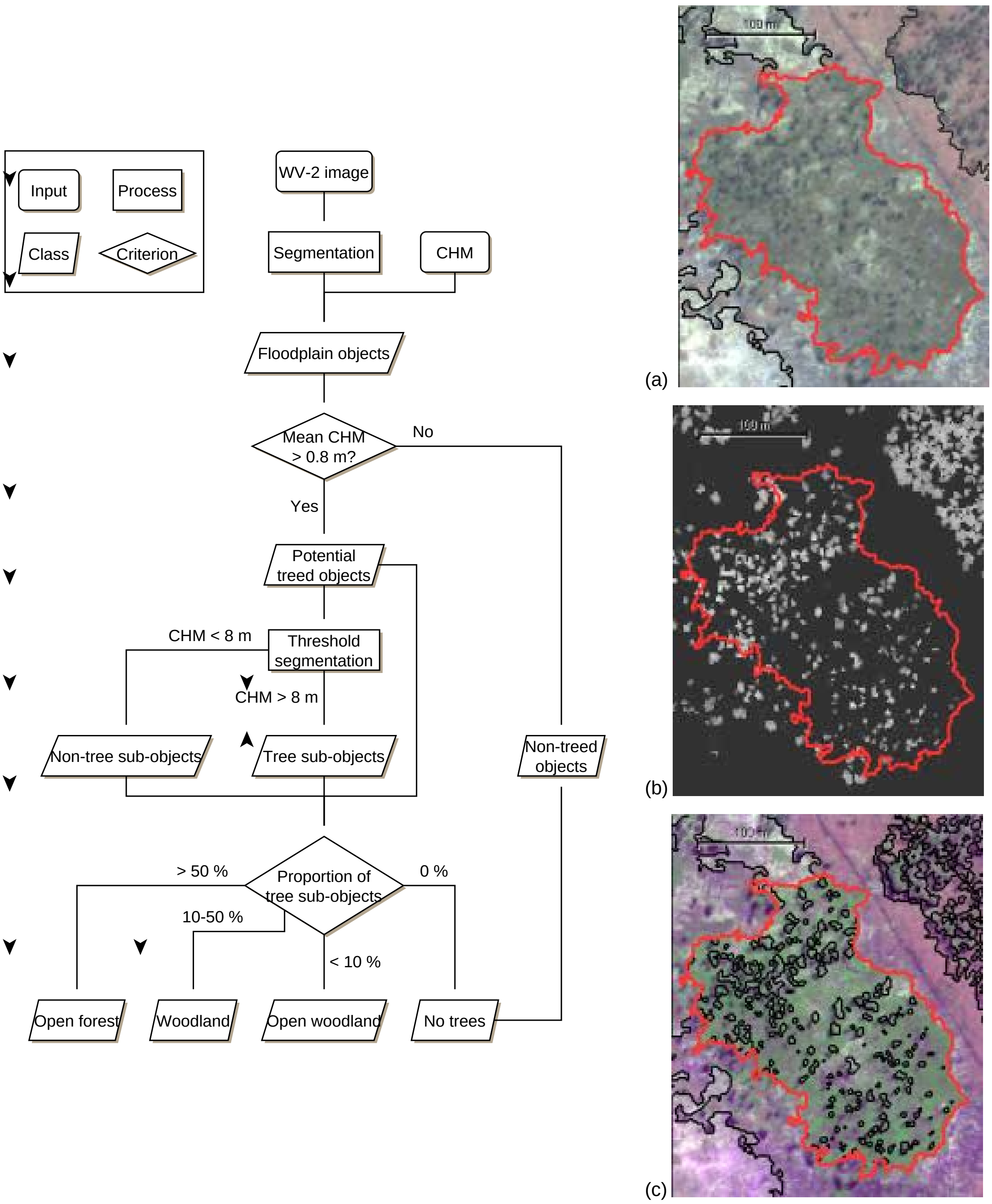

Figure 3.19 The flow diagram for creating treed classes (left) and its implementation (right). A potentially treed object (red polygon) (a), the CHM (b), and tree sub-objects (c).

3.4.8 Discriminating spectral cover classes within the floodplain

Four band ratios or indices were identified as being useful for class segregation and were used to segment and classify the objects within the image. The process involved a series of segmentations and classifications based on thresholds of band ratios that progressively discriminated vegetation classes within the floodplain regions. The band ratios used in this study included a version of FDI (Bunting & Lucas 2006) using NIR2, Red edge (RE) and Blue bands (Equation 5), an index created specifically for this project termed the Lily Index (LI) and the enhanced vegetation index EVI (Huete et al. 2002) using the NIR2 band (Equation 4). A normalised difference vegetation index (NDVI) (after Rouse et al. 1973) using the NIR2 band (Equation 3) was also used . The LI (Equation 6) derived its name from its ability, when initially formulated and applied to this imagery, to readily identify expanses of *Nelumbo nucifera*. Subsequently, the index was further found to readily distinguish between senescent vegetation and bare ground.

$$NDVI = \frac{NIR2 - Red}{NIR2 + Red} \tag{3}$$

$$EVI^{*} = \frac{G \times (NIR2 - Red)}{NIR2 + (C1 \times Red) + (C2 \times Blue) + L} \tag{4}$$

$$FDI = NIR2 - (RE + Blue) \tag{5}$$

$$LI = (NIR2 + RE) - Blue \tag{6}$$

where NIR2, B and R are the near infrared 2 (860 – 1040 nm), blue (450-510 nm) and red (625-690 nm) bands of the WV-2 data respectively. **G*=2.5, *C*1=6, *C*2=7.5 and *L*=1.

3.4.9 Delineating Region 1 vegetation classes

Due to the differing view angle for the Region 1 image (as described in section 3.1.1) and the increased reflective intensity from some surfaces (i.e. surface water), it was necessary to process Region 1 separately from Regions 2 and 3. Hence, a segment representing the Region 1 portion of the floodplain was separated from the other regions using a distance from pixel to bottom edge of image rule (Figure 3.20). The floodplain object was split so that Region 1 consisted of pixels that were of a distance greater than 17835 pixels from the bottom of the image.

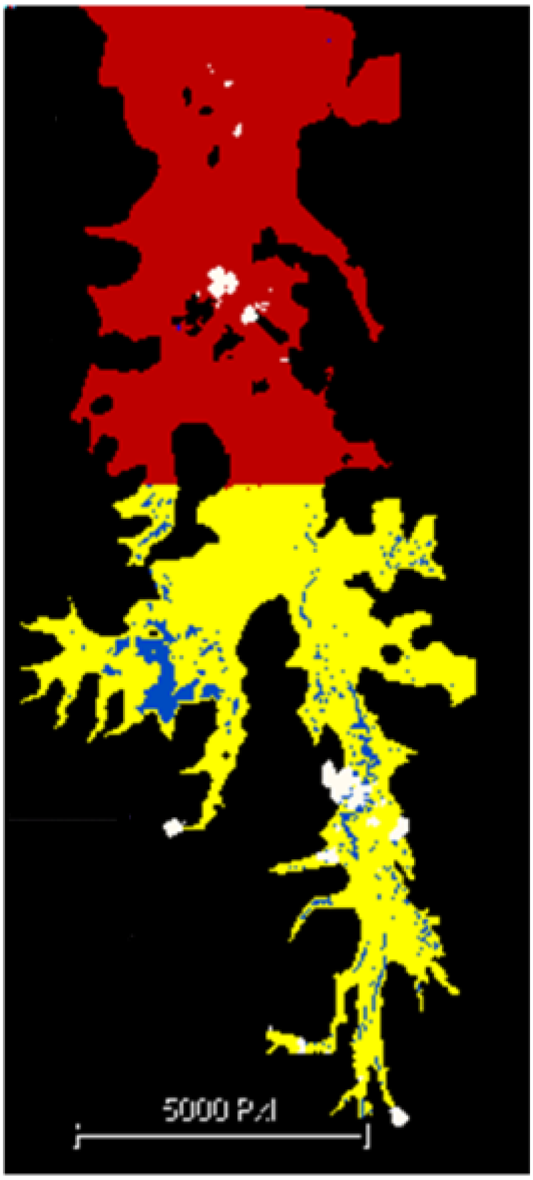

Figure 3.20 Masks applied to imagery. Red is region 1, yellow is regions 2 and 3. White is cloud, blue is water and black is either the non-floodplain landscape or cloud shadow.

Region 1 was then segmented with the multiresolution segmentation algorithm with the parameter values as listed in Table 3.3. These values were considered to be optimal (after an extensive visual trial and error assessment of a variety of parameter values) for segmenting the floodplain into objects displaying homogeneous vegetation community groups (Figure 3.21). After segmentation, the CHM process described in section 3.4.7 was applied to delineate the objects containing trees and create the three treed classes: Open woodland, Woodland and Open forest. Objects from the Open forest class were then assigned into either Melaleuca or Mangrove class objects using the following rule: distance to East Alligator River. This rule is based on the assumption that Mangroves are adjacent to the tidally influenced river

The remaining floodplain objects were subjected to a series of classification steps and some further finer segmentation. The steps formed a 'decision tree' with the end output being objects belonging to one of 29 classes (Figure 3.22). The threshold values at each step were determined through trial and error to be the best breaks in the continuous data for the classification of the floodplain vegetation. The first classification step assigned the initial floodplain objects to one of four categories based upon FDI threshold values (Figure 3.23). The class FDI<-350 contained of objects with mean FDI values less than -350, the class FDI<110 consisted of objects with mean FDI values between and including -350 and 109 (Figure 3.24). The class FDI<400 comprised of objects with mean FDI pixel values between and including 110 and 399. Segments within the class FDI≤1000 possessed mean FDI values from 400 up to and including 1000. Segments within the class FDI>1000 possessed mean FDI values greater than 1000.

Table 3.3 Parameters used for the multiresolution segmentation for Region 1.

Scale parameter	Shape criterion	Compactness	Layer weights
500	0.3	0.6	**Image layers**
			Coastal = 1
			Blue = 1
			Green = 1
			Yellow = 1
			Red = 1
			Red edge = 1
			NIR1 = 1
			NIR2 = 1
			CHM = 0
			Thematic layers
			Floodplain boundary = 0

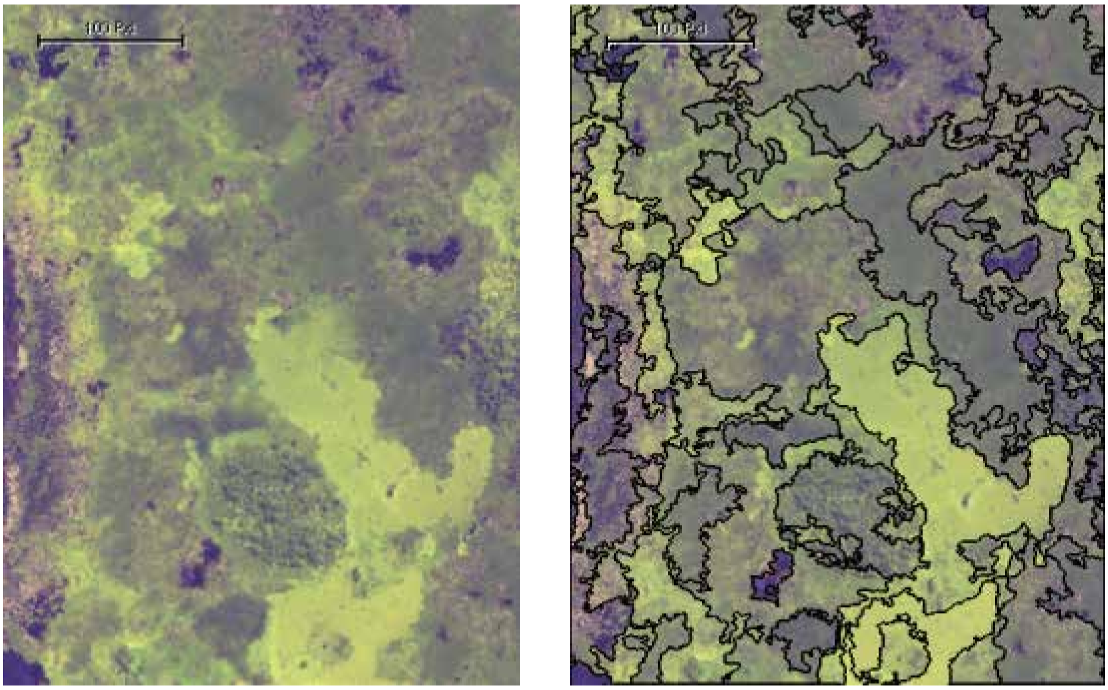

(a) (b)

Figure 3.21 A subset of the imagery show a portion of the Magela Creek floodplain within Region 1 (a), and showing the results of the initial image multiresolution segmentation (b). The segmentation algorithm used equal weights for all bands, a scale parameter of 500, a shape factor of 0.3, and compactness value of 0.6.

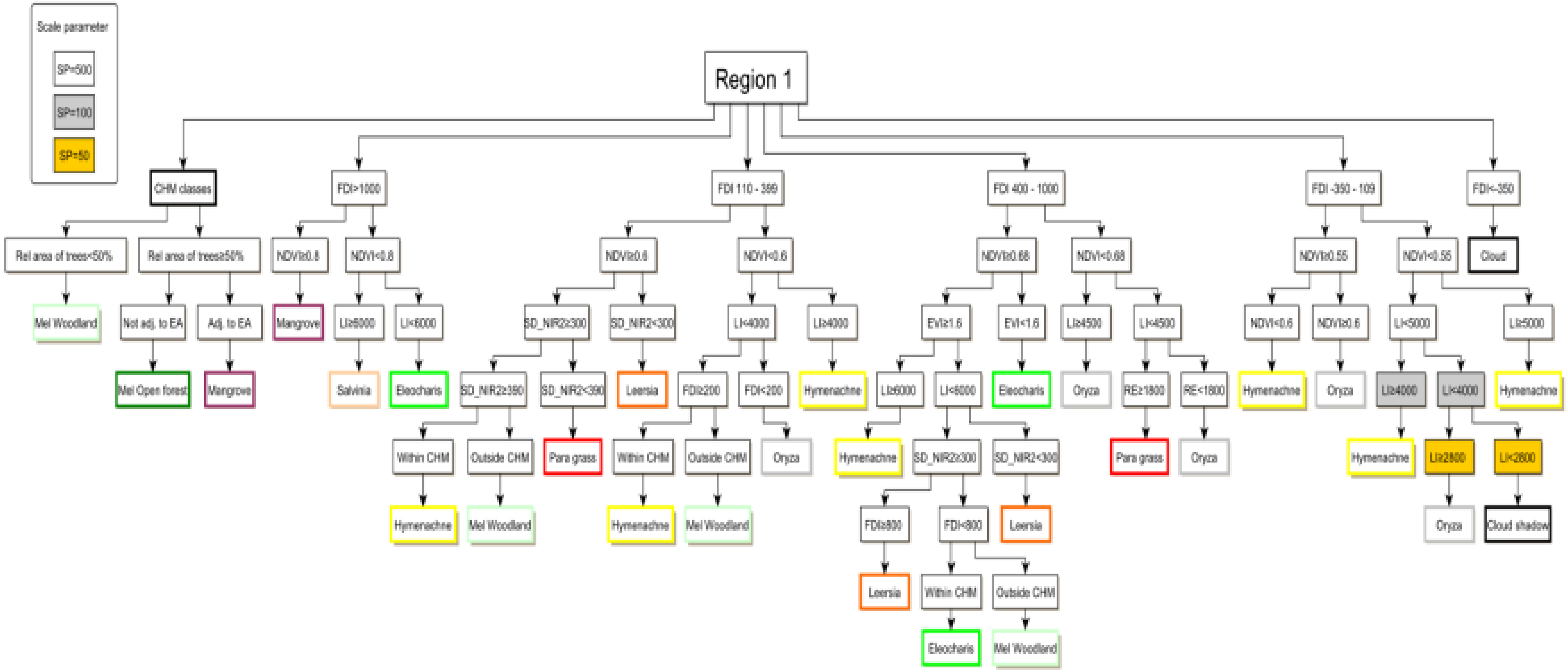

Figure 3.22 ‘Decision tree’ for the determination of spectral indices derived classes for Region 1. The clear boxes represent class splitting occurring on objects created with a scale parameter (SP) of 500 while the grey boxes have a SP of 100 and yellow boxes have a SP of 50. The colour borders on the terminal boxes correspond to the vegetation classes on the final map.

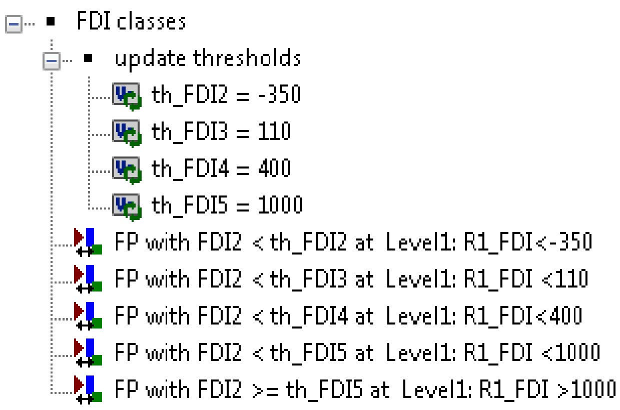

Figure 3.23 The first classification step for Region 1 from the eCognition process tree based on FDI thresholds.

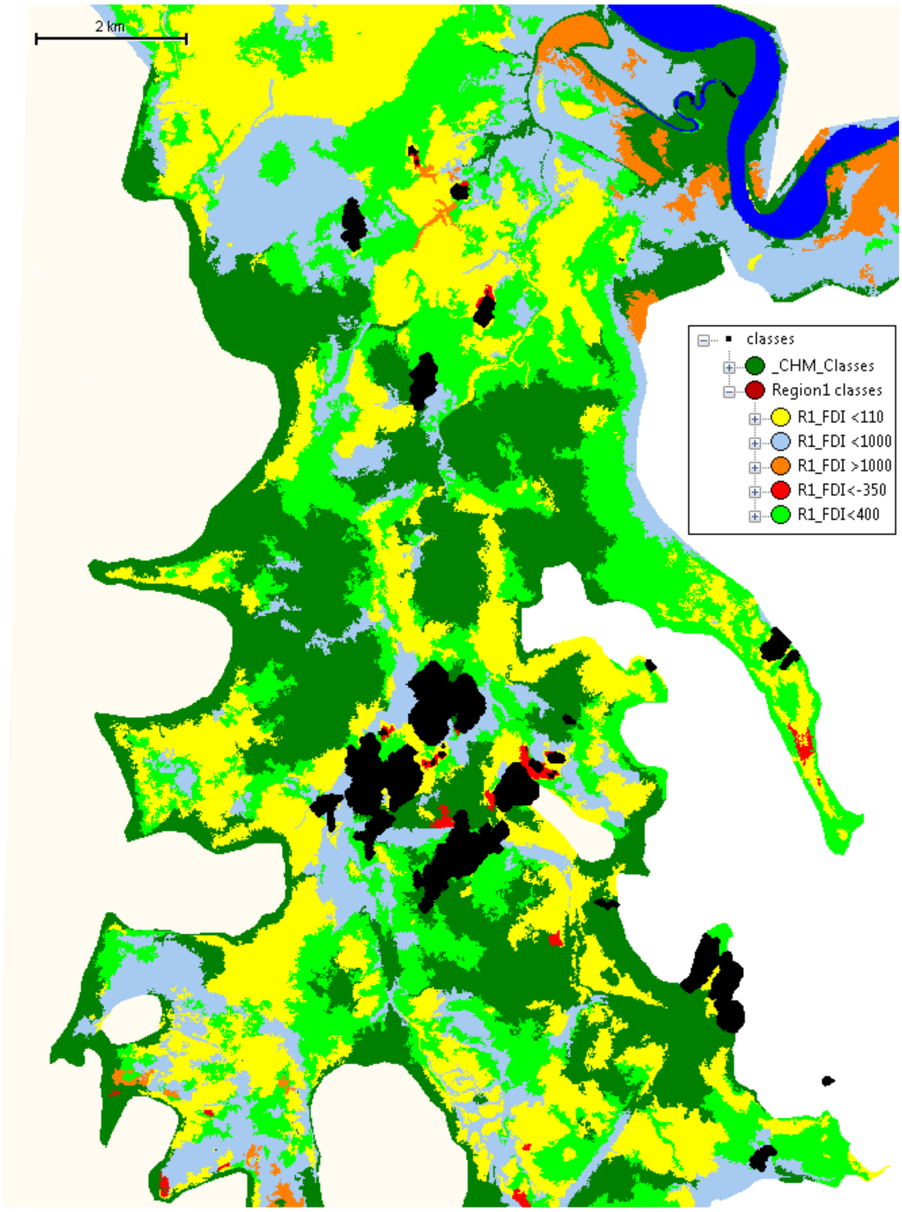

Figure 3.24 Region 1 after the initial classification into the 5 FDI classes. White represents non-floodplain regions, black is cloud or cloud shadow.

The second step of the classification process (Figure 3.25) involved splitting the four of the five FDI groups of classified objects created during the first processing step further into classes based on differences in NDVI (Figure 3.26). Again the threshold values at each step were determined through trial and error to be the best breaks in the continuous data for the further classification of the floodplain vegetation. Objects within the FDI<-350 class were not reclassified because these objects were identified as belonging to the Cloud class as they were mostly adjacent to Cloud objects and displayed similar feature values. Further reclassification and segmentation was conducted until satisfactory object separation was achieved. The end classes from this process were then assigned to vegetation classes using expert knowledge.

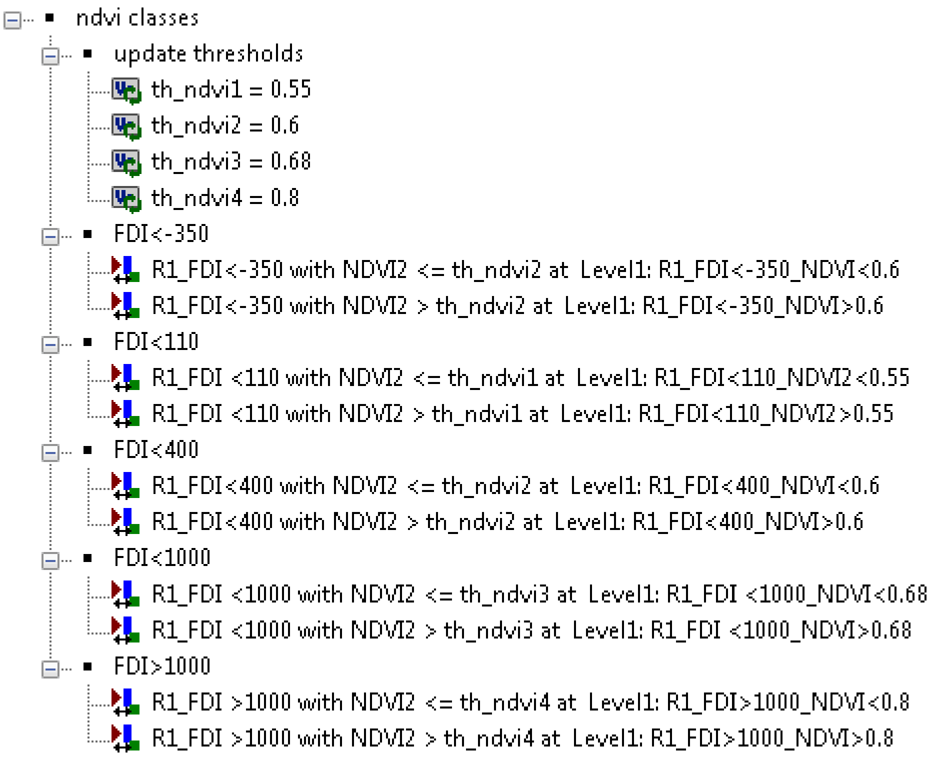

Figure 3.25 The second round of classifications for Region 1 from the eCognition process tree based on NDVI thresholds.

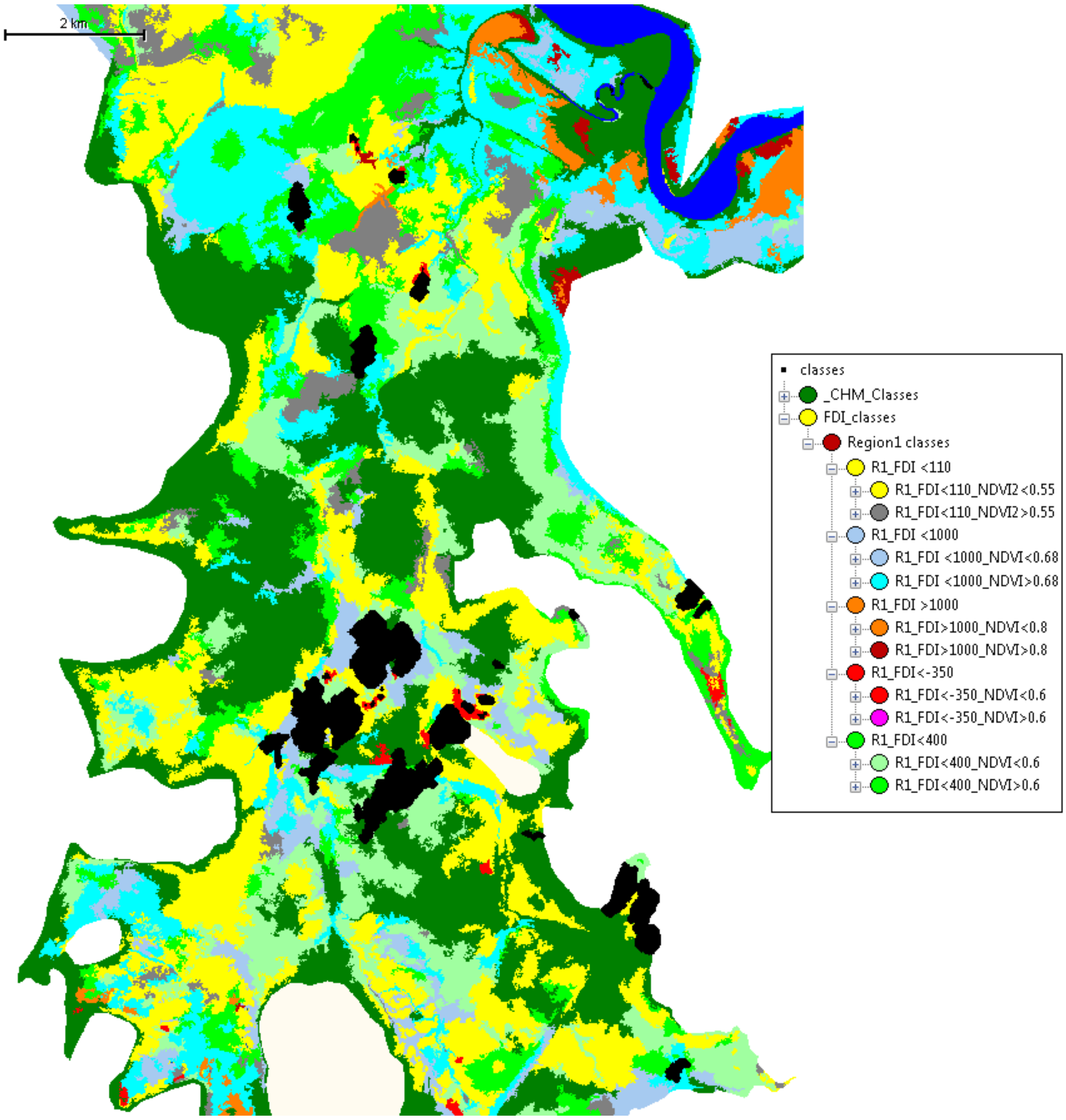

Figure 3.26 Region 1 after the second classification round into 10 NDVI classes. White is either non-floodplain regions or cloud, black is cloud shadow.

3.4.10 Delineating Regions 2 and 3 vegetation classes

Similar to the processing for Region 1, the imagery for Regions 2 and 3 was initially partitioned into clusters of pixels using the multiresolution segmentation algorithm. The parameters for the algorithm were the same as for Region 1: a scale parameter of 500, a shape factor of 0.3, and compactness value of 0.6 (Figure 3.27). After segmentation, the floodplain objects were subjected to a series of classification steps and some further finer segmentation (Figure 3.28).

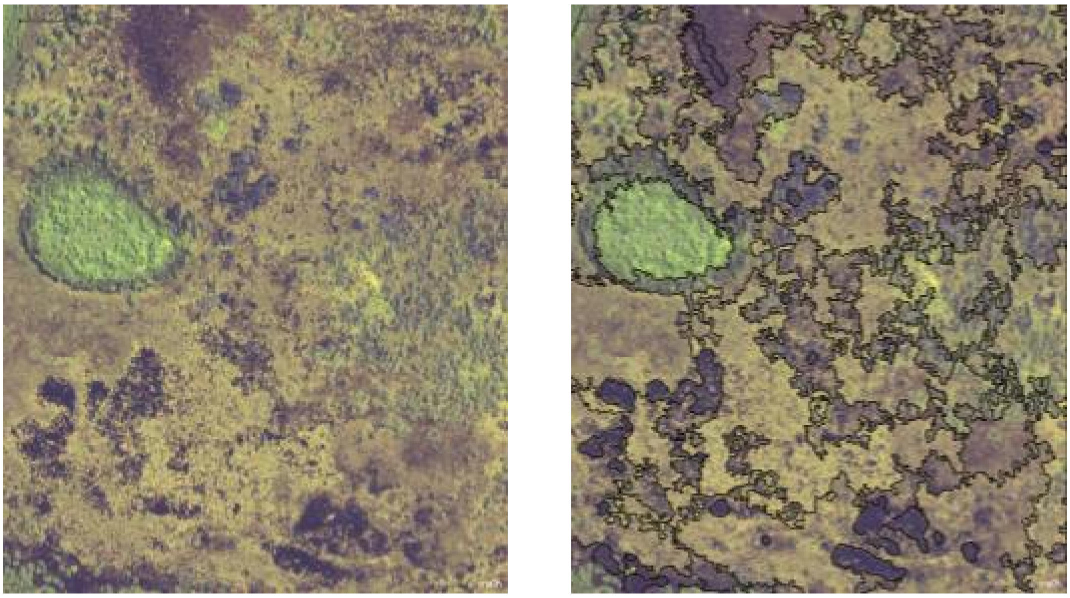

(a) (b)

Figure 3.27 A subset of the Magela Creek floodplain within Regions 2 and 3 (a), and showing the results of the initial image multiresolution segmentation (b). The segmentation algorithm used equal weights for all bands, a scale parameter of 500, a shape factor of 0.3, and compactness value of 0.6.

As per region 1, objects were identified as being potentially treed using a mean CHM value greater than 0.8 m within the potentially treed objects. Sub-objects representing trees or clusters were created using the threshold segmentation algorithm with trees being created from clusters of pixels within the CHM that were above 4 m. Sub-objects with spurious high values were removed from the tree sub-object class using 25 m as a ceiling value. The next step was to eliminate objects from the potentially treed objects if they contained no tree sub-objects. The remaining objects were then assigned to a tree class depending on proportional cover of tree in treed object: Open Forest was greater than 50% cover, Woodland 10–50% cover, Open Woodland < 10% cover (after Hnatiuk et al. 2009).

The remaining objects were then classified in steps that formed a 'decision tree' with the end output being objects belonging to one of 35 classes (Figure 3.28). The threshold values at each step were determined through trial and error to be the best breaks in the data for the classification of objects within the floodplain. Objects were first assigned to one of five classes based upon the five FDI threshold values (Figure 3.29). The class FDI<-350 segments contained pixels with FDI values less than -350, the class FDI<110 segments contained pixels with values between and including -350 and 109. The class FDI<400 clustered pixels with values between and including 110 and 399. Segments within the class FDI≤1000 possessed pixels with FDI values from 400 up to and including 1000. Segments within the class FDI>1000 possessed pixels with FDI values from 400 up to and including 1000. The second step of the classification process involved splitting the four of the five FDI groups of classified objects from the first processing step further into classes based on differences in NDVI (Figure 3.28). Objects within the FDI<-350 class were not reclassified because these were identified as belonging to the Cloud class as they were mostly adjacent to Cloud objects and displayed cloud features. Further reclassification and segmentation was conducted until satisfactory object separation was achieved. The end classes from this process were then assigned to vegetation classes using expert knowledge.

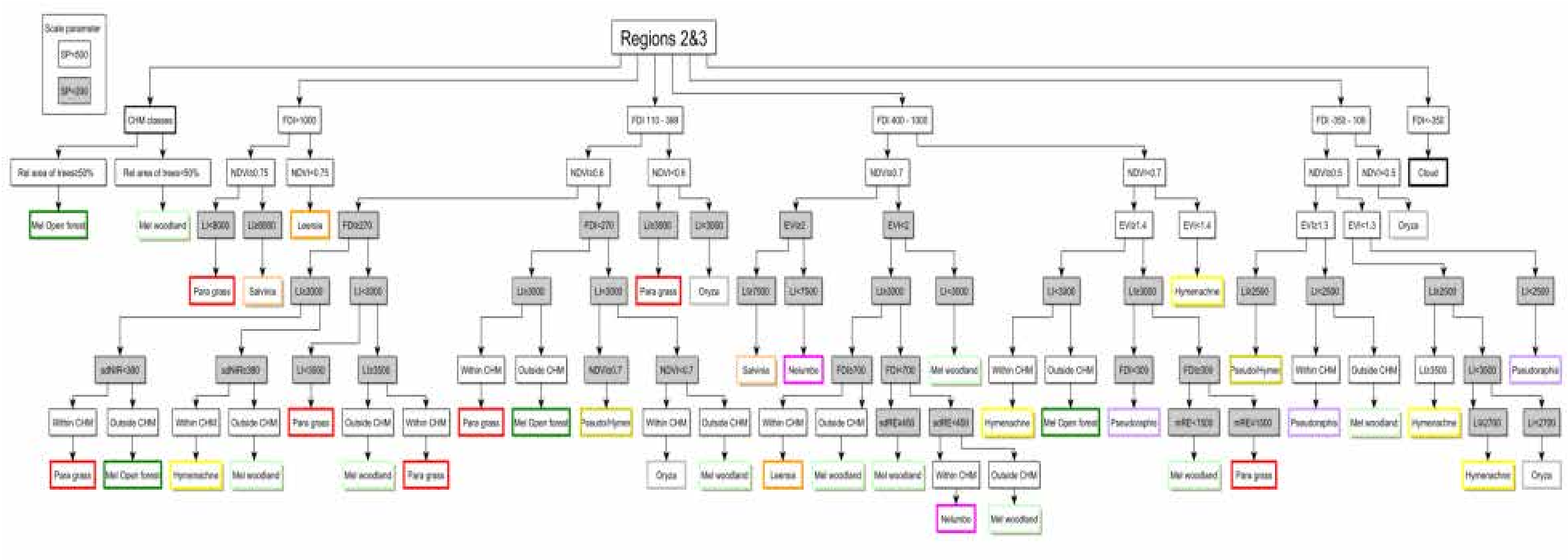

Figure 3.28 The 'Decision tree' for the determination of spectral indices derived classes for Regions 2 and 3. The clear boxes represent class splitting occurring on objects created with a scale parameter (SP) of 500 while the grey boxes have a SP of 200. The colour borders on the terminal boxes correspond to the vegetation classes on the final map.

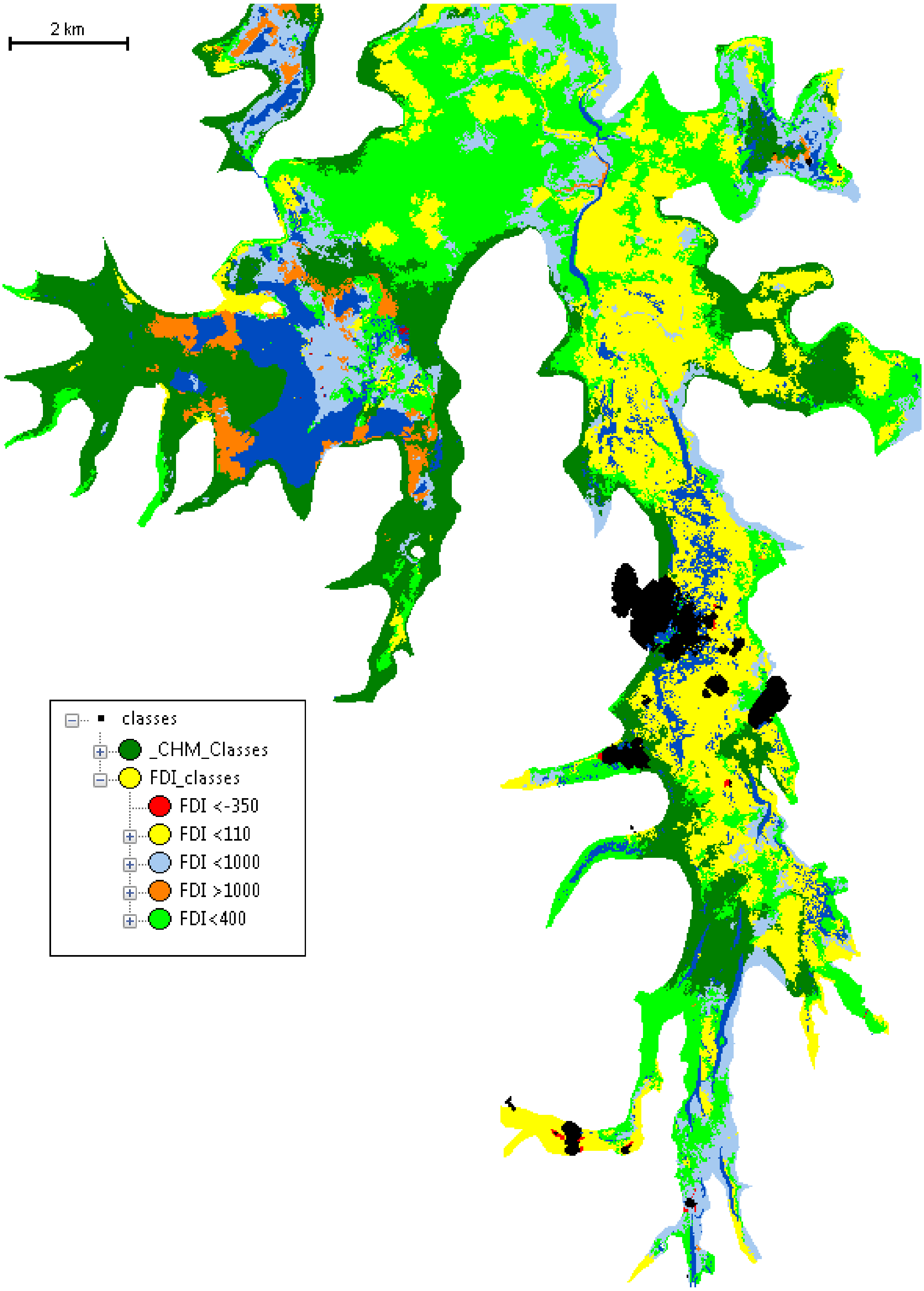

Figure 3.29 First classification step for regions 2 and 3. White represents non-floodplain regions,cloud and cloud shadow are black, dark blue is water.

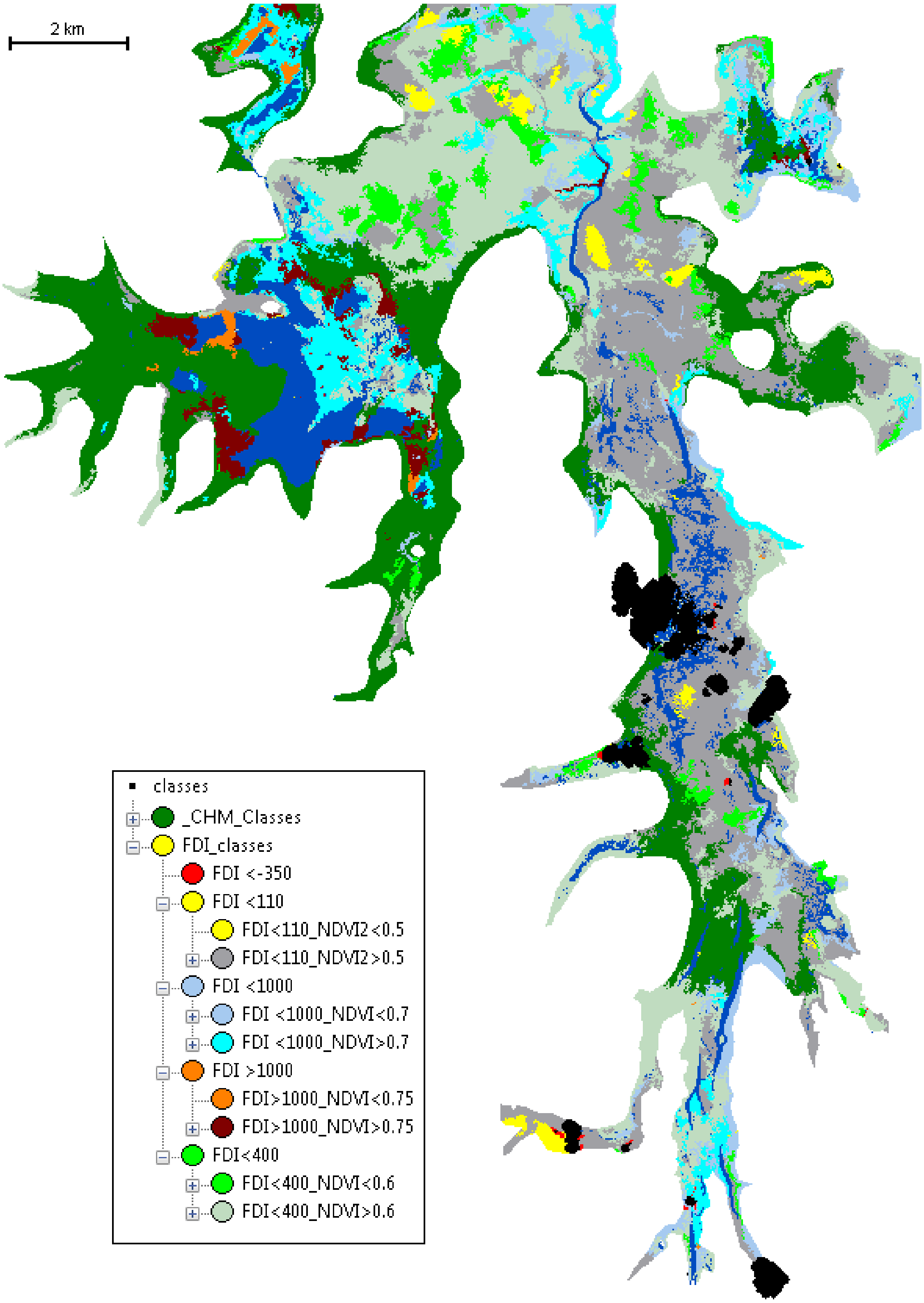

Figure 3.30 Regions 2 and 3 after the second classification round into 8 NDVI classes. Black is either cloud or cloud shadow.

3.5 Accuracy assessment

3.5.1 Field-based reference data

Validation was undertaken using two reference data sets (Figure 3.31). A systematic helicopter survey was undertaken on 29 May 2010, providing 100 reference sites identifying location, with dominant species and proportional cover for each site recorded based both on vertical visual estimates and photos. A ‘ground’ plot survey, undertaken 17–26 May 2010, provided a further 28 reference sites, each representing homogenous cover consisting of a single species. The sampling method used for the airboat survey was random with the reference data collected by the oblique visual estimation of the projected cover by species. These observations were made from the deck of an airboat while stationary. Classification accuracy at these sites was assessed against all the reference data using a confusion matrix (Congalton & Green 2009) and accuracy measures calculated.

Figure 3.31 Location of reference data sites.

3.5.2 Accuracy measures

To test the accuracy of the vegetation map, a site-specific accuracy assessment (Congalton & Green 2009) was conducted using a confusion matrix (Table 3.4) to compare the vegetation map to the classes at specific locations identified from the field-based reference data.

Table 3.4 The confusion matrix for assessing the accuracy of a classification of remotely sensed data.

		Reference data				
		A	B	C	Total	UA
Classified data	A	n_{AA}	n_{AB}	n_{AC}	n_{A+}	n_{AA}/n_{A+}
	B	n_{BA}	n_{BB}	n_{BC}	n_{B+}	n_{BB}/n_{B+}
	C	n_{CA}	n_{CB}	n_{CC}	n_{C+}	n_{CC}/n_{C+}
	Total	n_{+A}	n_{+B}	n_{+C}	n	
	PA	n_{AA}/n_{+A}	n_{BB}/n_{+B}	n_{CC}/n_{+C}		

Where n is the total number of samples, n_{+A}, n_{+B}, n_{+C} are the number of samples classified into class A, B and C respectively in the classified map; n_{A+}, n_{A+} and n_{A+} are the number of samples classified in to class A, B and C respectively in the reference data. n_{AA}, n_{BB} and n_{CC} are the number of samples classified into class A,B and C respectively for both the classified and reference data. n_{AB}, n_{AC}, n_{BA}, n_{BC}, n_{CA} and n_{CB} are the number of samples where the classification and reference sample do not belong to the same class. PA is the Producer's accuracy and UA is the User's accuracy.

User's and Producer's accuracies (Story & Congalton 1986) were calculated for each class along with the overall classification accuracy. The Producer's accuracy is a measure of omission error and termed as such because the producer of the classified image/map is interested in how well the area under study can be mapped. The User's accuracy measures errors of commission and named as such because the user is interested in the reliability of the map (how well the map represents what is really on the ground). The User's accuracy was calculated by dividing the number of correctly identified sample units for a given class (e.g. n_{AA} for class A in Table 3.4) by the total number of sample units for a given class according to the reference data (the row total e.g. n_{A+}). The Producer's accuracy was calculated by dividing the number of correctly identified sample units for a given class (e.g. n_{AA}) by the total number of sample units for given class based on the classification (the column total e.g. n_{+A}). The overall classification accuracy is given by dividing the total number of correctly identified sample units for all classes (the sum of the major diagonal e.g. n_{AA} + n_{BB} + n_{CC} in Table 3.4) by the total number of sample units for all classes (n).

4 Results

The map produced from the May 2010 WorldView-2 imagery contains 12 vegetation map classes representing typical vegetation communities found on the Magela Creek floodplain (Figure 4.1). The vegetation classes were named after the indicator or most abundant taxa for those objects at the time of data capture (early Dry season).

Figure 4.1 The vegetation map for the Magela Creek floodplain, May 2010.

4.1 Classes or vegetation mapping units

In May 2010, 828 ha were not mapped due to cloud cover or interference from cloud shadow and open water accounted for 3589 ha of the floodplain. The 12 vegetation mapping communities (Figure 4.1) are described below as is the extent and distribution of each of the classes at the time of data capture. For each community, image and derivative samples (chips) are provided along with descriptive written cues for the key interpretive elements that assisted in community discrimination. Selected feature values for representative objects for each community are also included.

4.1.1 *Hymenachne* grassland

The Hymenachne grassland class is dominated by *Hymenachne acutigluma* throughout the year. The community covers 3639 ha of the floodplain. Other species that may occur include *Oryza meridionalis*, *Nymphaea spp.*, and *Pseudoraphis spinescens* (Finlayson et al. 1989).

For the visual interpretation of *Hymenachne* communities there were a number of cues that were useful. In the May 2010 imagery, objects tended to be bright or highly reflective in most bands, particularly in the Region 1 image. Objects consisting of *Hymenachne* displayed as light green in the RGB true colour image (Figure 4.2a), and white or pale blue in NIR false colour image (Figure 4.2b). Areas tended to have higher LI and lower FDI, EVI and NDVI values for the time of year (early Dry) compared to neighbouring vegetation (Figure 4.2c-f). In regions 2 and 3, Hymenachne objects show more as a pale light brown colour. Table 4.1 highlights some of the values for features of the selected *Hymenachne* objects for Region 1 and Regions 2 and 3.

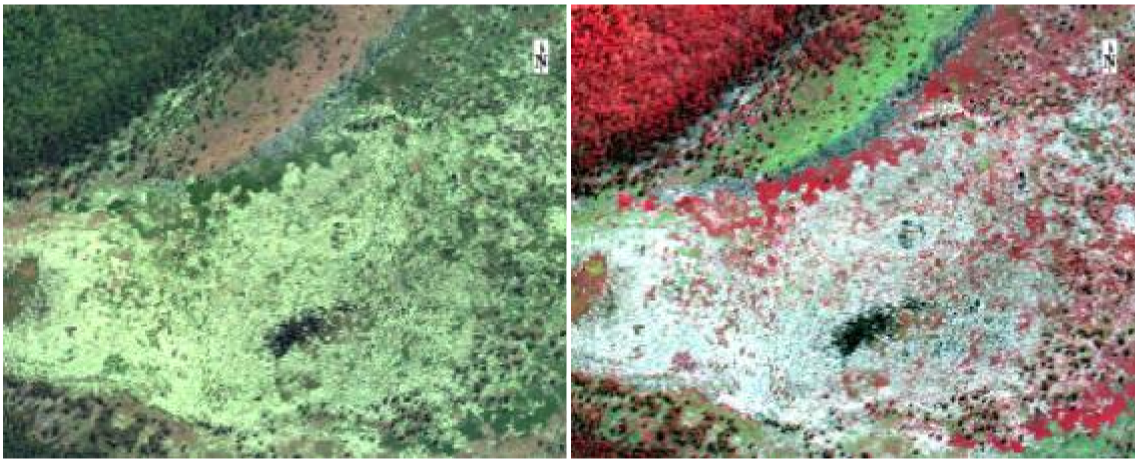

(a) (b)

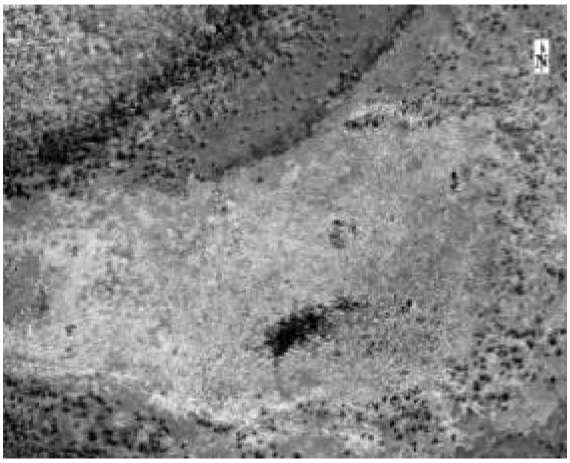

(c)

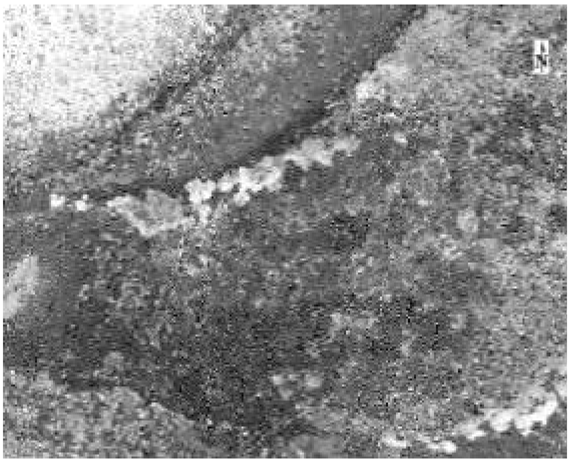

(d)

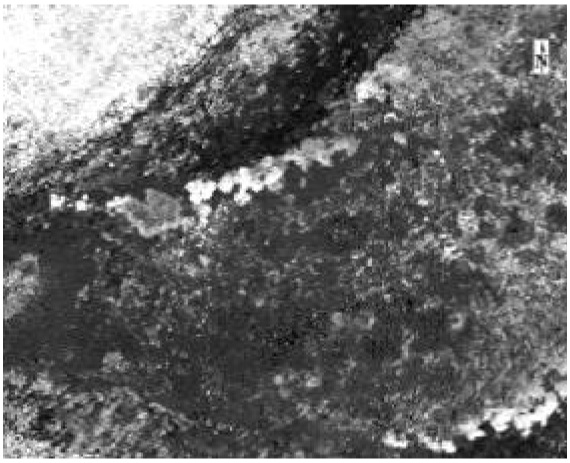

(e)

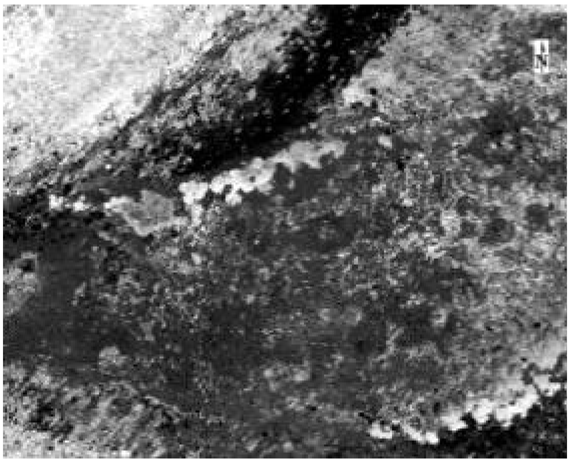

(f)

Figure 4.2 Image chip for *Hymenachne* grassland from Region 1 (a) True colour image with RGB=Bands 5,3,2, (b) NIR false colour image with RGB = Bands 8,5,3, (c) LI image, (d) FDI image, (e) EVI image and (f) NDVI image.

Table 4.1 Object feature values for the selected *Hymenachne* object in region 1 (top) and regions 2 and 3 (bottom).

Object	**Object feature values**	
Region 1	**Mean layer values**	
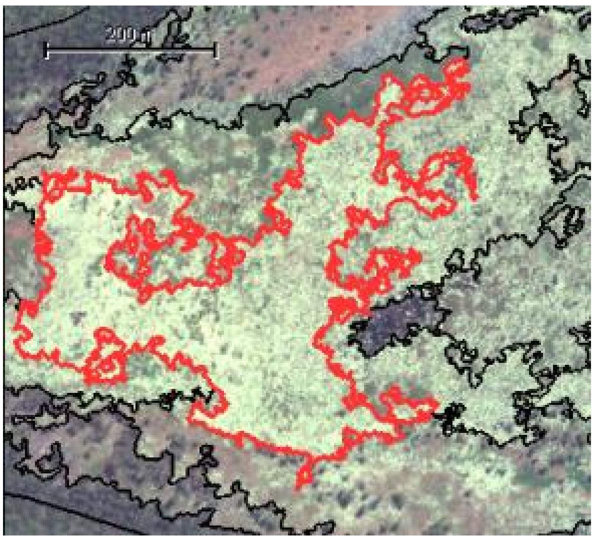	Coastal	316.2
	Blue	563.63
	Green	1193.71
	Yellow	1200.8
	Red	1086.83
	Red edge	2909.56
	NIR1	3572.38
	NIR2	3376.50
	Ratio values	
	EVI	1.009
	FDI	-96.69
	NDVI	0.5130
	LI	5722.43

Regions 2 & 3

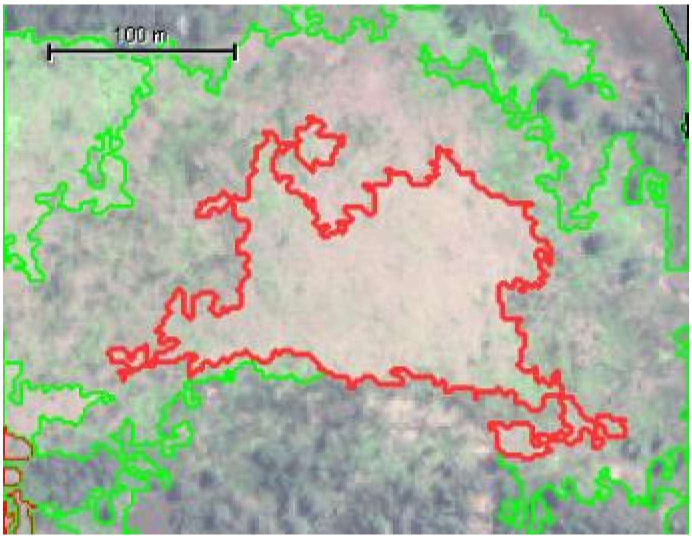

Mean layer values

Coastal	265.00
Blue	519.10
Green	959.26
Yellow	1103.07
Red	1077.75
Red edge	2186.06
NIR1	2631.40
NIR2	2515.30

Ratio values

EVI	0.7061
FDI	-189.86
NDVI	0.4001
LI	4182.25

4.1.2 *Melaleuca* woodland and open forest

The classes *Melaleuca* woodland and *Melaleuca* open forest typically contain *M. cajaputi* and *M. viridiflora* in the northern regions and at the edges of the floodplain, and *M. leucadendra* in the backswamps that are inundated for most of the year (Finlayson et al. 1989). Woodland communities have 10–50% woody cover (covering 5039 ha), whereas open forest communities have 50–70% cover (covering 821.8 ha). These communities are typically inundated for 5–8 months of the year.

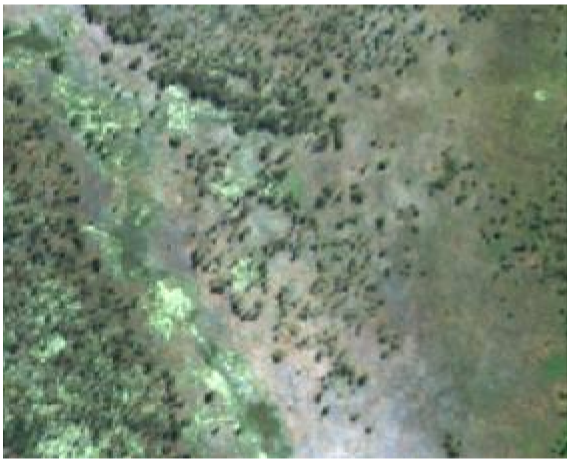

(a)

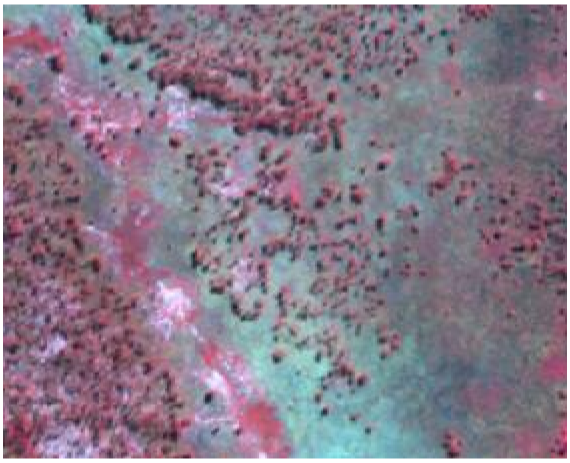

(b)

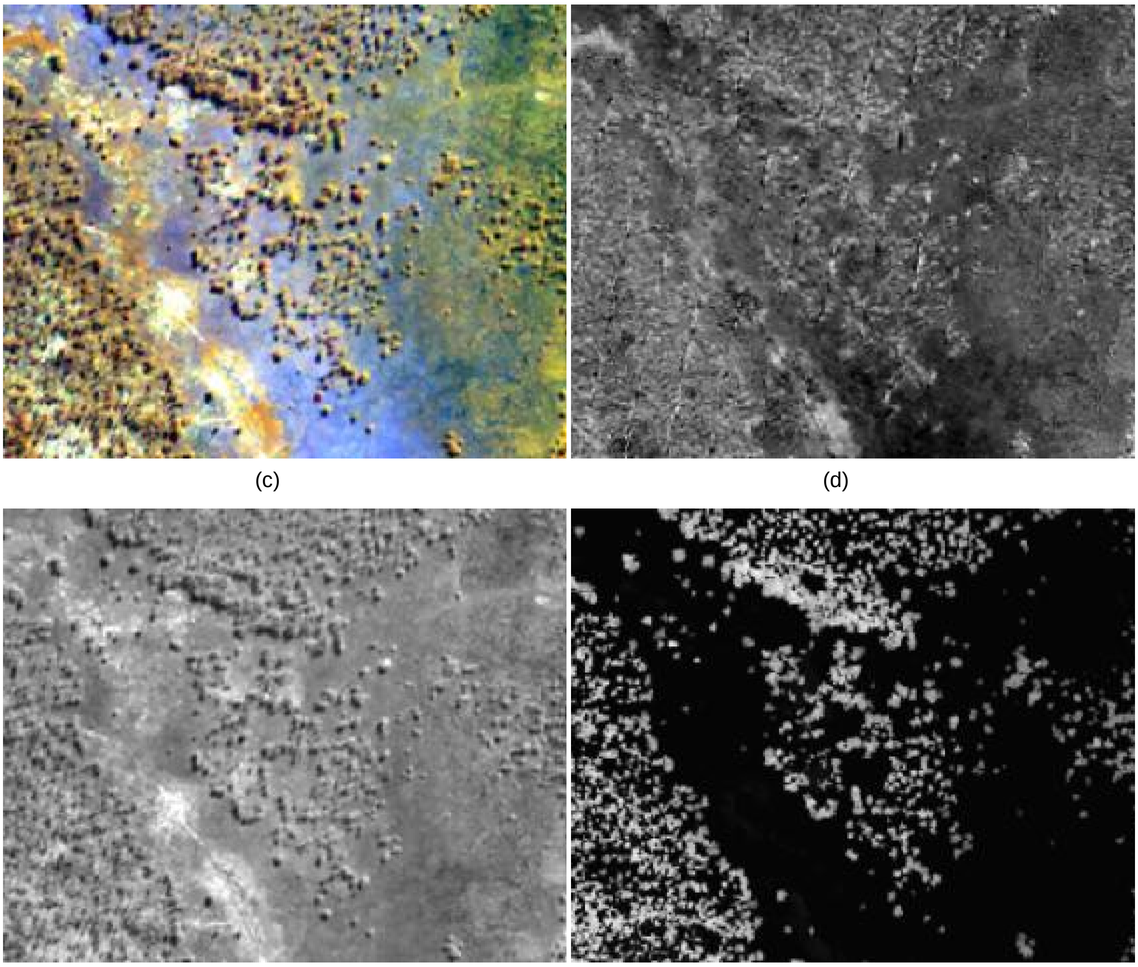

(c) (d) (e) (f)

Figure 4.3 Image chip showing a sample of *Melaleuca* woodland (a) true colour RGB=5,3,2, (b) false colour RGB= 8,5,3, (c) False colour RGB= 8,6,2, (d) FDI, (e) LI, (f) CHM.

There were a number of cues valuable for the visual interpretation of *Melaleuca* woodland communities. Regions of woodland showed obvious trees with shadows. Trees are displayed as dark green in the RGB image (Figure 4.3a), and crimson to red in the NIR false colour image (Figure 4.3b). Across an object the trees were in an irregular pattern and spaced apart, and the texture was course and uneven. Within the CHM, trees (or clusters of trees) were obvious (Figure 4.3f). Table 4.2 displays some of the values for features within the selected *Melaleuca* woodland object.

Table 4.2 Object feature values for the selected *Melaleuca* woodland object (top) and tree sub-objects (bottom).

Object	Object feature values	
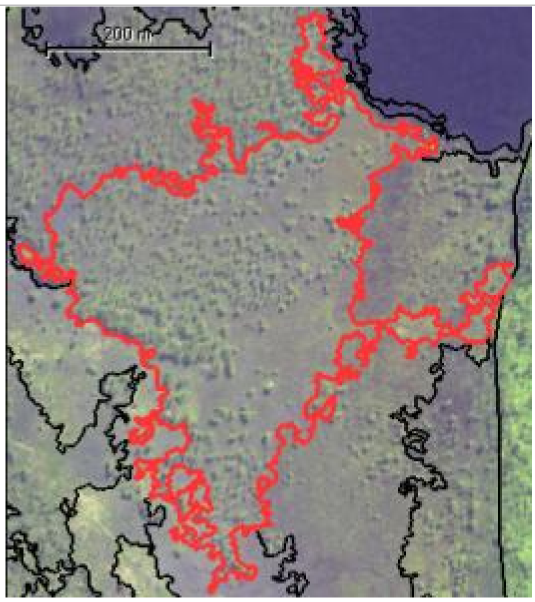	**Mean layer values**	
	Coastal	218.38
	Blue	377.71
	Green	678.33
	Yellow	730.54
	Red	696.94
	Red edge	1689.63
	NIR1	2248.19
	NIR2	2169.05
	CHM	2.478
	Ratio values	
	EVI	1.046
	FDI	101.71
	NDVI	0.5267
	LI	3480.97
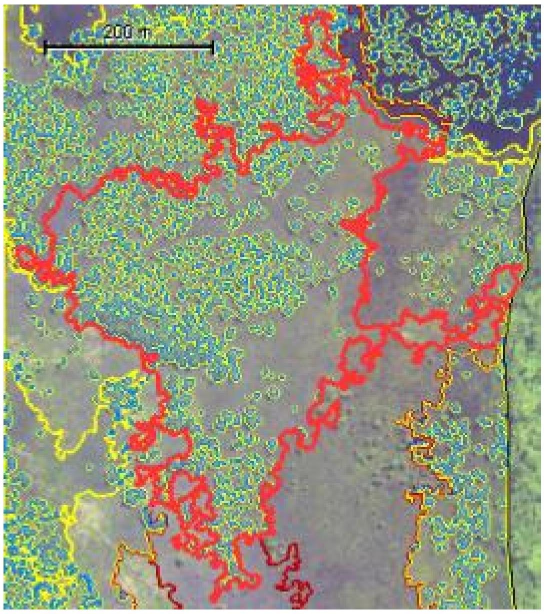	**Relative area of sub-objects**	
	Tree	26.5%

There were a number of cues that were useful for the visual interpretation of *Melaleuca* open forest objects. Within objects, trees displayed as dark green in the true colour RGB image (Figure 4.4a), or crimson in the NIR false colour image (Figure 4.4b). As trees are spaced close together and there are overlapping canopies, pixels within potential *Melaleuca* open forest objects displayed a regular pattern and fine texture. Shadows were obvious on the edges of stands but not so much for individual trees. In addition, trees were readily apparent in the CHM (Figure 4.4f). This land cover was mostly located in the southern reaches of the floodplain and around the perimeter. Table 4.3 shows some of the values for features of the selected *Melaleuca* open forest object.

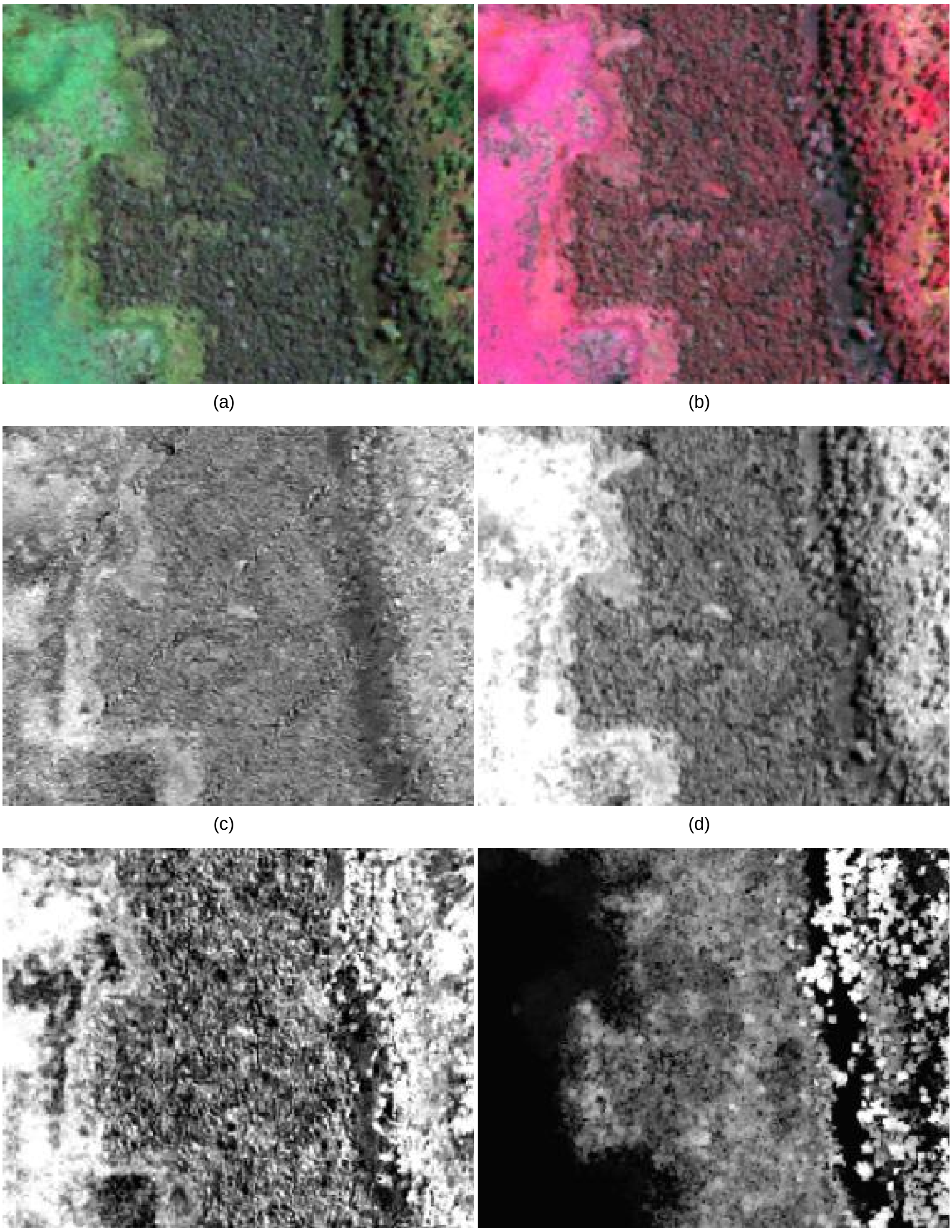

(a) (b) (c) (d) (e) (f)

Figure 4.4 Image chip for *Melaleuca* open forest (a) True colour RGB = bands 5,3,2, (b) False colour RGB = bands 8,5,3, (c) FDI, (d) LI, (e) EVI, and (f) CHM.

Table 4.3 Object feature values for selected the *Melaleuca* open forest object (left) and the tree sub-objects (right).

Object	Object feature values	
	**Mean layer values**	
	Coastal	116.58
	Blue	253.80
	Green	497.34
	Yellow	529.69
	Red	468.90
	Red edge	1502.42
	NIR1	2127.79
	NIR2	2188.58
	Ratio values	
	EVI	1.387
	FDI	432.36
	NDVI	0.6471
	LI	3437.2
	**Relative area of sub-objects**	
	Tree	51%

4.1.3 *Oryza* grassland

Objects within the *Oryza* grassland class are dominated by the annual grass, *Oryza meridionalis* towards the end of the Wet season. In the Dry season, these objects consist mostly of bare ground or dead *Oryza*. In 2010, the community occupied 4040 ha of the floodplain.

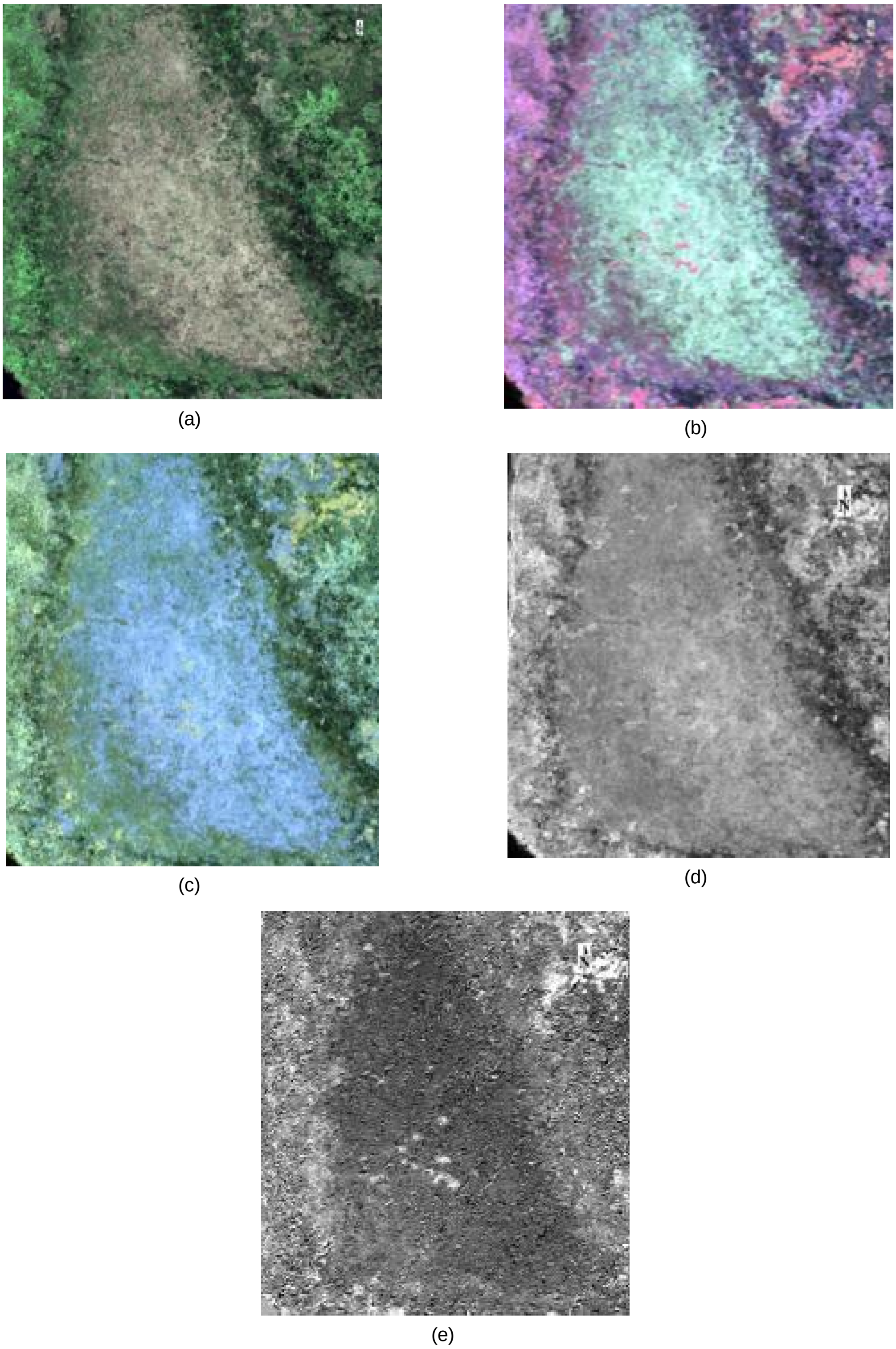

Figure 4.5 An image chip showing an example of Oryza grassland:(a) true colour image RGB=5,3,2, (b) nir false colour image RGB = 8,5,3, (c) red edge false colour image RGB = 8,6,2, (d) LI image, and (e) FDI image.

There were a number of visual cues for the interpretation of *Oryza* grassland: Areas with *Oryza* tended to have high reflectance in the visible bands (Figure 4.5a) and low NIR values (Figure 4.5b and c) typically associated with senescing vegetation. Areas dominated by *Oryza* also tended to display lower FDI values than the surrounding vegetation types. Table 4.4 highlights some of the feature values for the selected *Oryza* object.

Table 4.4 Object feature values for the selected *Oryza* object.

Object	**Object feature values**	
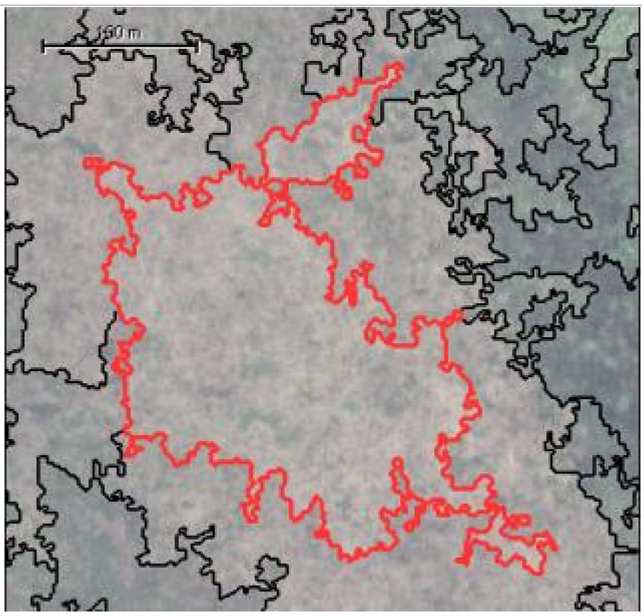	**Mean layer values**	
	Coastal	230.40
	Blue	475.39
	Green	828.57
	Yellow	967.39
	Red	963.88
	Red edge	1885.55
	NIR1	2349.80
	NIR2	2198.57
	Ratio values	
	EVI	0.6988
	FDI	-162.37
	NDVI	03904
	LI	3608.73

4.1.4 Pseudoraphis grassland

The *Pseudoraphis* grassland class is dominated by the perennial grass, *Pseudoraphis spinescens*. The class occupied 943 ha, particularly in the southern half of the floodplain.

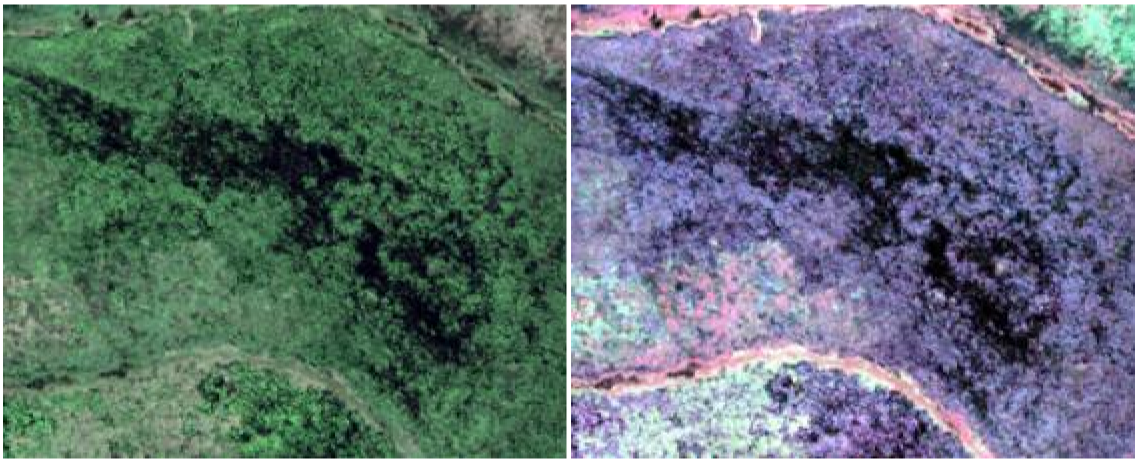

(a) (b)

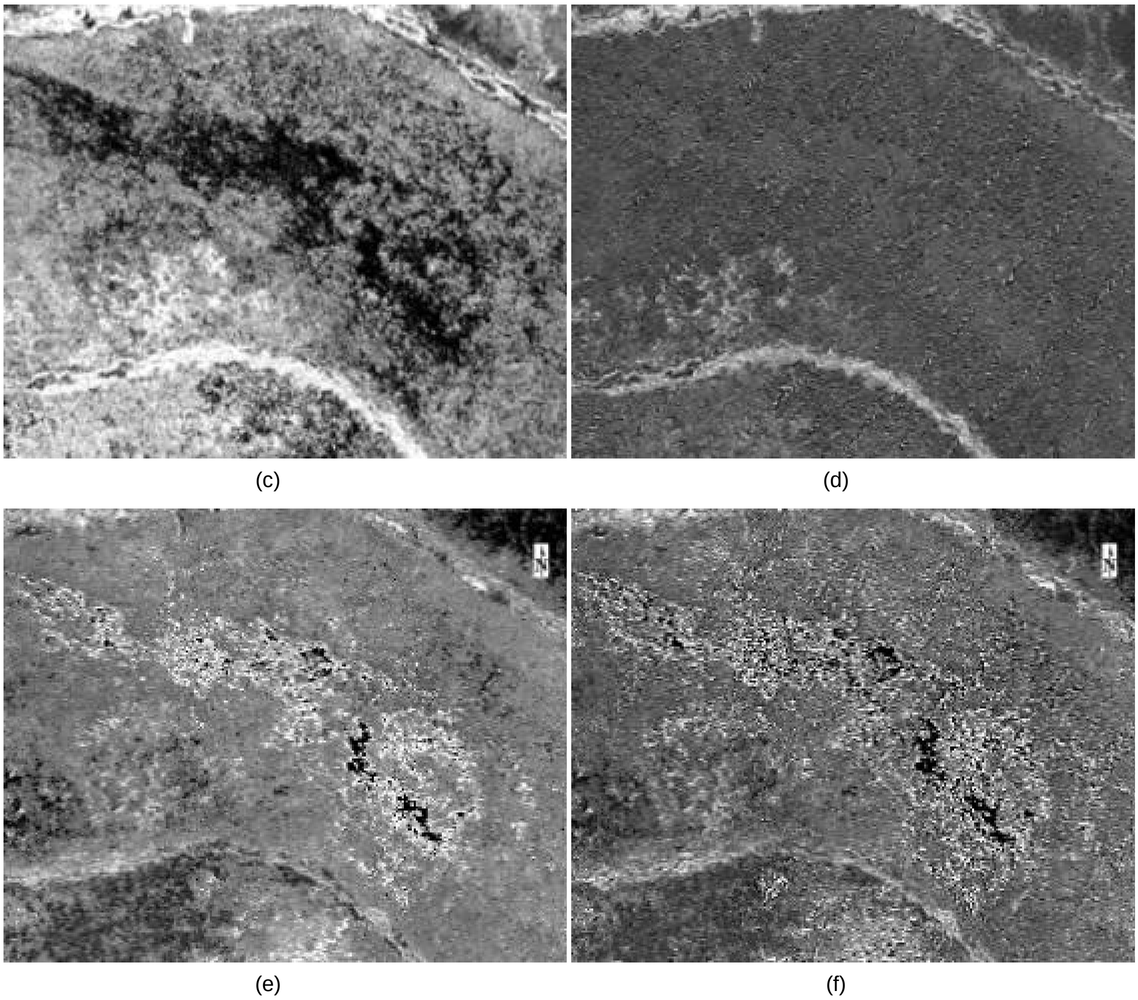

Figure 4.6 An image chip showing *Pseudoraphis* grassland (a) true colour imager RGB=5,3,2, (b) nir false colour image RGB = 8,5,3, (c) LI image, (d) FDI image, (e) NDVI image and (f) EVI image.

There were a number of cues that assisted in the visual interpretation of communities dominated by *Pseudoraphis spinescens*. Objects often contained vegetation mixed with water and as such displayed an irregular pattern and coarse texture. Plants typically displayed as dark green clumps in RGB imagery (Figure 4.6a), and purple in NIR false colour (Figure 4.6b). Table 4.5 highlights some of the values for features of the selected *Pseudoraphis* object.

Table 4.5 Object feature values for the selected *Pseudoraphis* object.

Object	Object feature values	
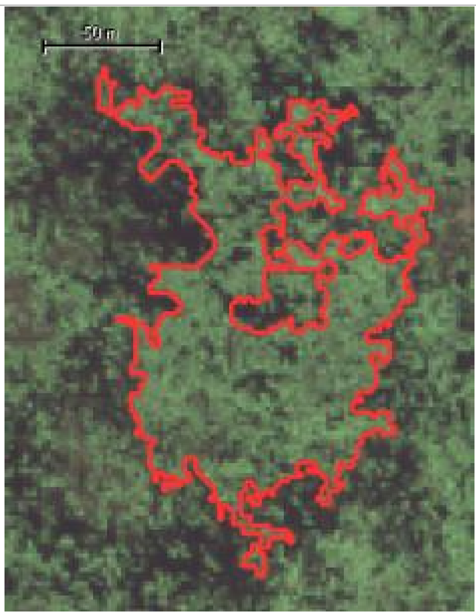	**Mean layer values**	
	Coastal	94.64
	Blue	249.44
	Green	699.88
	Yellow	611.73
	Red	420.35
	Red edge	1742.06
	NIR1	2066.79
	NIR2	1896.77
	Ratio values	
	EVI	1.448
	FDI	-94.73
	NDVI	0.6372
	LI	3389.38

4.1.5 Pseudoraphis/Hymenachne grassland

The class, Pseudoraphis/Hymenachne contains objects that are co-dominated by *Pseudoraphis spinescens* and *Hymenachne acutigluma*. The class covers approximately 375 ha of the floodplain.

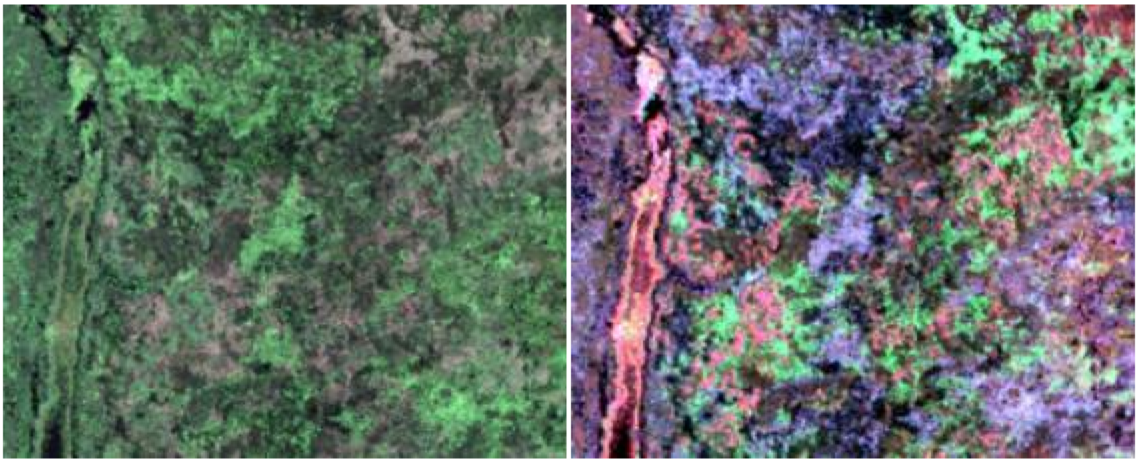

(a) (b)

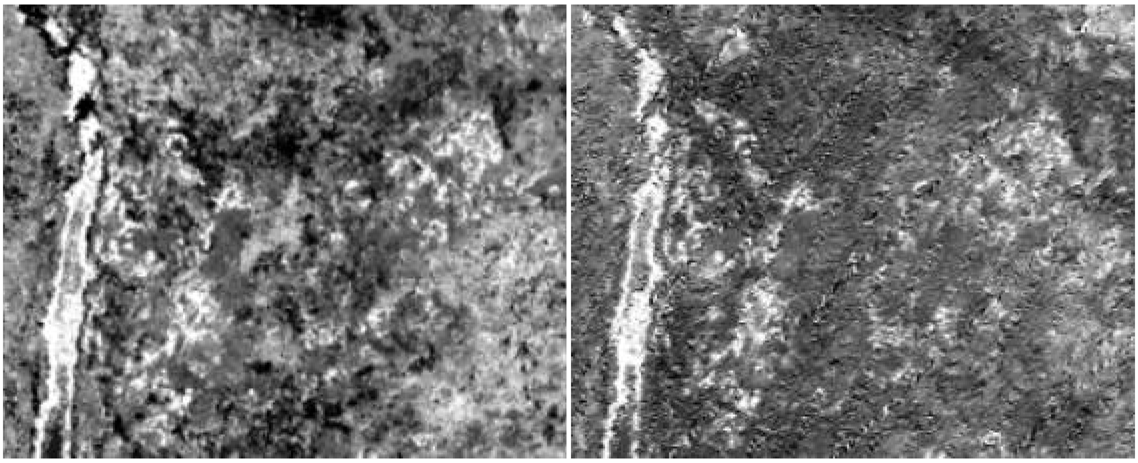

(c) (d)

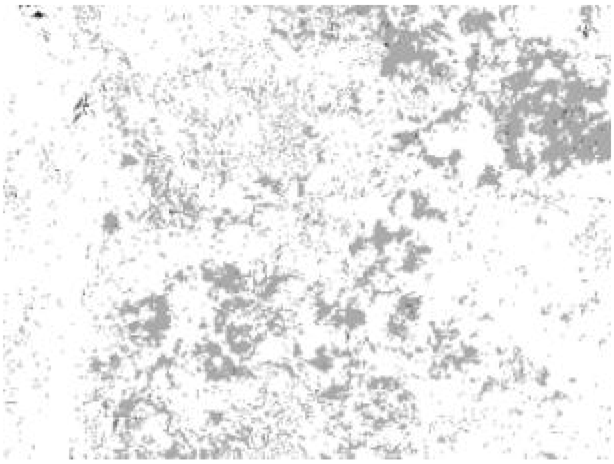

(e)

Figure 4.7 Image chip for *Pseudoraphis*/*Hymenachne* (a) True colour RGB =5,3,2, (b) false colour RGB=8,5,3, (c) LI, (d) FDI,and (e) EVI.

There are a number of cues that assisted with the visual interpretation of *Pseudoraphis*/*Hymenachne* grassland: Objects contained a mixture of green (*Pseudoraphis*) and light brown (*Hymenachne*) in the true colour RGB image (Figure 4.7a). Within the NIR false colour image, objects were a mixture of purple (*Pseudoraphis*) and green (*Hymenachne*) with the pink portions being Para grass (Fig 4.7b). There were pixels representing each species within the objects, thus displaying an irregular pattern and uneven texture (Figure 4.7c). Within and between the objects there was usually some water present (shown as dark patches). Table 4.6 highlights feature values for the selected Pseudoraphis/Hymenachne object.

Table 4.6 Object feature values for selected *Pseudoraphis* / *Hymenachne* object.

Object	Object feature values	
	**Mean layer values**	
	Coastal	160.70
	Blue	349.13
	Green	730.97
	Yellow	763.21
	Red	664.24
	Red edge	1859.55
	NIR1	2370.49
	NIR2	2283.78
	Ratio values	
	EVI	1.109
	FDI	75.10
	NDVI	0.5494
	LI	3794.20

4.1.6 Para grass

The weed grass, *Urochloa mutica* (Para grass), is an invasive species introduced from Africa as a pasture grass. It forms dense monocultures and can outcompete native vegetation in communities of *Hymenachne*, *Oryza* and *Eleocharis*. Based on the 2010 map, the community covered 2181 ha of the floodplain mostly in the central plains region.

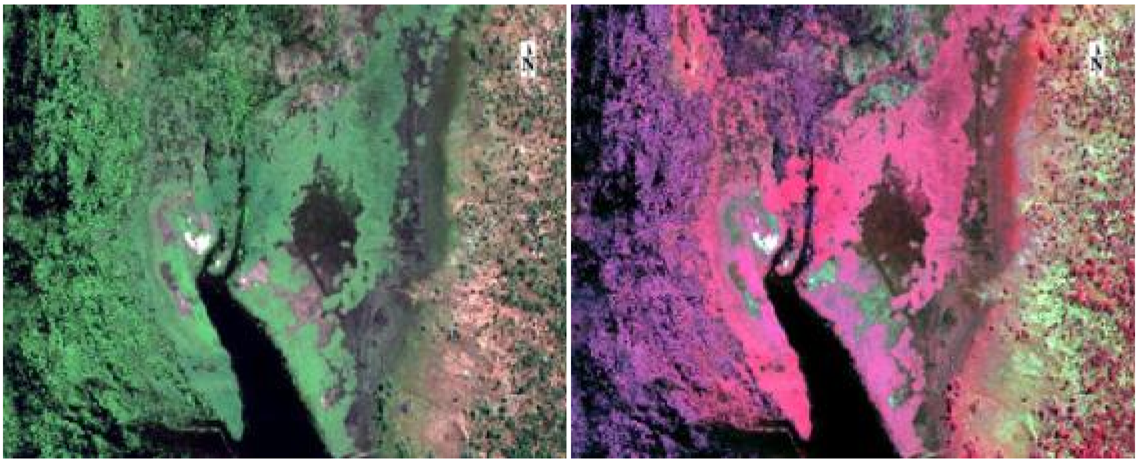

(a) (b)

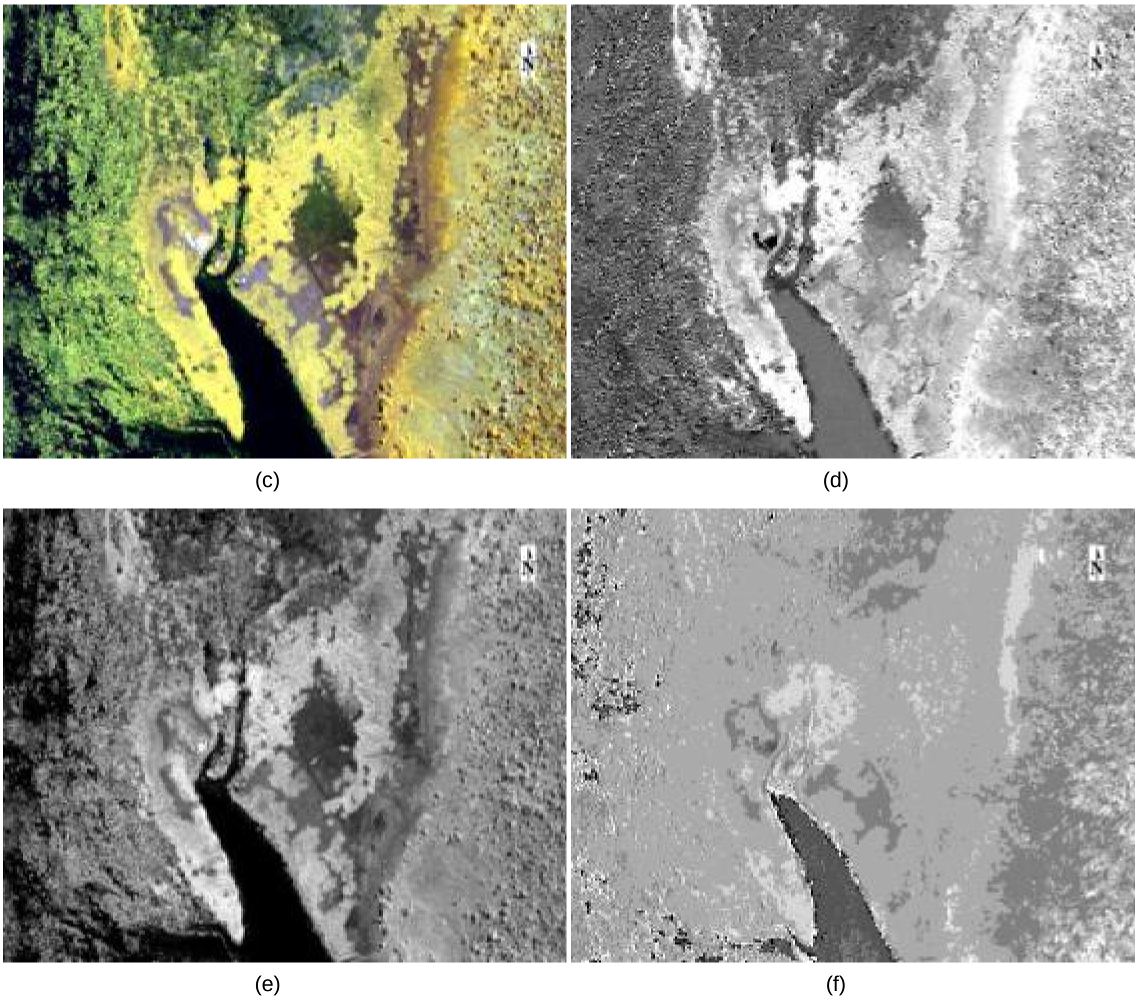

Figure 4.8 Image chip showing Para grass: (a) true colour RGB=Bands 5,3,2, (b) false colour RGB=Bands 8,5,3, (c) false colour RGB=Bands 8,6,2, (d) FDI, (e) LI and (f) EVI.

There were a number of cues for the visual interpretation of Para grass. Objects were of a typically smooth texture with irregular boundaries. Homogeneous areas displayed as a moss green colour in RGB imagery (Figure 4.8a) but with smoother texture than the similar coloured *Pseudoraphis*. Para grass also showed as bright pink in the NIR false colour whereas *Pseudoraphis* showed as purple and *Hymenachne*, greyish (Figure 4.8b). Smaller outbreaks tended to be elliptical in shape, due to runner activity. Table 4.7 lists some of the feature values for the selected para grass object.

Table 4.7 Object feature values for the selected para grass object.

Object	Object feature values	
	**Mean layer values**	
	Coastal	144.56
	Blue	313.26
	Green	765.35
	Yellow	672.60
	Red	500.18
	Red edge	2373.69
	NIR1	3425
	NIR2	3427.44
	Ratio values	
	EVI	1.794
	FDI	740.48
	NDVI	0.7453
	LI	5487.86

4.1.7 *Nelumbo* herbland

In 2010, the class *Nelumbo* herbland occupied 243.3 ha of the floodplain. This community is dominated by the water lilies, *Nelumbo nucifera* or to a lesser extent *Nymphoides* spp. These communities occur in permanent and semi permanent wet areas. Other species that may be present include *Leersia hexandra*, *Hymenachne acutigluma*, *Nymphaea* spp. The largest community is found on the eastern of Red Lily Swamp (the open body of water in the western part of the floodplain).

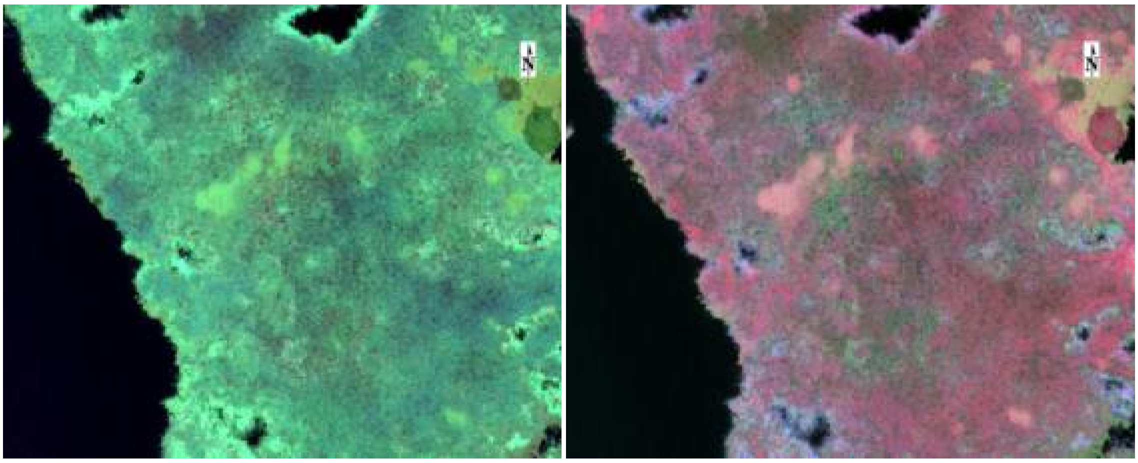

(a) (b)

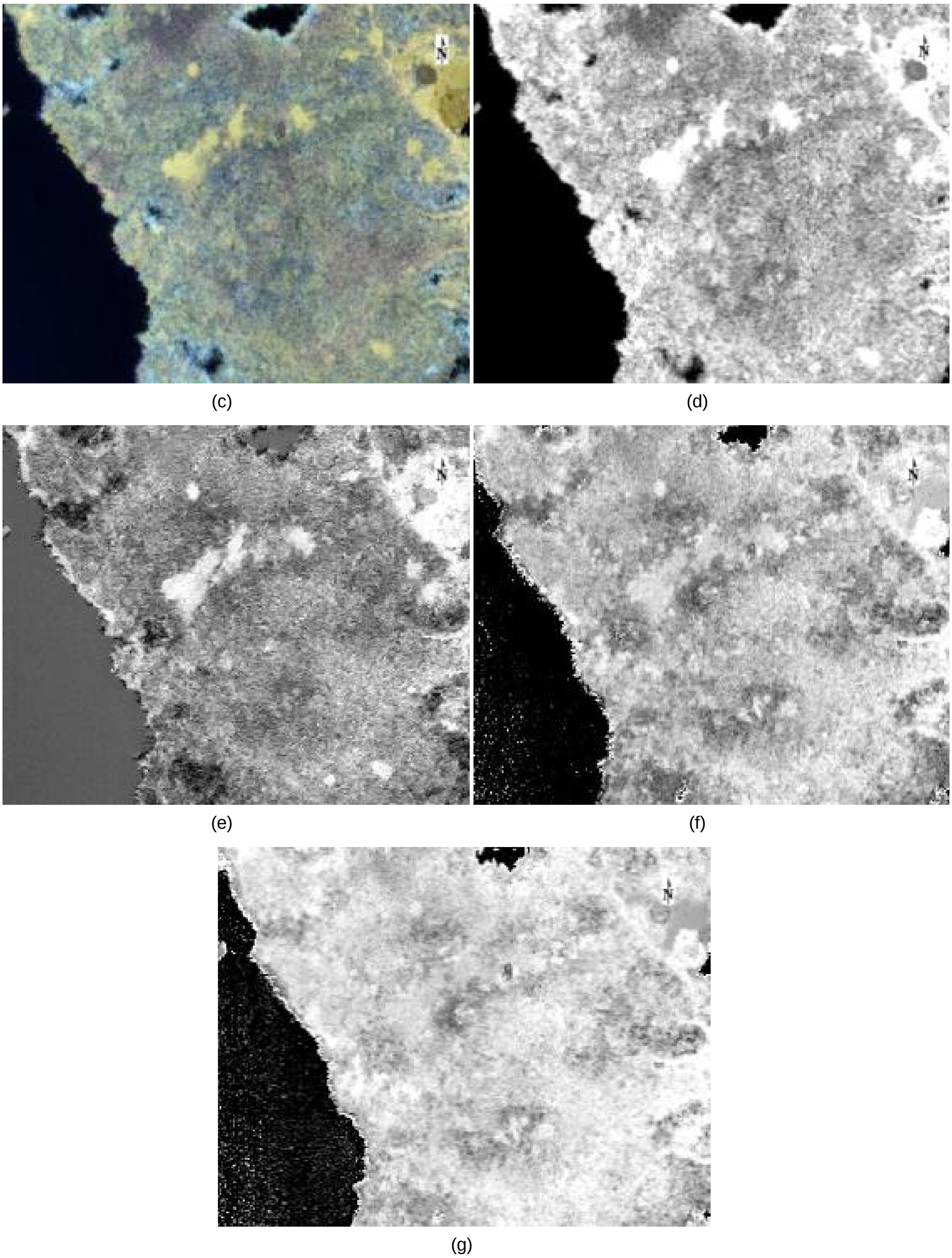

Figure 4.9 Image chip of *Nelumbo* herbland. (a) True colour RGB = Bands 5,3,2, (b) False colour NIR RGB=Bands 8,5,3, (c) False colour RGB = Bands 8, 6, 2, (d) LI, (e) FDI, (f) EVI and (g) NDVI.

There are several cues that assisted in the visual interpretation of *Nelumbo* herbland. The laminae of *N. nucifera* displayed as bright green in true colour RGB imagery (Figure 4.9a) and bright pink in NIR false colour imagery (Figure 4.9b). Nelumbo cover appeared bright in LI image (Figure 4.9c) but not in the FDI image (Figure 4.9d). Between the laminae water maybe visible; this was manifested as a blotchy appearance. This was characterised by a fine scale uneven texture. Large patches of *Nelumbo* adjacent to open water were characterised by a ragged boundary. Additionally, there were small patches of other cover types apparent within *Nelumbo* communities. Table 4.8 highlights the key feature values for the selected Nelumbo object.

Table 4.8 Object feature values for the selected *Nelumbo* object.

Object	Object feature values	
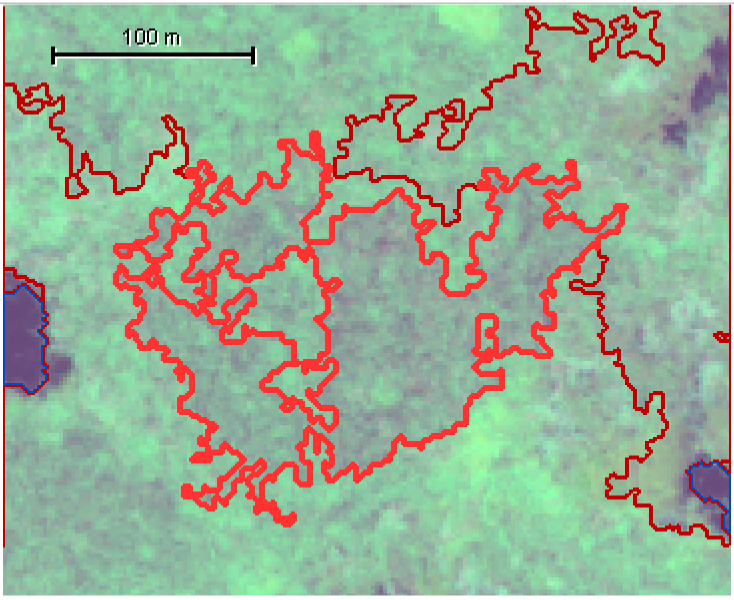	**Mean layer values**	
	Coastal	232.55
	Blue	348.36
	Green	743.50
	Yellow	614.09
	Red	457.85
	Red edge	2391.47
	NIR1	3157.34
	NIR2	3055.98
	Ratio values	
	EVI	2.035
	FDI	316.15
	NDVI	0.7394
	LI	5099.09

4.1.8 Salvinia

The class *Salvinia*, is dominated by the floating fern, *Salvinia molesta*. This weed can completely cover small areas of open water that are protected from wind. On larger stretches of open water, the fern can be found on the leeward edge. In the early Dry, the predominant wind is south easterly. This class covers 107.5 ha.

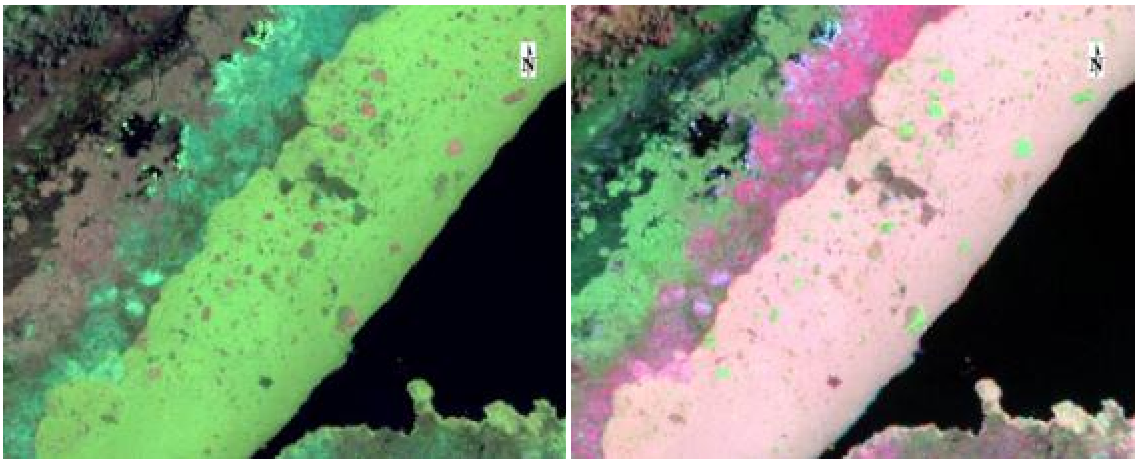

(a) (b)

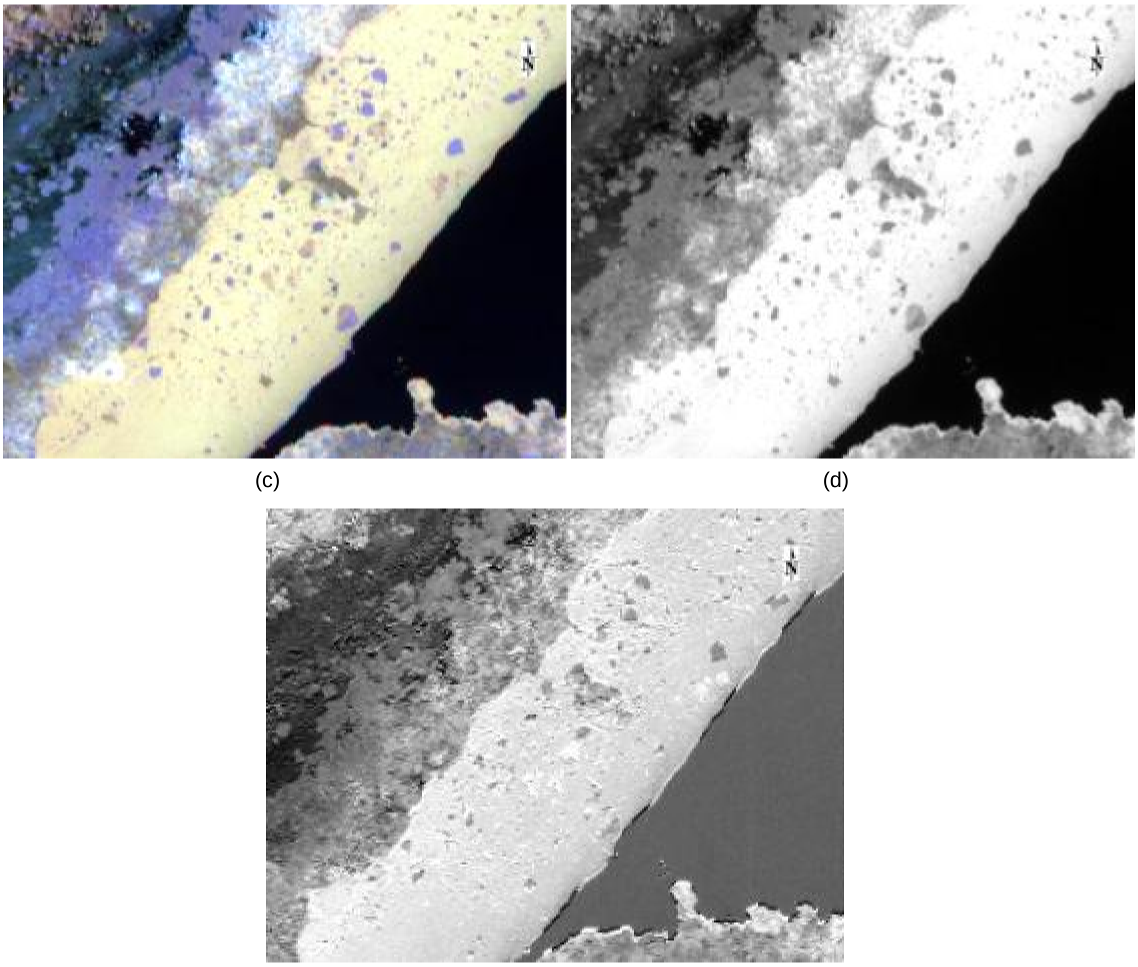

(c) (d)

(e)

Figure 4.10 Image chip for Salvinia. (a) RGB = 5,3,2, (b) RGB = 8,5,3, (c) RGB = 8,6,2, (d) LI, and (e) FDI. Note the smooth south eastern edge of infestation, matches prevailing winds at that time of year.

There were a number of cues for the visual interpretation of communities dominated by the floating fern, *Salvinia molesta*. Infestations abutting open water exhibited a smooth edge on leeward side (south east in the Dry season). Objects displayed a smooth texture although containing patches of other vegetation. Infestations displayed as a dull drab green colour in a RGB image (Figure 4.10a). Table 4.9 lists some of the values for key features for the selected *Salvinia* object.

Table 4.9. Object feature values for selected *Salvinia* object.

Object	Object feature values	
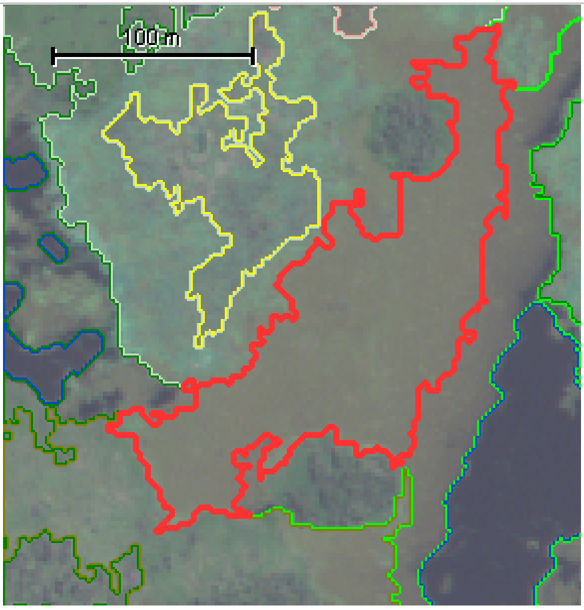	**Mean layer values**	
	Coastal	66.58
	Blue	222.12
	Green	670.87
	Yellow	828.83
	Red	676.05
	Red edge	2753.21
	NIR1	4076.17
	NIR2	4399.86
	Ratio values	
	EVI	1.371
	FDI	1424.53
	NDVI	0.7336
	LI	6930.95

4.1.9 *Eleocharis* sedgeland

The class, *Eleocharis*, dominated by the sedge, *Eleocharis dulcis* covers 1054 ha with larger areas mostly occupying the northern areas of the floodplain.

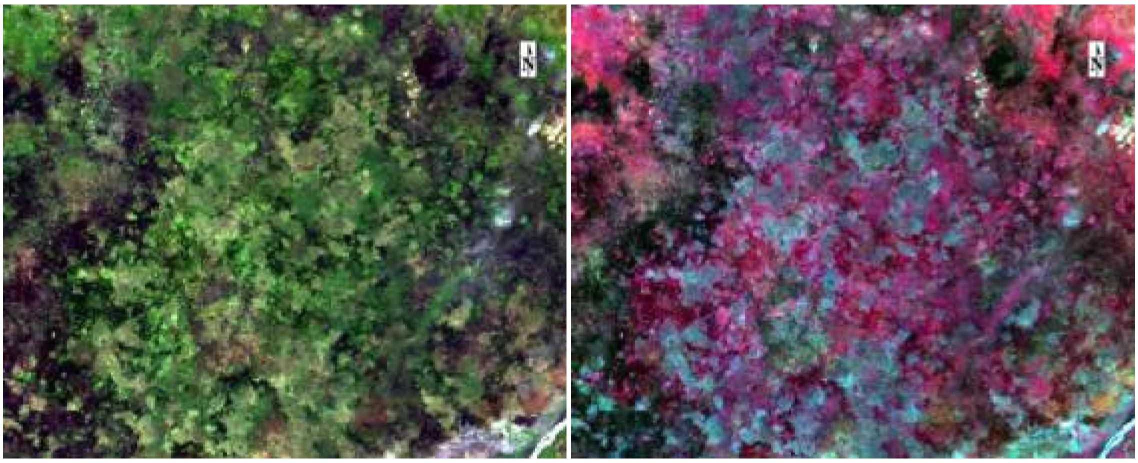

(a) (b)

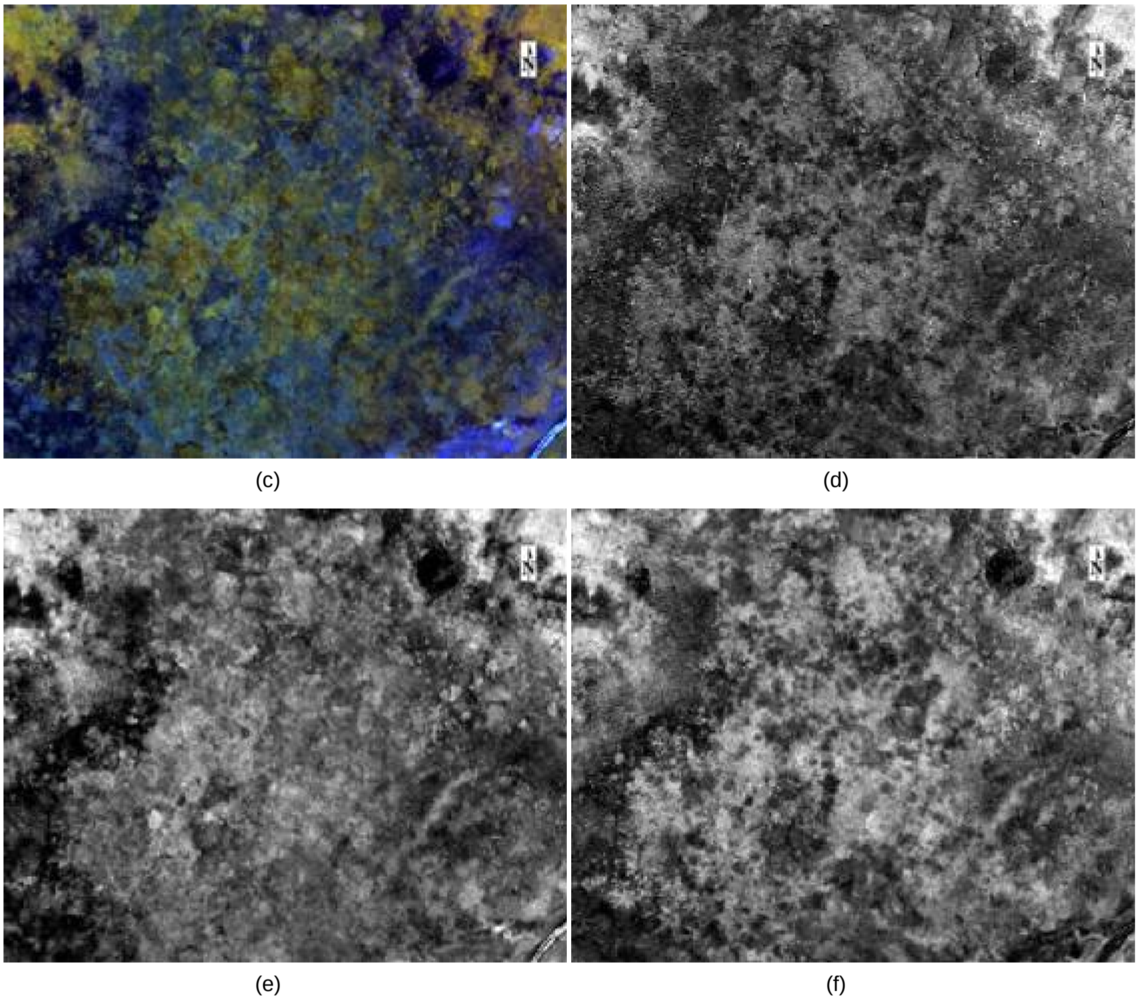

Figure 4.11 Image chip showing are of *Eleocharis*: (a) true colour RGB =5,3,2, (b) false colour RGB = 8,5,3, (c) false colour RGB = 8,6,2, (d) FDI, (e) LI and (f) EVI.

There were several key cues that assisted in the visual interpretation of *Eleocharis*. These included cover consisting of irregular and overlapping circles, intermingled with grass covers. The major regions for occurrence were in the backwater sections of the floodplain and downstream near East Alligator River. Objects containing *Eleocharis* were typically a dark green colour in RGB image. Table 4.10 lists some of the feature values of the selected *Eleocharis* object.

Table 4.10 Object feature values for selected *Eleocharis* sedgeland object.

Object	Object feature values	
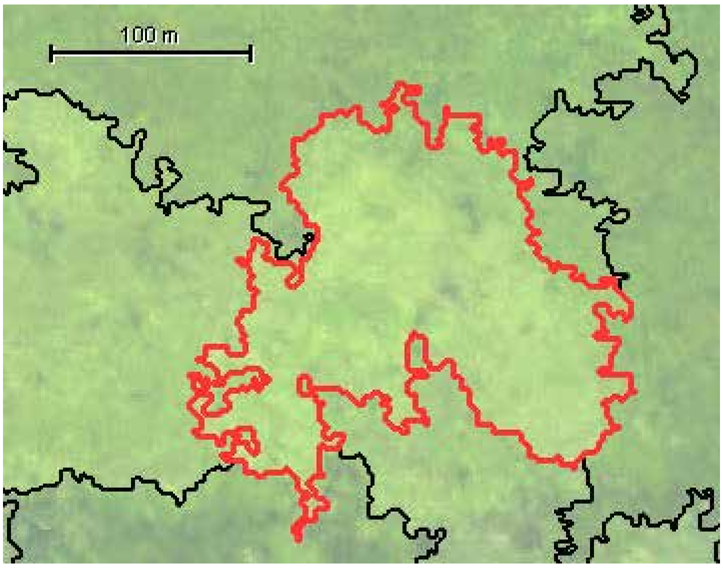	**Mean layer values**	
	Coastal	143.25
	Blue	316.74
	Green	696.68
	Yellow	898.10
	Red	906.91
	Red edge	2432.22
	NIR1	3467.80
	NIR2	3781.63
	Ratio values	
	EVI	1.049
	FDI	1032.67
	NDVI	0.6131
	LI	5897.1

4.1.10 *Leersia* grassland

The class, *Leersia* grassland covered 967 ha of the floodplain. Larger floating mats of *Leersia hexandra* can be found on the western border of Red Lily Swamp. As can be seen from Figure 4.12, the mats are distinctive, particularly in the LI image (Figure 4.12e).

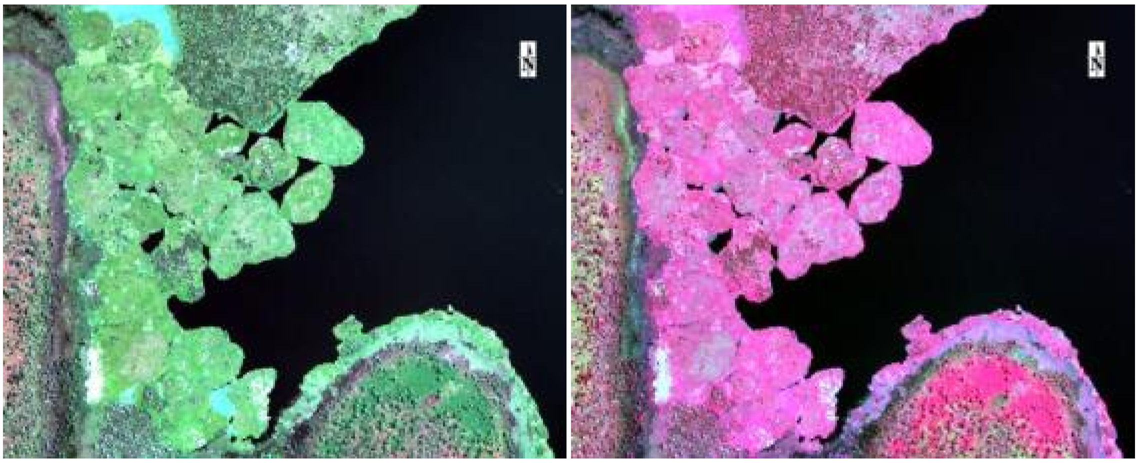

(a) (b)

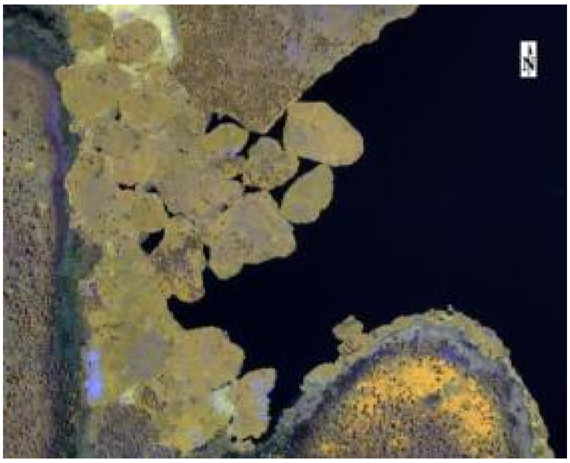

(c)

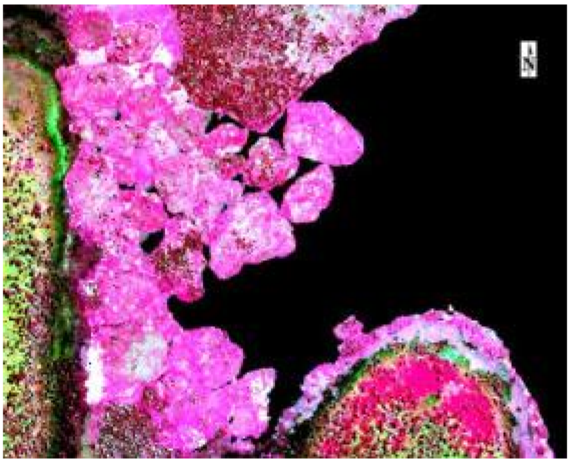

(d)

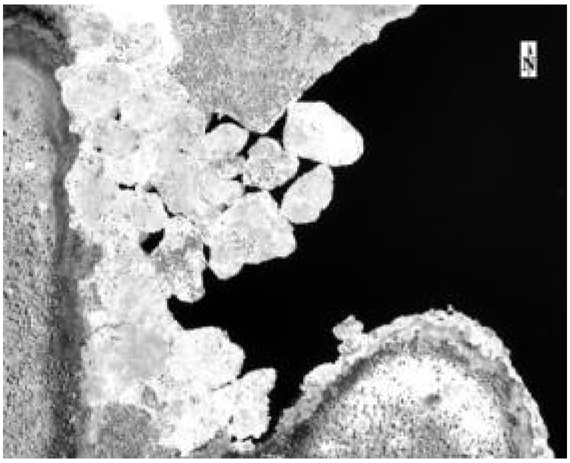

(e)

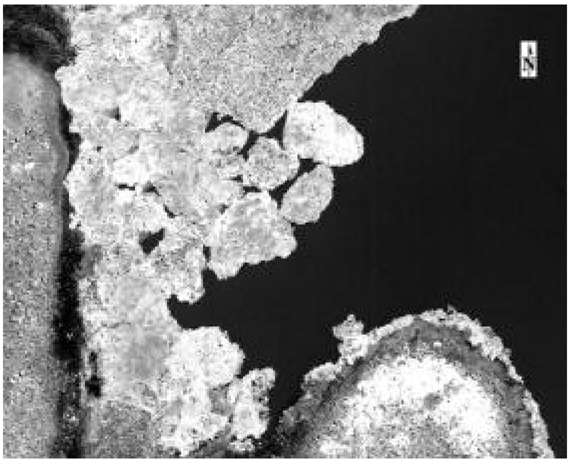

(f)

Figure 4.12 Leersia mats: (a) RGB = Bands 5,3,2, (b) RGB = 8,5,3, (c) RGB = 8,6,2, (d) RGB = Bands 6,5,3, (e) LI, and (f) FDI .

There were a number of cues useful for the visual interpretation of *Leersia* mats. The mats were generally elliptical in shape and display as light green in true colour image (Figure 4.12a). The mats are highly mobile when comparing imagery from different years. Some of the mats had a number of small trees growing on them. Most of the mats were located in the Red Lily Swamp in the western region of the floodplain. The mats appeared bright in LI image (Figure 4.12e) but not so in the FDI image (Figure 4.12f). Table 4.11 highlights some of the feature values for the selected *Leersia* object.

Table 4.11 Object feature values for selected *Leersia* object.

Object	Object feature value	
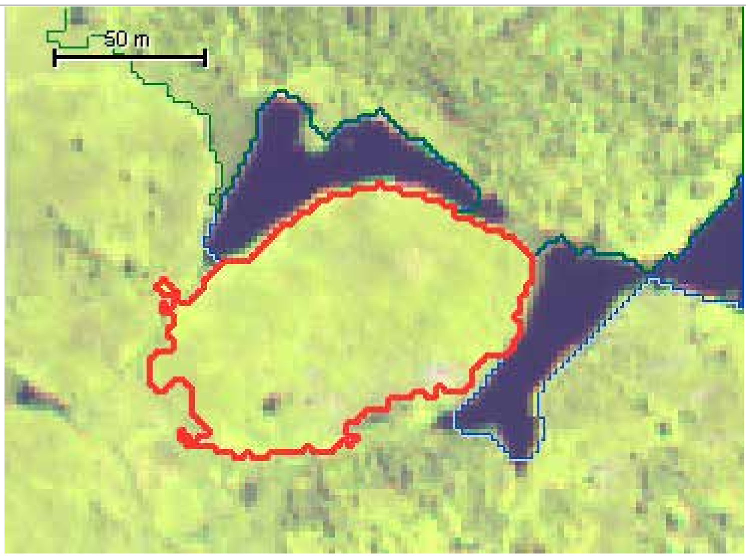	**Mean layer values**	
	Coastal	99.82
	Blue	235.07
	Green	711.67
	Yellow	627.28
	Red	461.81
	Red edge	2556.66
	NIR1	3862.26
	NIR2	4030.47
	Ratio values	
	EVI	1.770
	FDI	1238.73
	NDVI	0.7944
	LI	6352.06

4.1.11 Mangrove

The Mangrove community covered 249 ha, and is located mostly bordering the Magela Creek as it enters the East Alligator River.

(a)

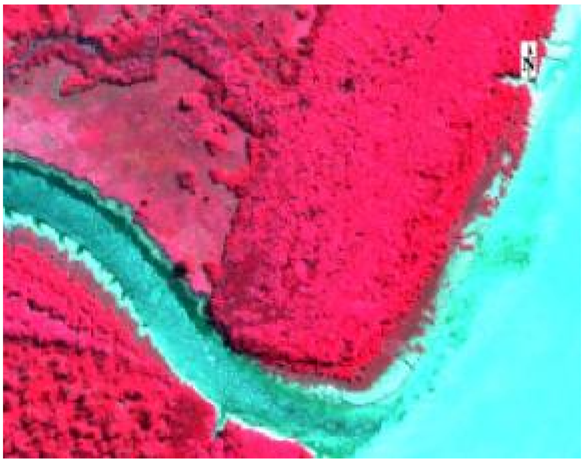

(b)

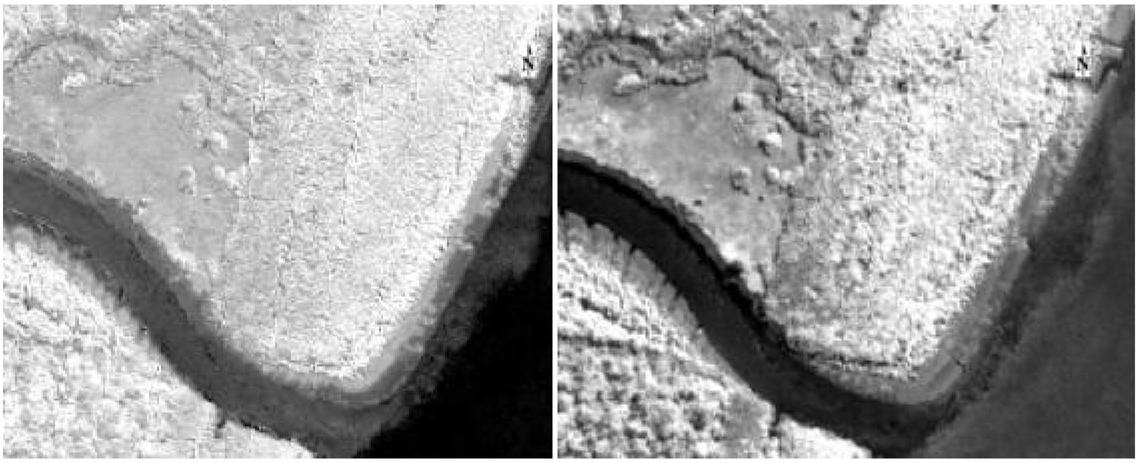

(c) (d)

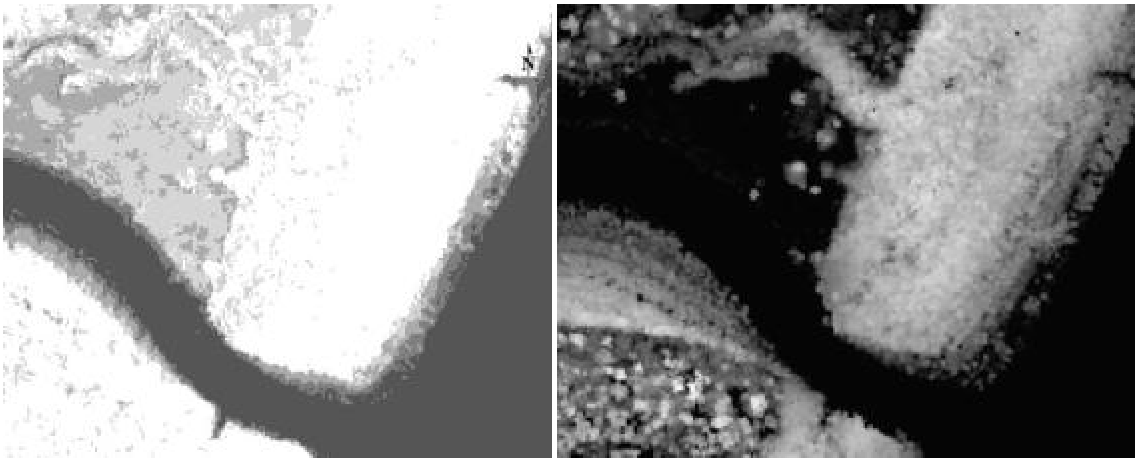

(e) (f)

Figure 4.13 Image chip showing Mangrove community: (a) true colour RGB = Bands 5,3,2, (b) false colour RGB = Bands 7,5,3, (c) FDI, (d) LI and (e) EVI, (f) CHM.

Key interpretive cues for mangroves included: Mangrove objects consisted of trees that were dark green and closely spaced in RGB image (Figure 4.13a), with a mostly overlapping canopy. Mangrove objects also tended to be adjacent to tidal influenced channels. The land cover displayed a fairly smooth texture with a regular pattern. Tree shadows were evident on the edges (Figure 4.13d). In the CHM image, mangroves could be distinguished from the surrounding woodland by texture (ie the dense canopy and similar heights of mangrove trees produced a smoother texture) (Figure 4.13f). Table 4.12 displays the feature values for the selected mangrove object.

Table 4.12 Object feature values for selected Mangrove object.

Object	Object feature value
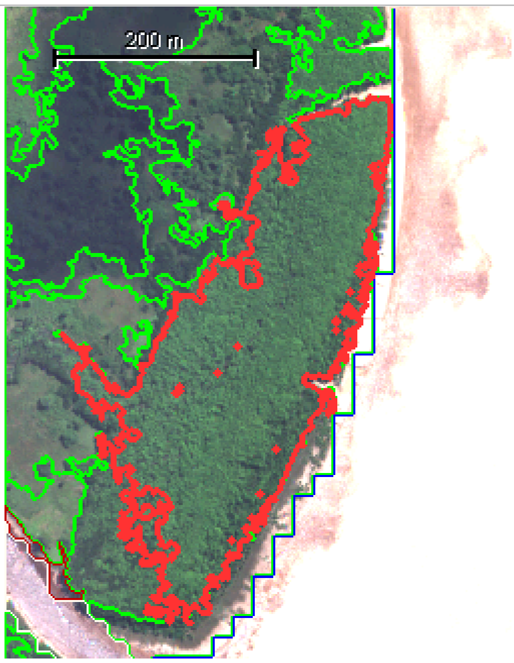	**Mean layer values** Coastal 32.66 Blue 123.83 Green 501.17 Yellow 381.12 Red 175.18 Red edge 2518.3 NIR1 4286.96 NIR2 4231.93 **Ratio values** EVI 2.329 FDI 1589.8 NDVI 0.9205 LI 6626.4 **Relative area of sub objects** Trees 98%

4.2 Accuracy assessment

The confusion matrix comparing reference data to the classification is displayed in Table 4.13. Overall accuracy for the map is 77.8%. User's and Producer's accuracies for each class are shown in Table 4.14. Based on the reference data, the most accurately delineated classes were *Leersia*, *Melaleuca* woodland and Para Grass with Producer's accuracies of 80.1%, 90%, and 87.5%, and User's accuracies of 100%, 90% and 87.5% respectively. The Mangrove and *Melaleuca* open forest classes also had high accuracies (Producer's accuracies of 100% and User's accuracies of 75%) however, the total number of reference samples for each of these classes was quite low (3 each). A low Producer's accuracy (57.9%) indicates there was confusion where *Eleocharis* was misclassified as *Hymenachne* (4 instances), *Oryza* (2 instances), Mangroves or *Melaleuca* woodland (both 1 instance). Of those classes with low User's accuracies, 24 sites that where classed as *Hymenachne*, 9 were other classes according to the reference data with 4 being *Eleocharis*. In addition, there was some confusion between the *Pseudoraphis*/*Hymenachne* class and the separate *Pseudoraphis* and *Hymenachne* classes.

Table 4.13 Confusion matrix for the 2010 Magela Creek floodplain vegetation map.

		Reference data													
		El	Hy	Le	Ma	MOF	MW	Ne	Or	PG	PH	Ps	S	W	Total
Classified data	El	11	1	0	0	0	0	0	0	0	0	0	0	0	12
	Hy	4	15	0	0	0	1	0	1	1	1	0	1	0	24
	Le	0	0	4	0	0	0	0	0	0	0	0	0	0	4
	Ma	1	0	0	3	0	0	0	0	0	0	0	0	0	4
	MOF	0	0	0	0	3	0	0	0	0	0	0	0	1	4
	MW	1	2	2	0	0	5	0	0	0	0	0	0	0	10
	Ne	0	0	1	0	0	0	5	0	0	0	0	0	1	7
	Or	2	0	0	0	0	0	0	6	0	0	0	0	0	8
	PG	0	1	0	0	0	0	0	0	7	0	0	0	0	8
	PH	0	1	0	0	0	0	0	0	0	13	2	2	0	18
	Ps	0	0	0	0	0	0	0	0	0	2	5	0	1	8
	S	0	0	0	0	0	0	0	0	0	0	0	8	2	10
	W	0	0	0	0	0	0	0	0	0	0	0	0	9	9
	Total	19	20	7	3	3	6	5	7	8	16	7	11	14	126
Overall Accuracy		98/126 = 77.8%													

Note: El=Eleocharis, Hy=Hymenachne, Le=Leersia, Ma=mangrove, MOF=Melaleuca open forest, MW=Melaleuca woodland, Ne=Nelumbo, Or=Oryza, PG=Para grass, PH= Pseudoraphis/Hymenachne, Ps=Pseudoraphis, S=Salvinia, W=water.

Table 4.14 Producer and User accuracies for each vegetation community class (plus water), based on confusion matrix results displayed in Table 4.13.

Class name	**Producer's accuracy**	**User's Accuracy**
Eleocharis	57.9	91.7
Hymenachne	83.3	62.5
Leersia	80.1	100.0
Mangrove	100.0	75.0
Melaleuca open forest	100.0	75.0
Melaleuca woodland	90.0	90.0
Nelumbo	100.0	71.4
Oryza	85.7	75.0
Para grass	87.5	87.5
Pseudoraphis/*Hymenachne*	81.3	72.2
Pseudoraphis	71.4	62.5
Salvinia	72.7	80.0
Water	64.3	100.0

5 Discussion

The vegetation classification process was able to distinguish between the spectrally and structurally distinct vegetation communities within the floodplain. The use of multiple indices and ratios were able to mostly differentiate between classes that appeared spectrally similar. From the results of the confusion matrix, there were a number of instances where objects were either not detected or misclassified. There was some difficulty in distinguishing between vegetation classes that are spectrally similar, most notably between the classes dominated by grasses. Previously, there has been noted some spectral similarity between different covers namely *Oryza* and Para grass (Boyden et al. 2007). In addition, there were objects that were of the same class that were spectrally different. This is possibly due to differences in growth phases as a result of water availability. For example, grasses on the edge of the floodplain will dry out quicker and either die or senesce earlier than those in the in the centre of the floodplain with access to water longer.

Due to sun glint it was difficult to detect open water and floating vegetation within Region 1. In addition, due to changes in reflectance associated with the view angle, the class rulesets developed for Regions 2 and 3 did not satisfactorily detect the classes in Region 1. This required a modified set of rules and threshold values for Region 1. Future data requests for WV-2 imagery need to ensure that imagery captured on a certain date has a consistent view angle, satellite azimuth and elevation. This may require a slight narrowing of the study area so that the image can be captured along a single path.

Although unable to successfully delineate the floodplain boundary using a simple height threshold based, the DEM data was useful in providing an initial delineation of the floodplain boundary that could be easily manually adjusted. This would have not been possible using only WV-2 imagery due to spectral similarities between floodplain and non-floodplain surfaces. However, both DEMs appear to contain uncertainty in elevation associated primarily with vegetation effects, consequently the boundary was not as accurate as was required and a manual modification of the boundary was necessary based upon visual interpretation of the multispectral imagery. This was possibly due to 30 m GSD of the SRTM DEM being too coarse a resolution whereas the 10 m aerial photograph derived DEM appeared to suffer from vegetation effects.

This report also highlights the development of the interpretive key. After decades of research and sporadic mapping the Magela Creek floodplain vegetation, this report contains the first documented attempt to provide key visual and image based cues for the interpretation and classification of vegetation within the Magela Creek floodplain. The key will be a valuable tool in the development of an ongoing systematic monitoring program for the floodplain.

The classification of HSR imagery does lead to an interesting problem associated with the scale and resolution. The high resolution (GSD = 2 m) of the WV-2 imagery produces a map scale including a level of detail that may mean some small objects only contain one individual of a species. For example, an object of 25 pixels that has been classified as *Melaleuca* open forest may in fact be a single tree. Objects of this scale may not be suitable for broader landscape analysis, therefore classes will need to be less broad in their inclusion and more specific and can describe an individual organism of a single species. Thus describing a class as a community dominated by a certain taxa may not be appropriate at finer scales.

The vegetation map within this report is representative of the vegetation that was on the floodplain in May 2010. The seasonal variation that is known to occur has not been captured on this map, such as changes in community composition associated with the water level and soil moisture in the floodplain. This mapping would be difficult to achieve, although (Boyden et al. 2013) achieved it to an extent for the 2006 dry season using Landsat data. For a large interval of the year, suitable quality data is unavailable due to either cloud cover or smoke haze and as the year progresses so does the area of fire affected land cover . In addition, using HSR data from a commercial satellite means data collection of such intensity will be cost prohibitive. As a result of the map being based on data from one date, the seasonal and inter-annual variation as described in the literature (e.g. Finlayson et al. 1989, Boyden et al. 2013) has not been captured in this map. The amount and periodicity of rainfall varies annually leading to different water levels and soil moisture availability means community distributions can vary greatly between years.

For reference data, it would be preferable to have more points to increase the rigour of the accuracy assessment, as several of the classes have limited reference data. However, gaining sufficient reference data is difficult to achieve using standard observation techniques due to accessibility issues associated with the landscape and the remote location, and resource limitations. For HSR image analysis, a number of studies have used the visual analysis of the base imagery to provide sufficient reference data for ground truthing providing what has been referred to as a pseudo accuracy assessment (Congalton & Green 2009). While this may be possible to undertake for easily discernible land covers, spectrally and texturally similar vegetation may be difficult to differentiate resulting in error. Further bias may be introduced by user influence (Foody 2002). New techniques for reference data collection using helicopter based GPS enabled videography and still photography at higher spatial resolutions than the satellite imagery will be trialled for future data captures to enable increased number of reference sites relative to field sampling effort.

5.1 Advantages and limitations of incorporating a CHM as part of the data set.

The inclusion of the CHM from the 2011 LiDAR data was extremely useful in discriminating between treed and non-treed vegetation cover classes. During the early development stage it was difficult to distinguish between *Melaleuca* classes and spectrally similar non-treed vegetation. Consequently on the map produced there was some confusion between these classes. This confusion occurred particularly where tree density was low, but also where objects of non-treed vegetation had similar spectral, spatial and textural features to treed objects. This issue was virtually eliminated using the CHM to define the treed classes.

One disadvantage, however, was that the CHM did not cover the entire area of Magela Creek floodplain with some upper reaches and backwater swamps being excluded from the coverage. Unfortunately, these areas are mostly treed. The treed classes on the areas outside the CHM were able to be discriminated using the spectral classification process. Another disadvantage in using the CHM was the difference in the dates of capture between the CHM and the WV-2 imagery (May 2010 for imagery and October 2011 for the LiDAR data). Therefore, an assumption was made that there was little change in tree cover during that time.

5.2 Advantages and limitations of WV-2 multispectral data for mapping wetlands

A spatial advantage of using WV-2 data is the resolution (2m GSD). Individual pixels within the data are generally one type of land cover or plant species. This is in contrast to data from moderate spatial resolution RS data (such as Landsat), where pixels may comprise multiple land cover or vegetation types. Thus, the spatial resolution of the WV-2 imagery was sufficient to readily identify most plants visually, which then provided some clues as to what to include in a class rule. In addition, the HSR data enables the analyst to readily identify class boundaries between classes that are spectrally distinct.

A spectral advantage of using WV-2 data is the inclusion of the red edge band which was found to be useful in vegetation analysis and discrimination, and consequently was included in two of the four indices used to classify objects into various communities.

Although containing 8 spectral bands, the WV-2 multispectral data only covers the VNIR (400–1050 nm) portion of the EM spectrum. The limited spectral range can inhibit spectral discrimination between classes. For example, information from the shortwave infrared (1400–1600 nm) can be useful in deriving the hydrological conditions that differentiate vegetation classes (Boyden et al. 2013). Using an image from a single date also limits opportunities to use the spectral variation of plant growth stages for discrimination between classes. The lack of temporal resolution means that the phenology of floodplain vegetation such as the grasses is limited as a tool for differentiation. Additionally, if imagery were acquired at intervals that could display the phenology of the different grasses, then cost becomes a limiting factor due to WV-2 being a commercial satellite.

Another limiting factor of using WV-2 data to consider is the potential variation in off-nadir sensor angles between multi-date imagery. The variation can make it difficult to compare between dates because even if radiometric calibration corrects for atmospheric effects, the differing view angle and relative position of the sun, some land covers will differ greatly in their spectral signature. Examples include highly reflective surfaces and vegetation with particular leaf angles.

5.3 Advantages and limitations of using a GEOBIA methodology.

There are a number of advantages in using a GEOBIA methodology including repeatability and semi –automation of the process. Once written a process is consistently repeatable, therefore rerunning the ruleset using the same parameters on the same data provides exactly same results. The ruleset is transparent in that the steps are visible and easy for any trained operator to follow. Once a rule set has been created and tested the classification procedure then becomes a semi-automated approach and can be implemented on other imagery with minimal adjustments to thresholds required. The iterative step wise approach enables a decision tree approach to classification, thus allows the input of expert knowledge of the land covers within the study area into the classification process.

The limitations of using a GEOBIA methodology include the software required to run a GEOBIA classification can be computer resource intensive and it may take a long time to process data unless the data is split into smaller regions. The rule sets for classifying such a heterogeneous landscape as the Magela Creek floodplain can take a long time to create and refine. However once a ruleset has been written and tested, it is readily transferrable to imagery over the study area from different dates although threshold values may need altering (due to differences in spectral information between images). The GEOBIA method also requires an *a priori* knowledge of the land covers and their features. This may not be possible if a researcher has limited or no experience in the region. As such, a successful classification relies on the extensive body of knowledge of Magela floodplain vegetation within the organisation that has been developed over many years of research.

A method that uses accurate training samples and a supervised statistical classifier such as Support Vector Machines (Cristianini & Shawe-Taylor 2000) or Random Forests ® (Breiman 2001), would reduce the need for expert knowledge in the classification; however the availability of reference data for this study was limited to 128 samples. This number of samples was not enough to provide both sufficient training and testing samples so all were used for testing.

6 Conclusion

This research highlights the application of GEOBIA for mapping variable floodplain vegetation using WorldView-2 high spatial resolution imagery. The method used produced a vegetation map of the Magela Creek floodplain for May 2010. Based on the field reference data the overall accuracy of the map was 78% with the majority of error being associated with confusion between classes that were spectrally similar but dominated by different species. The map, however, does not account for the temporal variability (seasonal or annual) of the extent and distribution of the communities. Due to the repeatability and semi-automated approach the method of iterative segmentation and classification based on spectral indices will be applied to mapping the floodplain vegetation in subsequent years to monitor the annual variation in distribution and extent of the communities. By applying relative measures (such as spectral indices) as opposed to absolute values (such as band values), we anticipate the rule set will be transferrable with minor threshold tweaks associated with radiometric differences as associated with growth as well as sun and view angle differences. Therefore the approach will be applied to imagery captured for May 2011, June 2012 and June 2013 and will form an integral component of an operational landscape scale off-site monitoring program.

Analysis will provide a quantitative measure of the interannual variation described previously in the literature but not measured (Finlayson et al. 1989). The program will enable quantitative analysis of the temporal and spatial change in vegetation communities within the downstream receiving environment for Ranger Uranium Mine. Future research may demonstrate the ability to link the monitoring of the health of vegetation communities using satellite imagery with the effects of mine rehabilitation.

7 References

Adam E, Mutanga O & Rugege D 2010. Multispectral and hyperspectral remote sensing for identification and mapping of wetland vegetation: a review. *Wetlands Ecology and Management* 18 (3), 281–296.

Adler-Golden SM, Matthew MW, Bernstein LS, Levine RY, Berk A, Richtsmeier SC, Acharya PK, Anderson GP, Felde G, Gardner J et al. 1999. Atmospheric correction for short-wave spectral imagery based on MODTRAN4. *SPIE Proceedings on Imaging Spectometry* 3753, 61–69.

Andersen AN, Cook GD & Williams RJ (eds) 2003. *Fire in Tropical Savannas: The Kapalga Experiment*. Springer-Verlag, New York.

Baatz M & Schäpe A 2000. Multiresolution segmentation - an optimization approach for high quality multi-scale image segmentation. In *Angewandte Geographische Informationsverarbeitung XII*, eds J Strobl, T Blaschke & G Griesebner, Wichmann-Verlag, Heidelberg, 12–23.

Bartolo R, Wasson R, Valentine E, Cleland S, Bayliss P & Winderlich S 2008. Climate change – The status of climate change research in the Kakadu landscape context. In *Kakadu National Park Landscape Symposia Series 2007–2009. Symposium 1: Landscape Change Overview, 17–18 April 2007*, eds DJ Walden & S Nou, Internal Report 532, Supervising Scientist, Darwin, 84–96.

Bayliss P, van Dam RA & Bartolo RE 2012. Quantitative ecological risk assessment of the Magela Creek floodplain in Kakadu National Park, Australia: comparing point source risks from the Ranger Uranium Mine to diffuse landscape-scale risks. *Human and Ecological Risk Assessment* 18 (1), 115–151. doi: 10.1080/10807039.2012.632290.

Bayliss P & Yeomans KM 1990. Seasonal distribution and abundance of magpie geese, *Anseranus semipalmata* Latham, in the Northern Territory and their relationship to habitat, 1983-1986. *Australian Wildlife Research* 17, 15–38.

Bellio MG, Bayliss P & Dostine P 2004. Landscape-scale analysis of the value of waterbirds in the Alligator Rivers Region, northern Australia. Internal Report 445, March, Supervising Scientist, Darwin.

Benz U, Hofmann P, Willhauck G, Lingenfelder I & Heynen M 2004. Multi-resolution, object-oriented fuzzy analysis of remote sensing data for GIS-ready information. *ISPRS Journal of Photogrammetry and Remote Sensing* 58 (3-4), 239–258.

Beringer J, Hutley LB, Tapper NJ & Cernusak LA 2007. Savanna fires and their impact on net ecosystem productivity in North Australia. *Global Change Biology* 13 (5), 990-1004.

Berk A, Anderson GP, Acharya PK, Bernstein LS, Muratov L, Lee J, Fox M, Adler-Golden SM, Chetwynd Jr JH & Hoke ML 2006. MODTRAN 5- 2006 update. *SPIE Proceedings, Algorithms and Technologies for Multispectral, Hyperspectral, and Ultraspectral Imagery XII* 6233, 508–515.

Blaschke T 2010. Object based image analysis for remote sensing. *ISPRS Journal of Photogrammetry and Remote Sensing* 65, 2–16.

Blaschke T & Hay GJ 2001. Object-oriented image analysis and scale-space: theory and methods for modelling and evaluating multiscale landscape structure. *International Archives of Photogrammetry and Remote Sensing* 34 (4/W5), 22–29.

Blaschke T & Strobl J 2001. What's wrong with pixels? Some recent developments interfacing remote sensing and GIS. *GeoBIT/GIS* 6 (1), 12–17.

Boyden J, Joyce KE, Boggs G & Wurm P 2013. Object-based mapping of native vegetation and para grass (*Urochloa mutica*) on a monsoonal wetland of Kakadu NP using a Landsat 5 TM Dry-season time series. *Journal of Spatial Science* 58 (1), 53–77. doi: 10.1080/14498596.2012.759086.

Boyden JM, Walden DJ, Bartolo R & Bayliss P Utility of VHR remote sensing data for landscape assessment of the environmental weed para grass [*Urochloa mutica*, (Forssk)]. In *Asian Conference on Remote Sensing*. Kuala Lumpur, Malaysia 12-16 November, Malaysian Centre for Remote Sensing and Ministry of Science (MACRES), Technology and Innovation (MOSTI), Malaysia, Kuala Lumpur, Malaysia.

Breiman L 2001. Random forests. *Machine Learning* 45, 5–32.

Bunting P & Lucas R 2006. The delineation of tree crowns in Australian mixed species forests using hyperspectral Compact Airborne Spectrographic Imager (CASI) data. *Remote Sensing of Environment* 101 (2), 230–248.

Clevers J, De Jong S, Epema G, Van der Meer F, Bakker W, Skidmore A & Scholte K 2002. Derivation of the red edge index using the MERIS standard band setting. *International Journal of Remote Sensing* 23 (16), 3169–3184.

Congalton RG & Green K 2009. *Assessing the accuracy of remotely sensed data: principles and practices.* 2nd edn, CRC Press, Boca Raton, Fl.

Cowie ID, Finlayson CM & Bailey BJ 1988. Alien plants in the Alligator Rivers Region, Northern Territory, Australia Technical Memorandum Technical Memorandum 23, 1988, Supervising Scientist, Canberra.

Cowie ID, Short PS & Osterkamp Madsen M 2000. *Floodplain Flora: A Flora of the Coastal Floodplains of the Northern Territory, Australia.* ABRS/PWCNT, Canberra/Darwin.

Cracknell AP 1998. Synergy in remote sensing-what's in a pixel? *International Journal of Remote Sensing* 19 (11), 2025–2047.

Cristianini N & Shawe-Taylor J 2000. *An introduction to support vector machines and other kernel-based learning methods.* Cambridge University Press, Cambridge.

Devhari A & Heck RJ 2009. Comparison of object-based and pixel based infrared airborne image classification methods using DEM thematic layer. *Journal of Geography and Regional Planning* 2 (4), 86–96.

Filella I & Penuelas J 1994. The red edge position and shape as indicators of plant chlorophyll content, biomass and hydric status. *International Journal of Remote Sensing* 15 (7), 1459–1470.

Finlayson CM 2005. Plant ecology of Australia's tropical floodplain wetlands: a review. *Annals of Botany* 96 (4), 541–555.

Finlayson CM, Bailey BJ & Cowie ID 1989. Macrophyte vegetation of the Magela Creek flood plain, Alligator Rivers Region, Northern Territory. Research Report 5, April 1989, Supervising Scientist, Canberra.

Finlayson CM, Cowie ID & Bailey BJ 1990. Characteristics of a seasonally flooded freshwater system in monsoonal Australia. In *Wetland Ecology and Management: Case studies*, eds RE Good & J Kvet, Kluwer Academic Publishers, Dordrecht, The Netherlands, 141–162.

Finlayson CM, Lowry J, Grazia Bellio M, Nou S, Pidgeon RWJ, Walden DJ, Humphrey C & Fox G 2006. Biodiversity of the wetlands of the Kakadu Region, northern Australia. *Aquatic Sciences* 68 (3), 374–399.

Fisher P 1997. The pixel: a snare and a delusion. *International Journal of Remote Sensing* 18 (3), 679–285.

Foody GM 2002. Status of land cover classification accuracy assessment. *Remote Sensing of Environment* 80, 185–201.

Hay GJ, Blaschke T, Marceau DJ & Bouchard A 2003. A comparison of three image-object methods for the multi-scale analysis of landscape structure. *ISPRS Journal of Photogrammetry and Remote Sensing* 57, 327–345.

Hay GJ & Castilla G 2008. Geographic Object-Based Image Analysis (GEOBIA): A new name for a new discipline. In *Object-based image analysis - Spatial Concepts for Knowledge-Driven Remote Sensing Applications*, eds T Blaschke, S Lang & GJ Hay, Springer Verlag, Berlin, 75–89.

Hay GJ, Castilla G, Wulder MA & Ruiz JR 2005. An automated object-based approach for the multiscale image segmentation of forest scenes. *International Journal of Applied Earth Observation and Geoinformation* 7, 339–359.

Hayder K 2001. Study of remote sensing and GIS for the assessment of their capabilities in mapping the vegetation form and structure of tropical savannas in Northern Australia. PhD thesis, Northern Territory University, Darwin.

Herold M, Woodcock CE, Loveland TR, Townshend J, Brady M, Steenmans C & Schmullius CC 2008. Land-Cover Observations as Part of a Global Earth Observation System of Systems (GEOSS): Progress, Activities, and Prospects. *Systems Journal, IEEE* 2 (3), 414–423. doi: 10.1109/JSYST.2008.925983.

Hnatiuk RJ, Thackway R & Walker J 2009. Vegetation. In *Australian Soil and Land Survey Field Handbook*, 3rd edn, Australian Soil and Land Survey Handbooks, CSIRO, Melbourne.

Huete AR, Didan K, Miura T, Rodriguez EP, Gao X & Ferreira LG 2002. Overview of the radiometric and biophysical performance of the MODIS vegetation indices. *Remote Sensing of Environment* 83 (1–2), 195–213.

Isbell RF 1996. *The Australian Soil Classification.* Australian Soil and Land Survey Handbooks, Vol. 4, CSIRO Australia, Collingwood.

Jawak SD & Luis AJ 2013. Improved land cover mapping using high resolution multiangle 8-band WorldView-2 satellite remote sensing data. *Journal of Applied Remote Sensing* 7 (1), 073573-073573. doi: 10.1117/1.JRS.7.073573.

Johansen K, Arroyo LA, Armston J, Phinn S & Witte C 2010. Mapping riparian condition indicators in a sub-tropical savanna environment from discrete return LiDAR data using object-based image analysis. *Ecological Indicators* 10 (4), 796–807.

Johansen K, Phinn S, Lowry J & Douglas M 2008. Quantifying indicators of riparian condition in Australian tropical savannas: integrating high spatial resolution imagery and field survey data. *International Journal of Remote Sensing* 29 (23), 7003–7028.

Kay S, Hedley J & Lavender S 2009. Sun glint correction of high and low spatial resolution images of aquatic scenes: a review of methods for visible and near-infrared wavelengths. *Remote Sensing* 1 (4), 697–730.

Lymburner L, Tan P, Mueller N, Thackway R, Lewis A, Thankappan M, Randall L, Islam A & Senarath U 2011. The National Dynamic Land Cover Dataset. Record 2011/31, Geoscience Australia, Symonston, ACT.

Moffett KB & Gorelick SM 2012. Distinguishing wetland vegetation and channel features with object-based image segmentation. *International Journal of Remote Sensing* 34 (4), 1332–1354. doi: 10.1080/01431161.2012.718463.

Morley AW (ed) 1981. *A review of Jabiluka environmental studies*. Pancontinental Mining Limited, Sydney.

Mutanga O, Adam E & Cho MA 2012. High density biomass estimation for wetland vegetation using WorldView-2 imagery and random forest regression algorithm. *International Journal of Applied Earth Observation and Geoinformation* 18 (0), 399-406. doi: http://dx.doi.org/10.1016/j.jag.2012.03.012.

Riley J & Lowry J 2002. An initial assessment of changes to Melaleuca distribution on a selected area of the Magela floodplain using aerial photography. Internal Report 394, September, Supervising Scientist, Darwin.

Roberts SJ 1997. Gunak, gapalg dja gungod ('Fire, floodplain and paperbark'): a study of fire behaviour in the Melaleuca-flooplain communities of Kakadu National Park, Northern Territory, Australia. PhD thesis, University of London, London.

Rossiter NA, Setterfield SA, Douglas MM & Hutley LB 2003. Testing the grass-fire cycle: alien grass invasion in the tropical savannas of northern Australia. *Diversity and Distributions* 9, 169–176.

Rouse JW, Haas RH, Schell JA & Deering DW 1973. Monitoring vegetation systems in the Great Plains with ERTS. In *Proceedings of the 3rd ERTS Symposium*. NASA, 309–317.

Russell-Smith J, Needham S & Brock J 1995. The physical environment. In *Kakadu: natural and cultural heritage and management*, eds T Press, D Lea, A Webb & A Graham, Australian Nature Conservation Agency & North Australian Research Unit, Australian National University, Darwin, 94–126.

Sanderson NT, Koontz DV & Morley AW 1983. The ecology of the vegetation of the Magela Creek floodplain: upper section from Oenpelli road crossing to Nankeen Billabong. Paper presented at *Scientific Workshop on Environment Protection in the Alligator Rivers Region*. Jabiru 17–20 May 1983.

Schaeffer M, Hare W, Rahmstorf S & Vermeer M 2012. Long-term sea-level rise implied by 1.5° C and 2° C warming levels. *Nature Climate Change* 2 (12), 867–870. doi:

http://www.nature.com/nclimate/journal/v2/n12/abs/nclimate1584.html#supplementary-information.

Saynor, MJ & Erskine, WD 2013. Classification of river reaches on the little disturbed East Alligator River, northern Australia. *International Journal of Geosciences* 4, 53–65.

Staben G 2008. Mapping the spatial and temporal distribution of *Melaleuca* spp. on the Magela floodplain between 1950 and 2004 using object-based analysis and GIS. Internal Report 545, June, Supervising Scientist, Darwin.

Staben G, Pfitzner K, Bartolo R & Lucieer A 2012. Empirical line calibration of WorldView-2 satellite imagery to reflectance data using quadratic prediction equations. *Remote Sensing Letters* 3 (6), 521–530.

Story M & Congalton RG 1986. Accuracy assessment - a user's perspective. *Photogrammetric Engineering and Remote Sensing* 52 (3), 397–399.

Story R 1976. Vegetation of the Alligator Rivers area. In *Lands of the Alligator Rivers area, Northern Territory*, Land Research Series No. 38, Commonwealth Scientific and Industrial Research Organisation, Melbourne, 89–110.

Trimble 2012. *eCognition Developer 8.8 Reference Book*. Trimble, Munich, Germany.

Updike T & Comp C 2010. Radiometric use of WorldView-2 imagery, Longmont, Colorado, USA.

Walden D, Boyden J, Bayliss P & Ferdinands K 2012. *A preliminary ecological risk assessment of the major weeds on the Magela Creek floodplain, Kakadu National Park*. SSR, Supervising Scientist Division, Darwin NT.

Wasson RJ & Bayliss P 2010. River flow and climate in the 'Top End' of Australia for the last 1000 years, and the Asian-Australian monsoon. In *Kakadu National Park Landscape Symposia Series 2007–2009. Symposium 4: Climate change*. Gagudju Crocodile Holiday Inn, Kakadu National Park 6–7 August 2008, ed S Winderlich, Internal Report 567, January, Supervising Scientist, 15–36.

Whiteside T, Bartolo R, Pfitzner K & Staben G 2013. Geometric and radiometric correction of WorldView-2 satellite imagery. Internal Report 617, May, Supervising Scientist, Darwin.

Whiteside TG, Boggs GS & Maier SW 2011. Comparing object-based and pixel-based classifications for mapping savannas. *International Journal of Applied Earth Observation and Geoinformation* 13 (6), 884–893.

Willhauck G, Schneider T, De Kok R & Ammer U 2000. Comparison of object oriented classification techniques and standard image analysis for the use of change detection between SPOT multispectral satellite images and aerial photos. In *ISPRS Archives, Vol. XXXIII*, Amsterdam.

Williams A 1979. Vegetation and stream pattern as indicators of water movement on the Magela Floodplain, Northern Territory. *Australian Journal of Ecology* 4, 239–247.

Williams AR 1984. Changes in Melaleuca forest density on the Magela floodplain, Northern Territory, between 1950 and 1975. *Australian Journal of Ecology* 9 (3), 199–202. doi: 10.1111/j.1442-9993.1984.tb01357.x.

Wulder MA, Hall RJ, Coops NC & Franklin SE 2004. High spatial resolution remotely sensed data for ecosystem characterization. *BioScience* 54 (6), 511–521.

Appendix A

Project data is located in the following folders:

Vegetation map

\\pvnt01flpr01\nas2\2010_Magela_veg_map\GIS\veg_map

WV-2 image data

\\pvnt01flpr01\gis\MASTER_RASTER\Magela\WorldView2\2010-05-11

Image mosaic

\\pvnt01flpr01\nas2\2010_Magela_veg_map\Mosaic

CHM data

\\pvnt01flpr01\nas2\2010_Magela_veg_map\CHM

Floodplain boundary data

\\pvnt01flpr01\nas2\2010_Magela_veg_map\GIS\fp_bound

eCognition project file and process tree

\\pvnt01flpr01\nas2\2010_Magela_veg_map\eCog_project

\\pvnt01flpr01\nas2\2010_Magela_veg_map\ecog_ruleset

Appendix B

Descriptions of the major vegetation communities within the Magela Creek floodplain.

B.1 *Eleocharis* spp. sedgeland

Eleocharis sedgelands (Figure B.1) are dominant in the Wet season but are usually replaced by herblands (such as *Phyla nodiflora* and *Heliotropium indicum*) during the Dry season. This community occurs in shallow flooded areas mostly in the northern portion the floodplain. For most species of *Eleocharis*, flowering is from May to September while fruiting is April to September. The growth habit of *E. dulcis*, the most common species of *Eleocharis* on the floodplain, grows to 1 m tall but tends to be smaller in shallower water with some saline influence (Cowie et al. 2000). *E. sphacelata* grows to 1.5 m.

Figure B.1 *Eleocharis* sedgeland indicated by the areas of darker green vegetation.

B.2 Oryza spp. (wild rice) grassland

The dominant annual, *Oryza meridionalis* is at its vegetative peak toward the end of the wet season. Plants can be between 0.3 and 2 m tall with linear leaf blades 6-35 cm long (Cowie et al. 2000). In the Dry season, the grassland is mostly bare ground or dead stems (Figure B.2). *O. meridionalis* is germinated by early Wet season storms along with other annual species such as *Digitaria* sp., *Hygrochloa aquatica* and *Heliotropum indicum*. These species are reliant on flooding up to 1 m for successful establishment. Once flooding has commenced other species such as *Nymphaea* spp., *Nymphoides* spp. and *Eleocharis* spp. may occur amongst the grass. Flowering and fruiting occurs between April and August (Cowie et al. 2000). In the drying out phase there is an increased abundance of *Ludwigia adscendens* and a number of herbs (Finlayson et al. 1989).

Figure B.2 Oryza grassland as indicated by red arrow.

B.3 Pseudoraphis spinescens grassland

P. spinescens is a perennial emergent grass. In the Dry season it displays a turf like habit, whereas in the Wet season it grows up through the water (Figure B.3) (Finlayson et al. 1989). Plants are either prostrate of decumbent 20–50 cm tall with linear or triangular linear leaves 1–2 cm long (Cowie et al. 2000). Flowering and fruiting occur mainly from January to June. During the Wet season, aquatic plants including *Eleocharis* spp., *Nymphaea* spp., *Najas tenuifolia*, and *Salvinia molesta* can exist amongst this grass (Finlayson et al. 1989).

Figure B.3 *Pseudoraphis spinescens* grassland.

B.4 *Hymenachne acutigluma* grassland

This is a perennial grassland occurring year long. Plants can be up to 1.3 m tall with linear or linear triangular blades 8–30 cm long. Flowering and fruiting occur between January and October (Cowie et al. 2000). Minor species that may occur in the grassland include *Ludwigia adscendens*, *Oryza meridionalis* and *Pseudoraphis spinescens*. According to Finlayson et al. (1989) the community is susceptible to invasion from Para grass (Figure B.4).

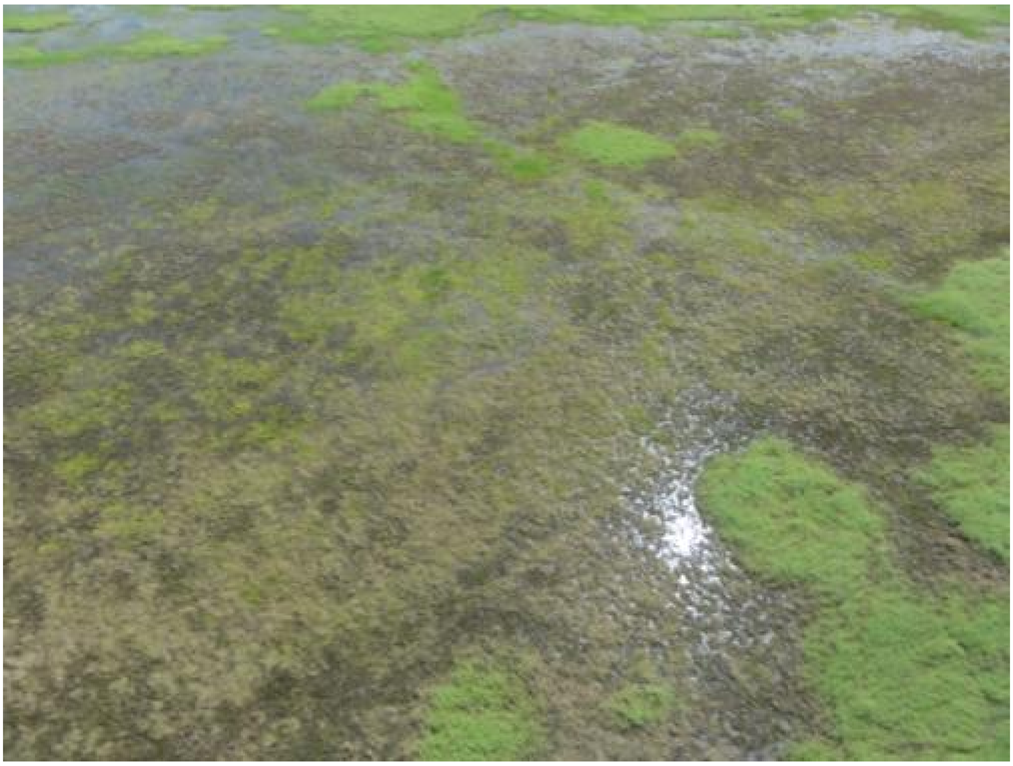

Figure B.4 *Hymenachne acutigluma* grassland with Para grass encroaching on right hand side.

B.5 Melaleuca spp. woodland and open forest

Melaleuca spp. woodland (Figure B.5) and open forest (Figure B.6) communities are dominated by trees from one or more *Melaleuca* spp. Floodplain edges and the northern region tend to be dominated b *M viridiflora* and *M. cajaputi*, while *M leucadendra* is prevalent in the backswamps that are inundated for most of the year. Understorey in these communities is varied most likely as a response to water depth and shade (Finlayson et al. 1989). In areas with a dense canopy, the understorey tends to consist of shade tolerant species, in the more open areas the understorey is similar to adjacent grassland communities with *Hymenachne acutigluma*, *Pseudoraphis spinescens* or *Oryza meridionalis* present (Finlayson et al. 1989).

Figure B.5 *Melaleuca* woodland with a mixed grass/ sedge understorey.

Figure B.6 *Melaleuca* open forest.

B.6 Nelumbo nucifera (red lily) herbland

This community (Figure B.7) occurs in permanently or semi-permanently wet areas. Perennial and emergent *N. nucifera* can form dense stands in the Dry season. *N. nucifera* is typified by large orbicular blue green leaf blades (18–70 cm in diameter) that are either floating or emergent from the water (Cowie et al. 2000). Flowering occurs between March and December while fruiting occurs between June and December.

Figure B.7 *Nelumbo* herbland.

B.7 Nymphoides/Nymphaea (small lilies) herbland

Nymphoides/*Nymphaea* (small lilies) herbland are aquatic communities with floating leaves (Figure B.8). *Nymphoides* spp. leaf blades are much smaller (typically less than 10 cm diameter) than the leaf blades of *Nymphaea* spp.

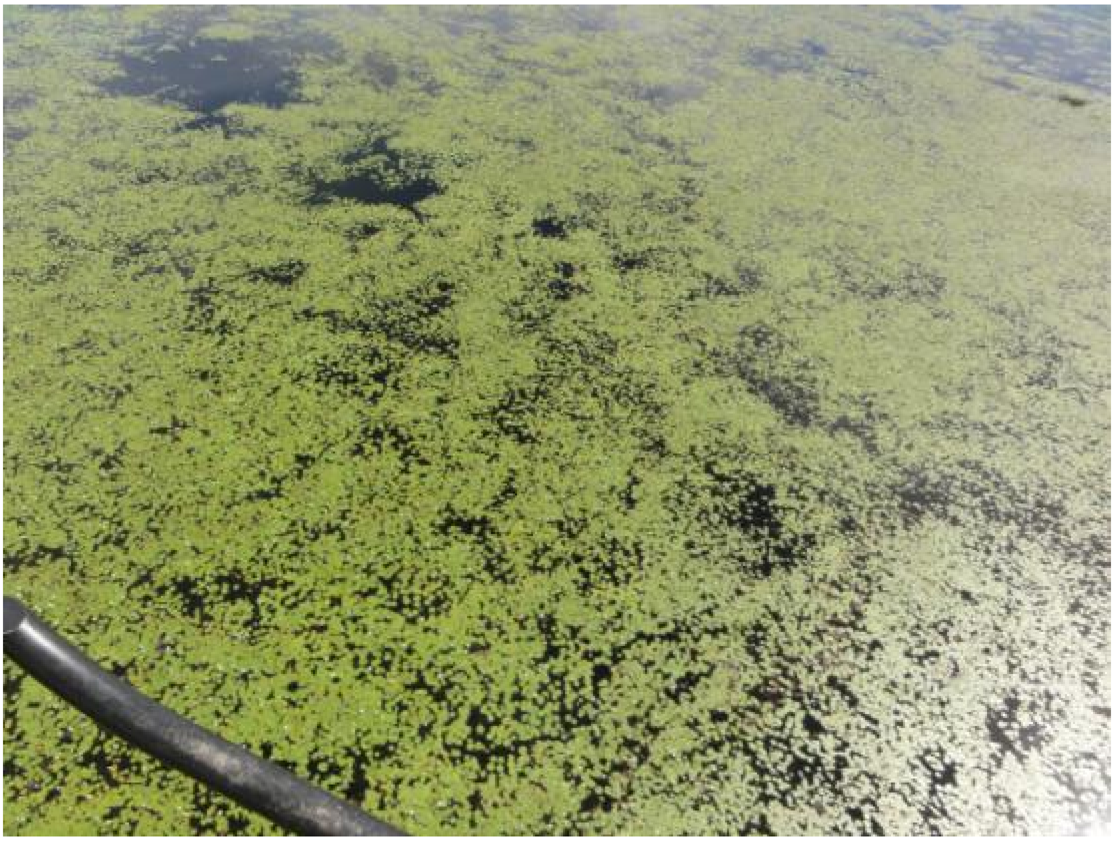

Figure B.8 A large expanse of *Nymphaea*/*Nymphoides* herbland.

B.8 Leersia hexandra grassland

The *Leersia hexandra* grassland that commonly occurs in floating mats located on floodplain and backwater swamps (Cowie et al. 2000). Plants are tall and slender (0.6–2 m long) with linear-acuminate blue-green leaf blades, 4–20 cm long. *L hexandra* flowers and fruits between March and June.

B.9 Other vegetation

The major ecological weed within the floodplain is Para Grass, *Urochloa mutica* (Boyden et al. 2007, Boyden et al. 2013), occupying a large area in the central plains region of the floodplain (Figure B.9). Other weeds include *Mimosa pigra* and *Salvinia molesta* (Figure B.10) but these are under effective biological control on the floodplain (Cowie et al. 1988, Walden et al. 2012). Vegetation surrounding the floodplain is primarily a tropical savanna matrix consisting of the co-dominants: a continuous annual grass cover and a discontinuous tree cover (mostly *Eucalyptus* spp.) (Story 1976).

Figure B.9 The invasive Para grass, *Urochloa mutica*.

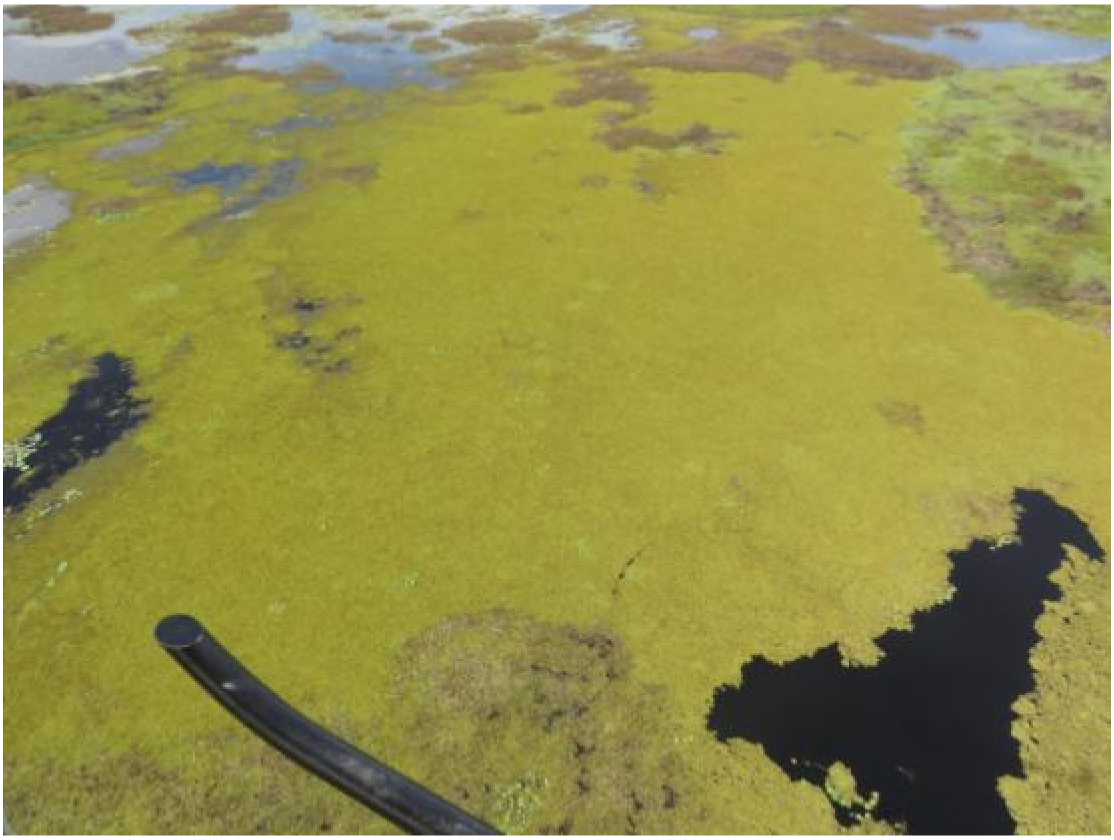

Figure B.10 The floating fern, *Salvinia molesta*.